OPTICAL EMISSIONS FROM ENSEMBLES OF NANOCLUSTERS WITH HIGH CONCENTRATIONS OF STABILIZED NITROGEN ATOMS

A Dissertation

by

PATRICK THOMAS MCCOLGAN

Submitted to the Office of Graduate and Professional Studies of
Texas A&M University
in partial fulfillment of the requirements for the degree of

DOCTOR OF PHILOSOPHY

Chair of Committee,	David Lee
Committee Members,	Glenn Agnolet
	Roland Allen
	Philip Hemmer
Head of Department,	Grigory Rogachev

December 2018

Major Subject: Physics

ABSTRACT

Ensembles of nanoclusters are formed in bulk HeII by the injection of products of a radiofrequency discharge in impurity-helium gas mixtures into bulk superfluid ^{4}He (HeII). The ensembles of nanoclusters contain high concentrations of stabilized nitrogen atoms residing mostly on the surfaces of rare gas or nitrogen nanoclusters. These samples are characterized by a high energy density which allows the study of energy release processes in chemical reactions initiated by warming ensembles of nanoclusters. Optical spectra in the ultra-violet, visible, and near-infrared ranges were recorded during the destruction of these ensembles of nanoclusters, accompanied by a rapid release of chemical energy stored in the samples.

Rare gases such as neon, argon, and krypton were used to study the effects of changing the relative concentrations of nitrogen in rare gases used for sample preparation on thermoluminescence spectra during destruction of nitrogen-rare gas-helium samples. Spectra obtained during the bright flashes of the final destruction of the samples contain M- and β-bands of NO molecules the intensities of which depend on concentration of molecular nitrogen in the gas mixture as well as on the type of rare gas present in the gas mixture.

During the destructions of samples containing stabilized nitrogen, oxygen, hydrogen, and deuterium atoms, the known bands of atomic nitrogen and oxygen, and bands of molecular nitrogen, oxygen, and NO were observed as well as several other interesting features including a broad band near $\lambda \sim 360$ nm, which has been identified as an emission corresponding to the $2A_g \rightarrow 1A_g$ transition of $N_4(D_{2h})$ polymeric nitrogen. Also the sharp lines at λ = 336 nm, 473 nm, and 1170 nm were observed, which were assigned to the emission of the ND radicals formed due to recombinations of nitrogen atoms in excited metastable states and deuterium atoms in the ground state during the destruction of ensembles of molecular nitrogen nanoclusters.

The influence of rotation speed of a beaker containing HeII on the intensity of luminescence of collections of nanoclusters immersed in HeII was also studied. Luminescence was found to increase with the concentration of molecular nitrogen in the nitrogen-helium gas mixtures used

for the formation of the molecular nitrogen nanoclusters. The intensity of α-group emission of nitrogen atoms (^{2}D $\rightarrow$ ^{4}S transition) in nanoclusters also increased with the rotational speed of the beaker. We suggest that this effect is connected to the processes of recombination of nitrogen atoms residing on the surfaces of nanoclusters after their trapping into quantum vortices in HeII. Increasing the rotation speed of the beaker results in the increasing density of quantum vortices in HeII. The probability for nanoclusters to become trapped in the vortex cores increases with the vortex density. Inside the vortex cores, the collision rate of nanoclusters increases substantially, leading to more efficient recombination of nitrogen atoms stabilized on the surfaces of nanoclusters and, therefore to more intense atomic nitrogen luminescence.

DEDICATION

For my parents and brothers.

ACKNOWLEDGMENTS

I would like to articulate my sincere gratitude to my advisor, Prof. David M. Lee for supporting, and encouraging me throughout my academic career. It was a privilege to participate in research in his group.

I would like to thank our senior scientist Dr. Vladimir Khmelenko for his patient guidance throughout my participation in research here at A&M. He is an exceptional experimental physicist, and under his careful direction, I have gained experience in many skills and techniques required for scientific research. Together we turned an empty room into a fully-functional condensed matter laboratory.

I would like to thank our collaborator Dr. Roman Boltnev in Russia, for his steadfast and patient approach which greatly strengthened every paper he participated on.

The physics machine shop offered experience in scientific instrument manufacturing, and precisely fabricated many parts that allowed our experimental setups to function. Garrick Garza, the shop supervisor, eagerly offered advice and technical assistance on many occasions. Research Instrumentation Specialists Andrew Jaisle and John Newkirk manufactured many parts integral to our research to exacting specifications.

I would also like to thank the my colleagues in my research group for their diligent work. During long hours in the lab, I learned a lot from each of them. A special thanks to Dr. Shun Mao, Dr. Adil Meraki, and Dr. Sergei Sheludiakov.

Finally, I would like to thank the diligent work put forward by the administrative staff of this department. Without their patient assistance, this dissertation would not be possible.

CONTRIBUTORS AND FUNDING SOURCES

Contributors

This work was supported by a dissertation committee consisting of Professor David Lee, Dr. Glenn Agnolet, Dr. Roland Allen, of the Department of Physics and Astronomy and Dr. Philip Hemmer of the Department of Electrical and Computer Engineering. Research was supervised by Dr. Vladimir Khmelenko (senior research scientist) of the Department of Physics and Astronomy.

Material in chapter 3 was obtained by the student in collaboration with Dr. Adil Meraki, Dr. David Lee, and Dr. Vladimir Khmelenko, of the department of Physics and Astronomy, as well as Dr. Roman Boltnev of Talroze Institute for Energy Problems of Chemical Physics, Russian Academy of Sciences, Chernogolovka, Russia. Dr. Adil Meraki assisted with obtaining and analysis of the ESR data in this chapter.

Material in chapter 4 was obtained by the student in collaboration with Dr. Adil Meraki, Dr. Sergei Sheludiakov, Dr. David Lee, and Dr. Vladimir Khmelenko of the department of Physics and Astronomy, as well as Dr. Roman Boltnev of Talroze Institute for Energy Problems of Chemical Physics, Russian Academy of Sciences, Chernogolovka, Russia.

Material in chapter 5 was obtained by the student in collaboration with Dr. Sergei Sheludiakov, Dr. David Lee, and Dr. Vladimir Khmelenko of the department of Physics and Astronomy, as well as Dr. Roman Boltnev of Talroze Institute for Energy Problems of Chemical Physics, Russian Academy of Sciences, Chernogolovka, Russia.

Material in chapter 6 was obtained by the student in collaboration with Dr. Sergei Sheludiakov, Dr. David Lee, and Dr. Vladimir Khmelenko of the department of Physics and Astronomy, as well as Dr. Peter Rentzepis of the Department of Electrical and Computer Engineering.

All optical spectra were obtained, and processed by the student. All other work conducted for the dissertation was completed by the student independently.

Funding Sources

Graduate study was supported by the CF Squire Condensed Matter Fellowship and Grants from the National Science Foundation Award numbers: DMR 1209255, and DMR 1707565.

NOMENCLATURE

IHC	Impurity Helium Condensate
RF	Radio-Frequency
HeII	Superfluid Helium II
LN_2	Liquid Nitrogen
LHe	Liquid Helium
ESR	Electron Spin Resonance
RG	Rare Gas
UV	Ultraviolet
VIS	Visible
NIR	Near-Infrared
UHP	Ultra High Purity
PID	Proportional-Integral-Derivative
BNC	Bayonet Neill-Concelman
USB	Universal Serial Bus
TTL	Transistor-Transistor Logic
PSI	Pounds per Square Inch
V-K	Vegard-Kaplan
HEDM	High-Energy Density Material

TABLE OF CONTENTS

Page

LIST OF FIGURES

FIGURE Page

LIST OF TABLES

TABLE Page

1. INTRODUCTION AND LITERATURE REVIEW

1.1 Introduction

Investigations of thermoluminescence of solid nitrogen and rare gases containing stabilized atoms at low temperates have a long history [11, 12, 13, 14, 15, 16, 17, 18]. Later, investigations of destruction of ensembles of nanoclusters containing stabilized atoms formed in bulk superfluid helium (HeII) were performed [19, 20, 21, 22, 23].

The ensembles of nanoclusters were created by injecting products of discharges in nitrogen-helium or nitrogen-rare gas-helium mixtures into bulk HeII [24, 25]. This method allows the formation of a porous structure consisting of a collection of impurity nanoclusters with high concentrations of stabilized atoms inside superfluid helium (HeII). This method has also been used to examine oxygen impurities $\sim$ 10 ppm in low temperature plasmas [26].

Injecting radiofrequency discharge products into HeII creates highly porous aggregates of nanoclusters immersed in HeII. The characteristic size of the impurity nanoclusters is of order 5 nm and the overall density of the impurity atoms and molecules inside HeII is of order 10^{20} cm^{-3} as determined from ultrasonic and x-ray experiments [27, 28, 29, 30, 31, 32]. The nanoclusters form porous aerogel-like structures known as impurity-helium condensates, which have a broad distribution of pore sizes ranging from 8 to 860 nm [28, 33, 34]. Just after preparation of the samples the pores are filled with liquid helium. The highest concentrations of stabilized atoms were achieved in nitrogen-helium condensates with relative concentration of stabilized nitrogen atoms (N/N$_2$ $\times$ 100 %) in the range 10-30 % [35].

The stabilized atoms reside mostly on the surfaces of the nanoclusters [36, 37, 38]. It is believed that a layer of solid helium covered the surfaces of impurity nanoclusters thus preventing reactions between nitrogen atoms residing on the surfaces of nanoclusters. The average concentration of stabilized nitrogen atoms was of order 10^{19} cm^{-3} [36, 39, 40]. The values of local concentrations of N atoms are substantially larger, 8×10^{20} cm^{-3} [36, 39, 40, 41] as determined from the width

of electron spin resonance spectra. The ensembles of molecular nitrogen nanoclusters with stabilized nitrogen atoms contain high densities of stored chemical energy [35, 36, 37]. As a result, these ensembles of nanoclusters are characterized by high specific energy content (up to 10^4 J/g) [39, 41]. The investigations of thermoluminescence of the ensembles of nanoclusters containing stabilized atoms were performed for samples prepared from nitrogen atoms and molecules [3] and also atoms of rare gases [19, 21, 22].

High concentrations of nitrogen atoms stabilized in molecular nitrogen nanoclusters provide substantial chemical energy for promoting recombination reactions of stabilized atoms during warming of the samples [39, 40, 41]. These porous structures are stable while immersed in bulk superfluid helium. Removing liquid helium from the porous structures led to a collapsing of the pores, resulting in approaching and colliding of nanoclusters which initiated chemical reactions of atoms residing on the surfaces of the nanoclusters. The rapid release of stored chemical energy resulted in rapid heating and intense thermoluminescence of the samples. In the past, studies of thermoluminescence during the destruction of samples were performed for impurity-helium condensates containing N_2 molecules, N atoms, and rare gas atoms, as well as small amounts of oxygen atoms ($N_2/O_2 \sim 10^{-3} - 10^{-4}$). Strong emissions from N atoms (α, α', δ, δ'-groups), O atoms (β, β', β'' groups), N_2 molecules (VK bands), NO molecules (M and β-bands), XeO molecules (green bands), O_2 molecules (second Herzberg bands), and N^- anions (γ-line) were observed in these experiments [3, 5, 19, 21, 22, 23, 42]. These studies provided examples of chemical reactions at low temperatures in collections of nanoclusters containing stabilized nitrogen and oxygen atoms.

Previously, work has been performed via ESR studies on hydrogen and nitrogen atoms stabilized in corresponding molecular matrices [43] as well as N_2:RG Matrices [2, 36]. The method of matrix isolation provides possibilities for studying exotic highly unstable species. In the past, considerable efforts were made to create systems with high concentrations of matrix-isolated free radicals [16]. Different practical applications were proposed for those systems such as clean energy storage and more efficient rocket fuel. An additional application could be research on cryochemi-

cal reactions of exotic species. Conditions inside of our Dewar are similar to those in outer space, so it may be possible to examine processes that occur in the interstellar medium.

Fascination with quantum vortices in superfluid helium (HeII) started with their discovery in the 1950s, and continues today [44]. Investigations of quantum vorticies in superfluid helium have recently attracted great attention [45, 46, 47]. The visualization of vortex cores [44] has led to the observation of the reconnection of vortices and direct observation of Kelvin waves excited by quantized vortex reconnections [48, 49], characterization of the probability density function representing particle velocity [50] and acceleration in thermal counterflow [51]. Metastable helium molecules were used as tracers in superfluid helium [52], providing the possibility to study quantum turbulence in He in the T = 0 limit [53] and examine the normal fluid behavior in thermal counterflow [54, 55]. The technique of nanowire formation by ablating metallic nanoparticles from a target in HeII was realized on the basis of coalescence of the nanoparticles in the vortex cores [56, 57]. The luminescence of ensembles of molecular nitrogen nanoclusters containing stabilized nitrogen atoms was initiated in HeII by quantum vortices [58]. In this latter case the dependence of luminescence intensity on temperature was correlated with that of the vortex density in the temperature range 1.2 - 2.1 K.

There are two main goals in this work: To study the optical spectra of thermoluminescence emitted during the warming and destruction of ensembles of molecular nitrogen nanoclusters with high concentrations of stabilized nitrogen atoms, and to study quantum vortex initiation of luminescence of molecular nitrogen nanoclusters with stabilized atoms submerged in HeII.

Chapter 2 describes the experimental setups and the processes used to create and study our samples. In our stainless steel cryostat, the samples can be simultaneously investigated with electron spin resonance (ESR) and optical spectroscopy techniques. In the glass Dewar setup, all stages of sample preparation, luminescence, and destruction can be observed directly, and by multiple optical spectroscopy techniques. The large inner diameter of the glass Dewar allows the possibility for many different experiments to be conducted inside. This permitted us to mount a stepper motor to investigate luminescence resulting from chemical reactions of atoms stabilized on the surfaces

of nanoclusters initiated by the rotation of a beaker containing HeII.

In Chapter 3, the experiments describe the addition of rare gases: argon, neon, and krypton to the nitrogen-helium gas mixtures from which the samples were created. Optical spectra were recorded during the destruction of these samples, and striking differences were found in the observed spectra. A correlation between molecular nitrogen content in the gas mixture used to prepare the samples and the concentration of stabilized atoms was observed using ESR spectroscopy techniques.

Spectra of the luminescence emitted during the destruction of samples prepared from nitrogen-helium gas mixtures with small admixtures of molecular hydrogen isotopes are described in Chapter 4. The admixture of hydrogen or deuterium in the gas mixtures used to prepare our samples enhanced the broad band at λ = 360 nm, which was determined to be emission from the N_4 polynitrogen. Emission from several transitions of the ND radical were also observed in the visual range. Bands at λ = 336 and 473 were tentatively assigned to the emission of the $A^3\Pi_i^+ \rightarrow X^3\Sigma^-$ and $b^1\Sigma^+ \rightarrow X^3\Sigma^-$ transitions of the ND radical respectively.

In Chapter 5 we discuss the investigations of luminescence during the destruction of samples which were performed in the ultraviolet (UV), visual (VIS), and near-infrared (NIR) optical ranges simultaneously. The spectra taken in the NIR range revealed a band at λ = 1170 corresponding to the $b^1\Sigma^+ \rightarrow a^1\Delta$ transition of the ND radical. The presence of this band further supported the assignment of the band observed at λ = 473 nm, as the $b^1\Sigma^+ \rightarrow X^3\Sigma^-$ transition of the ND radical.

Chapter 6 presents studies of the influence of the rotation speed beaker containing HeII on the α-group N(^{2}D $\rightarrow$ ^{4}S transition) luminescence during the injection of gas mixtures. The increase of vortex density led to the increased recombination probability of the nitrogen atoms residing on the surfaces of the nanoclusters.

2. EXPERIMENTAL APPARATUS AND TECHNIQUE

2.1 Combined Optical and ESR Spectroscopy Setup

2.1.1 Experimental Setup

The experimental setup used to study the impurity-helium samples at low temperature allows application for both optical and electron spin resonance (ESR) spectroscopies simultaneously. It utilizes a custom-designed Janis research cryostat and a home-made insert. These have been thoroughly described elsewhere [1]. The cryostat has a variable temperature insert (VTI) where the sample is created and studied. Investigations can be performed in the temperature range from 1 K to 300 K.

The temperature inside the VTI during sample preparation is maintained at 1.45 K using an Edwards model E2M80 two-stage mechanical pump and is measured by a germanium thermometer. Generally, sample accumulation lasts 10 minutes and the volume of the accumulated sample is $\sim$1 cm^3. After sample preparation the beaker is lowered into the microwave cavity, located in the tail of the cryostat and the center of the electromagnet where ESR and optical studies can take place. There is only optical access through the quartz windows at the bottom of the tail of the cryostat.

2.1.2 ESR and optical spectra registration systems

This experimental setup consists of a custom-fabricated Janis research cryostat whose tail sits within the poles of a 1.5T Varian research electromagnet (see Fig. 2.1). This cryostat has concentric LN_2 and LHe baths surrounding the VTI as well as a vacuum-insulated jacket that reduces liquid cryogen loss due to heat leaks. There are two fused quartz-silica windows in the tail of the Janis Research cryostat, which is located between the poles at the center of an electromagnet which allow optical access. Outside of the window, a focusing lens is installed for directing light emitted from the sample into a bifurcated fiber optic cable which feeds simultaneously into an Ocean optics HR2000+ and an Andor SR-500i spectrometer.

Inside the bore of the research cryostat we have installed a custom-fabricated insert. The vari-

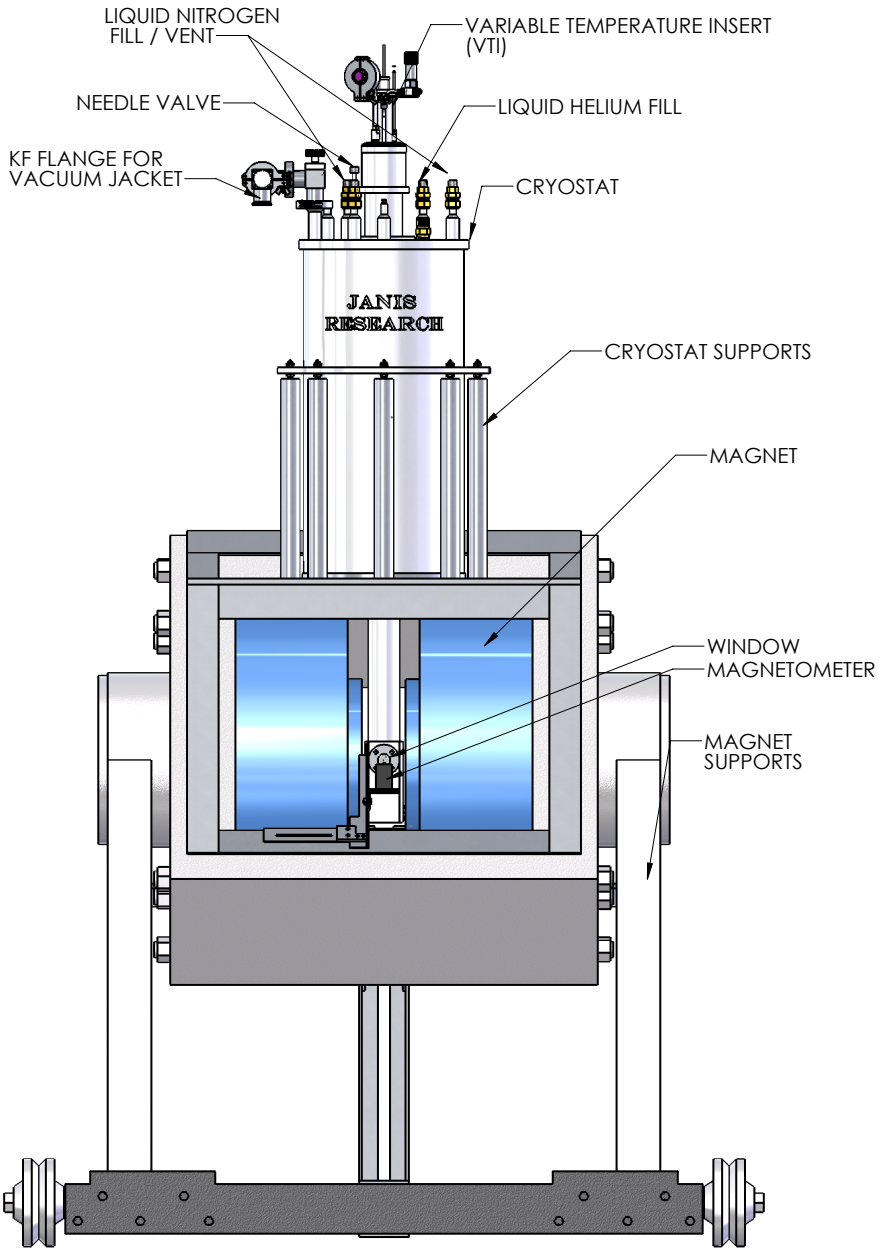

Figure 2.1: Diagram showing the scheme of the combined optical and ESR spectroscopy setup.

able temperature insert (VTI) houses all of the equipment required for the experiment: The atomic source, quartz sample collection beaker, stainless steel control rods, modulation coils, and ruby crystal. The atomic source provides the excited atoms and molecules. Temperatures above 2.8K

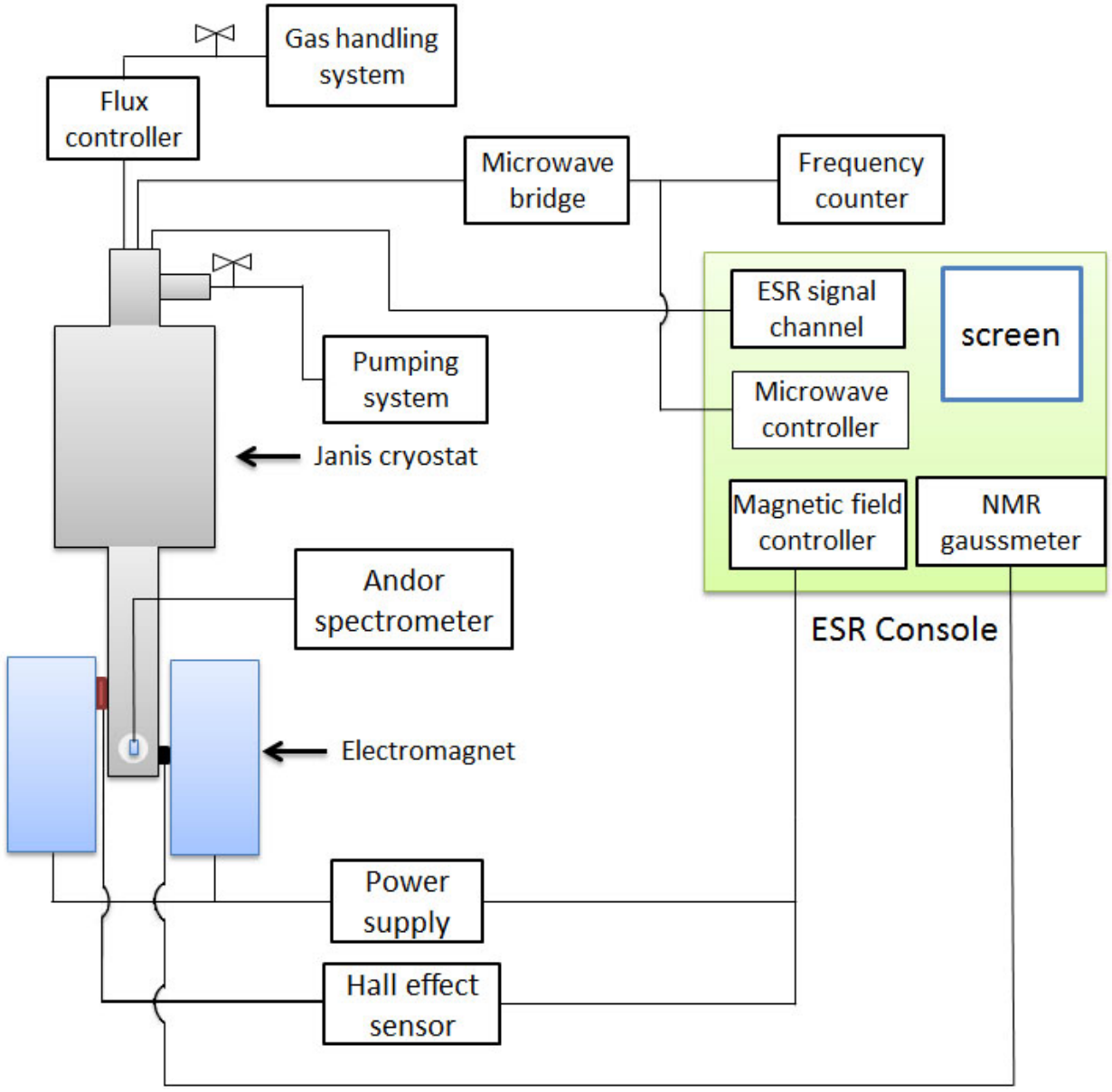

Figure 2.2: Diagram showing a block diagram of the combined optical and ESR spectroscopy setup. Reprinted with permission from [1].

inside of the variable temperature insert (VTI) can be stabilized by a computer-controlled PID heater and regulating the pumping speed of the mechanical pump, as well as the flow of helium liquid or vapor from the main bath through the needle valve.

A Bruker EMXPLUS spectrometer was used to record ESR spectra of stabilized atoms. This spectrometer can record standard definition spectra with 1024 points or high resolution spectra

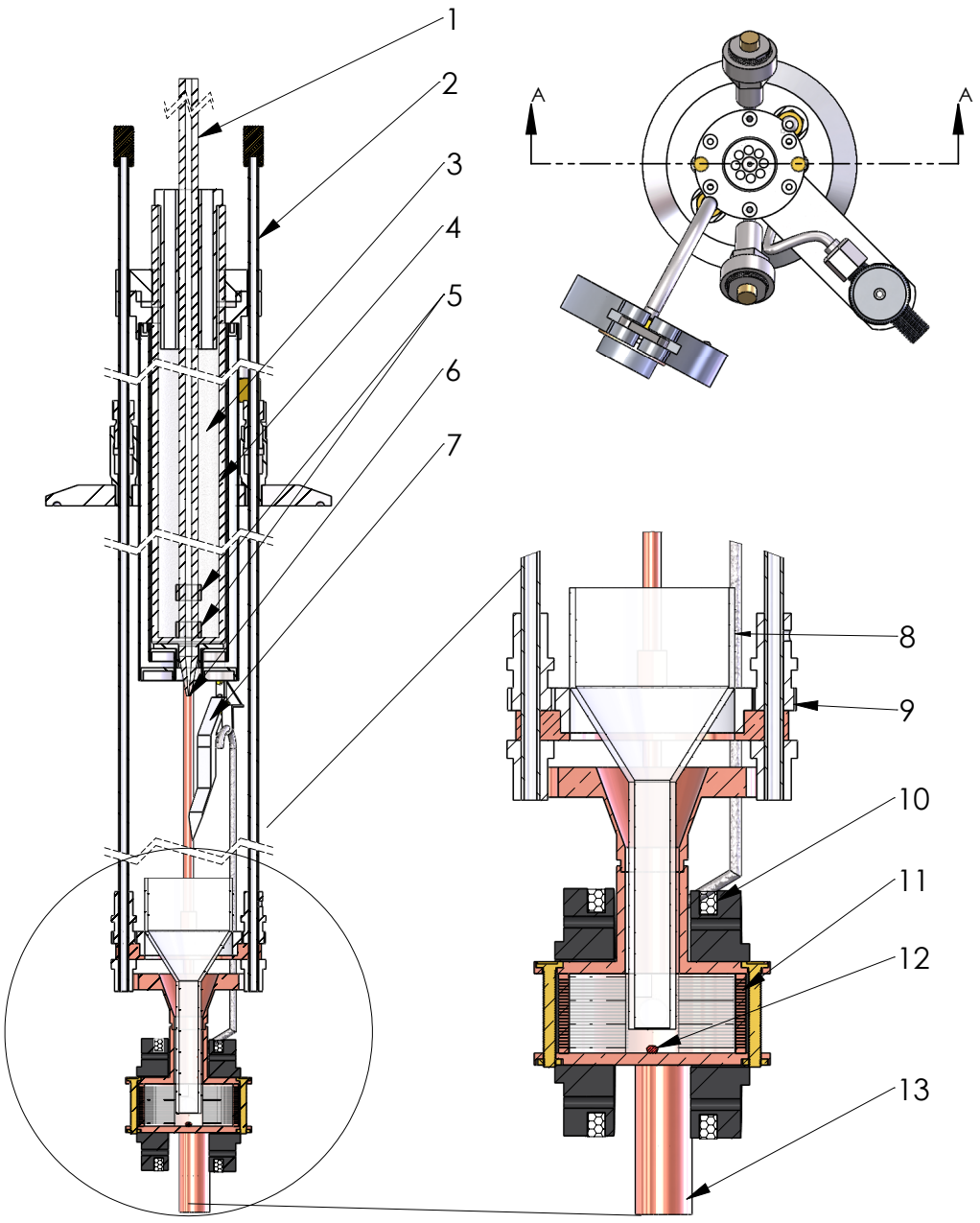

Figure 2.3: Schematic of the combined optical ESR spectroscopy VTI. 1: Quartz capillary, 2: Stainless steel control rods, 3: LN_2 volume, 4: Quartz discharge tube, 5: Discharge electrodes, 6: Orifice, 7: Teflon blade, 8: Quartz beaker, 9: Teflon gear, 10: Modulation coils, 11: Slits in the copper cavity, 12: Ruby crystal, 13: Fountain pump. Reprinted with permission from [2].

with 2048 points. The ESR parameters for the registration of the derivative of atomic nitrogen absorption signals are as follows: Center field for N atoms is 3190 G with a sweep of 200 G in four minutes. The klystron microwave bridge provides ∼10-20 microwatts of power. The modulation frequency is 100 kHz with an amplitude of 0.5 G. For the ruby crystal used as secondary a standard, the center field is 1820 G. To measure the concentration of stabilized N atoms, ESR signals from the sample are compared to signals from the ruby crystal. This ruby was permanently affixed to the bottom of the microwave cavity where it is used as a secondary standard. The calibration of the absolute value of the number of spins was performed using a standard organic diphenyl-picrylhydrazl (DPPH) sample with a known number of spins $\sim 2.4 \times 10^{17}$. The atomic nitrogen concentrations were calculated by dividing the number of atoms by the volume of the sample. Typically samples are studied at different temperatures. Starting directly after sample preparation, the temperature is stabilized at 1.3 K while scans are taken. Typically a series of scans are performed at different temperatures until the sample is destroyed.

2.2 Optical Setup

Our experimental setup has been described elsewhere [3]. The cryogenic portion of the experimental setup consists of two concentric, silvered glass double-walled Dewars. These Dewars are silvered to prevent the radiative transfer of heat. To allow optical access, there are two slit windows in the silvering. An advantage of this system, is that all processes from sample creation to sample destruction can be optically studied. The outer Dewar is filled with Liquid nitrogen (LN_2) and the inner Dewar is filled with liquid helium (LHe). The glass helium Dewar is connected by a pumping line to an Edwards model E2M80 two-stage mechanical pump, and an Edwards model EH1200 roots blower. The inside of the Dewar is cooled by the evaporation of He^4 removed by these two pumps. With the roots blower running, temperatures inside the helium Dewar of 1.1 K are achievable.

The glass Dewars are supported by an aluminum frame connected to a vibration isolation table. The hollow spaces inside of this frame were filled with lead shot, which loads the vibration isolation table helping reduce vibration transmission to the setup. To prevent transmission of vi-

brations from footsteps, a false floor was constructed using aluminum I-beams and CNC water-jet cut quarter inch aluminum plates. The main pumping line also has a series of bellows to reduce vibrations from the vacuum pumps.

2.2.1 Optical Insert

The optical insert houses the atomic source and mechanically supports the experimental apparatus inside of the glass helium Dewar. The optical insert is connected to the vacuum system with a large flange with a rubber o-ring. The top flange of the cryogenic system houses all of the connections to room-temperature equipment, including a vacuum feed-through for our cryogenic fiber assembly, and a vacuum feed-through for all electrical connections. Directly below the top flange are 4 Styrofoam baffles which help reduce heat transfer from the room-temperature top flange. The insert connects the support for the sample collection beaker to the top flange with a series of thin-wall stainless steel tubes connected to brass flanges. These stainless steel tubes terminate in a brass flange which can be used to mount additional equipment inside of the Dewar.

2.2.2 Rotating Beaker Assembly

One unique feature of this setup is the ability to rotate our beaker at cryogenic temperatures. The possibility of rotating a beaker containing HeII was demonstrated in previous work [59, 60]. In our setup rotation of the beaker is accomplished by connecting the quartz beaker to the output shaft of a stepper motor (see Fig. 2.5). The quartz beaker sits in a Teflon holder which is attached to a brass flange with screws. The brass flange is secured to the output shaft of the stepper motor with a set screw.

The electric motor is powered by a 24 VDC power supply controlled by a stepper motor driver and an Arduino UNO development board with an ATMEGA 328 microcontroller. The microcontroller is running a program which enables the motor, controls the direction of rotation, and “ramps up" the rotational speed from zero to the desired speed, as well as displaying this speed on a seven-segment display. The microcontroller provides a chain of TTL pulses to the DM320T stepper motor driver. This driver has built-in current limiting capabilities that reduce heating inside

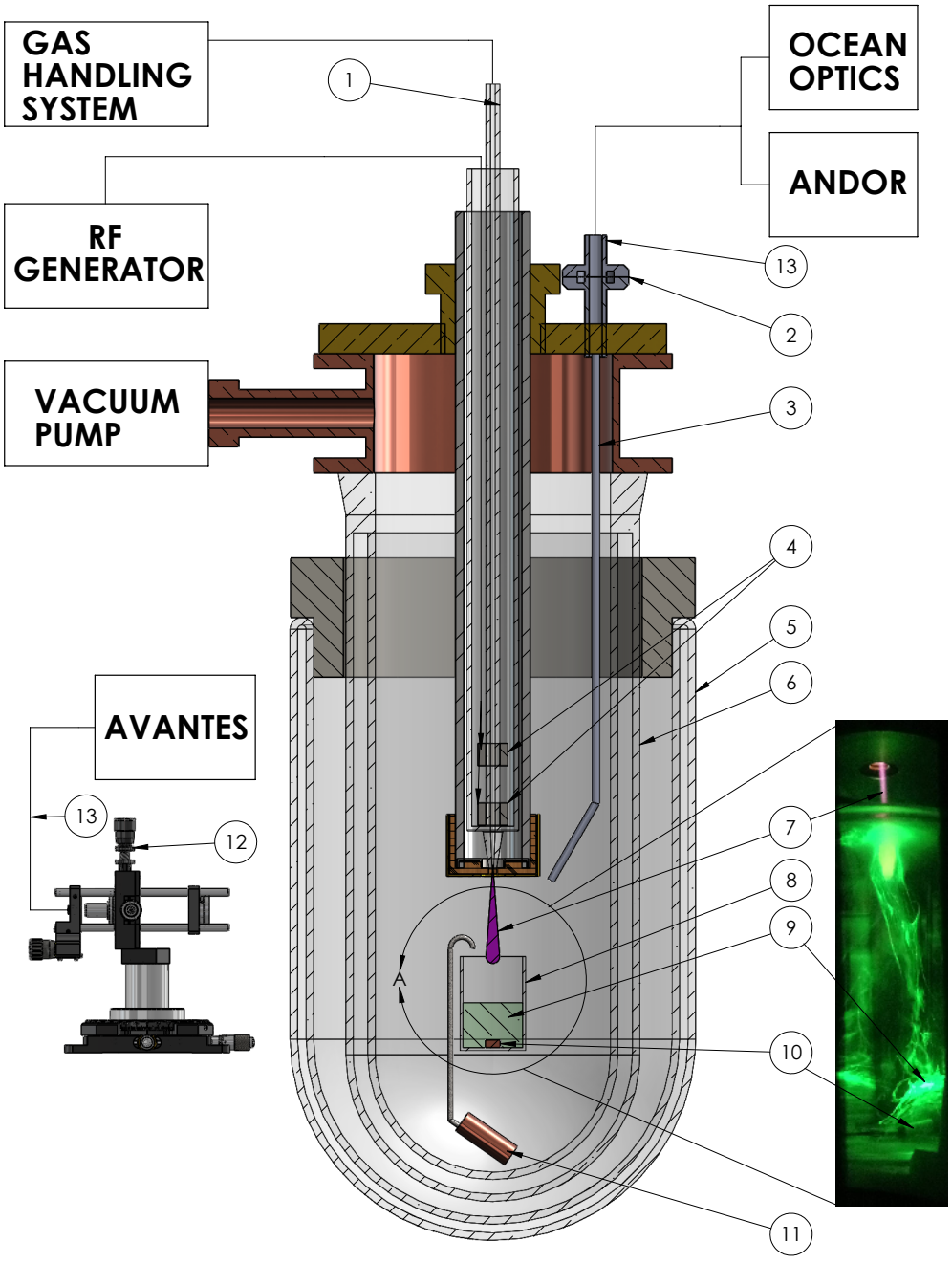

Figure 2.4: Diagram showing the scheme of the optical experiment. 1: Quartz capillary, 2: Optical-vacuum feed-through, 3: Cryogenic optical fiber assembly, 4: Discharge electrodes, 5: LN_2 Dewar, 6: LHe Dewar, 7: Jet, 8: Sample collection beaker, 9: Sample in HeII, 10: Germanium thermometer, 11: Thermo-mechanical fountain pump, 12: Fiber launch, 13: Bifurcated optical fiber. Reprinted with permission from [3].

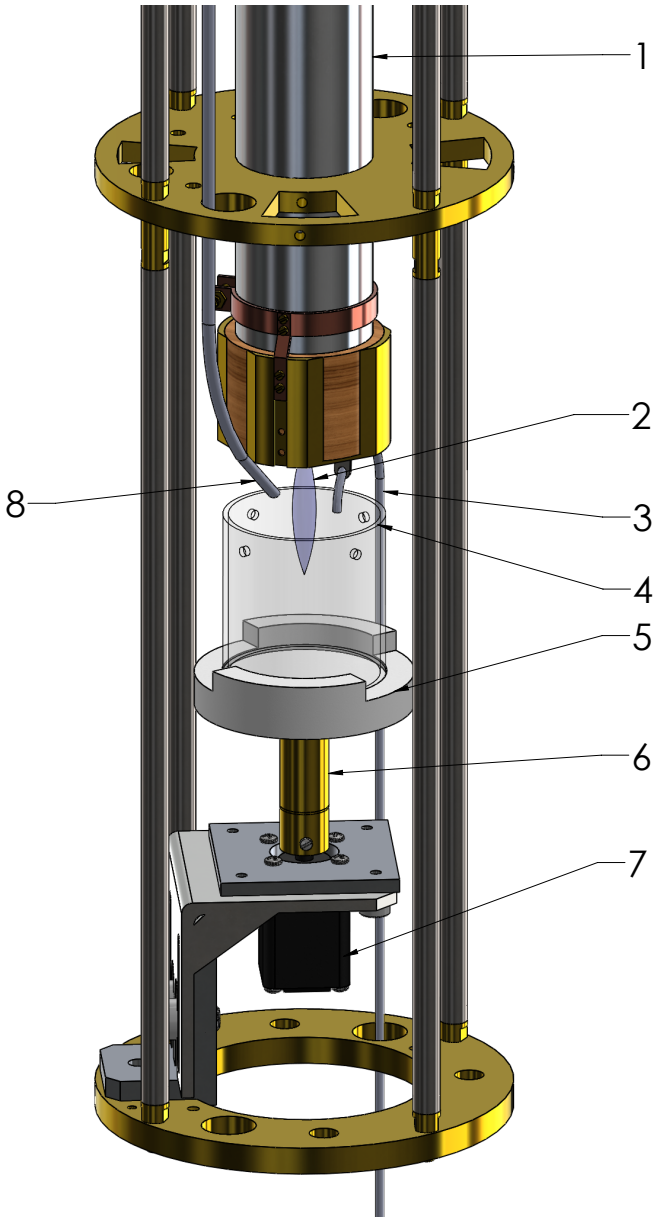

Figure 2.5: Rotating beaker assembly. 1: Atomic source, 2: Nitrogen-helium jet, 3: Fountain pump line, 4: Quartz beaker, 5: Teflon beaker holder, 6: Brass flange, 7: NEMA 8 stepper motor, 8: Optical fiber.

of the stepper motor coils, as well as providing the microstepping. These are controlled by dip-switches located on the side of the stepper motor driver. The motor is a standard NEMA 8 motor with 200 steps per revolution, or 1.8 deg. per step. With the microstepping from the driver, there are a total of 1600 microsteps per revolution (13.5 arcmin per microstep). Each TTL pulse from

the microcontroller advances the motor one step. The use of microstepping allows for smoother rotation of the beaker.

The motor itself is an off-the shelf part, which was modified to perform in cryogenic conditions. The two bearings connected to the rotor were removed and throughly cleaned using an aerosol solvent. This solvent is generally used to remove oil and debris from automotive sensors, and it is safe for sensitive electronics. The liquid oil lubricants would be frozen at cryogenic temperatures. The bearings were then lubricated using a molybdenum disulfide (MbS_2) dry lubricant applied with an aerosol solvent. After application, the solvent is evaporated, leaving a thin film of dry MbS_2.

The operation of the motor provided an additional heat load so that all experiments were performed at a slightly elevated temperatures 1.53-1.54 K compared to the optimal condition (T = 1.5 K).

2.3 Optics

The emission of the ultraviolet (UV) and visible (VIS) light is collected using a cryogenic fiber assembly installed inside the helium Dewar that withstands liquid helium temperatures. This fiber assembly collects light from the bottom of the sample collection beaker and terminates at a vacuum-tight optical feed-through on the top flange.

A bifurcated optical fiber is connected on the atmospheric side of the vacuum feed-through. This optical fiber transfers the light emitted from the sample to the Andor Shamrock SR-500i with Newton EMCCD camera and the Ocean Optics HR2000+ spectrometers [3]. By employing this bifurcated fiber assembly, we can make simultaneous measurements with two different spectrometers.

The Andor spectrometer can take high resolution spectra (0.53 nm, first grating) for a narrower spectral range ($\Delta\lambda = 340$ nm), but has a much higher sensitivity, allowing for an exposure time of 3 ms during registration. The quantum efficiency of the Andor spectrometer using the Newton EMCCD camera and the 1st grating is shown in Fig. 2.6a. The Ocean Optics spectrometer can record spectra continuously over a large wavelength range from 200 to 1100 nm, with spectral

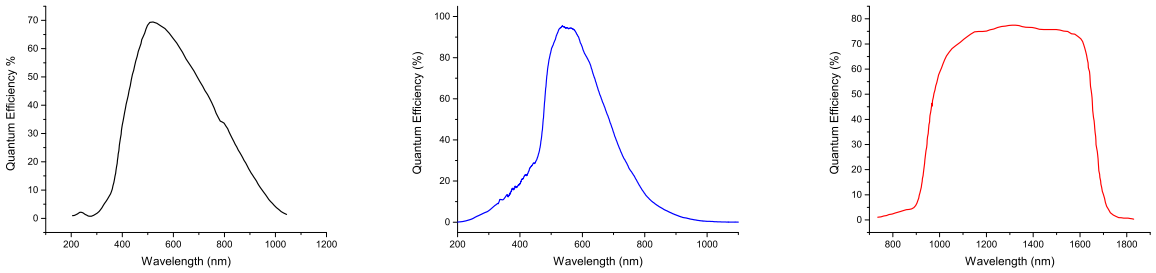

(a) (b) (c)

Figure 2.6: a) Quantum Efficiency of Andor SR-500i spectrometer while using Newton EMCCD camera with the 1st grating, b) Quantum efficiency of the Ocean Optics HR2000+ spectrometer, c) Quantum efficiency of Avantes NIR 512-1.7 TEC spectrometer.

resolution 1.3 nm (generally used with a registration time from 100 to 500 ms). The quantum efficiency of the Ocean Optics spectrometer is shown in Fig. 2.6b.

The Ocean Optics and Andor Spectrometers were wavelength calibrated using an Ocean Optics HG-1 Mercury Argon Calibration source. This source emits light with known wavelengths and intensities from λ = 253 - 922 nm.

The spectra of NIR emission is observed from the exterior of the Pyrex Dewars through a strip window in the silvering. A collection lens focuses light emitted by the sample onto the entrance of a collimating lens where a fiber optic cable is attached. The fiber connects to an Avantes NIR 512-1.7 TEC spectrometer. This spectrometer can continuously record spectra in a range from 944-1650 nm, with an exposure time of 100-500 ms, and a resolution of 5 nm. The quantum efficiency of the Avantes spectrometer is shown in Fig. 2.6c.

The Ocean Optics and Avantes Spectrometers were externally synchronized using a home-made trigger box connected to each spectrometers accessory port. The connections are illustrated in Fig. 2.7. The Ocean Optics HR2000+ was connected using the HR4-CBL-DB15 accessory cable which converts from the 3M Pak-50 connector on the spectrometer to a standard DB-15HD. The Avantes spectrometer was connected using a standard DB26HD cable. The trigger-box enclosure houses DB15HD and DB26HD breakout boards which connect the external trigger input

and ground connections for each spectrometer. It also has a BNC bulkhead for the TTL input of an external trigger, which was provided by a Tektronix CFG250. The TTL signal is sent on the inner conductor, with the outer conducted being grounded. The TTL input signal was externally switched using a physical relay actuated by an Arduino UNO development board using the LINX firmware connected via USB to a computer running Labview. Both spectrometers were externally triggered to the rising edge, and controlled via USB by their respective programs; Ocean Optics SpectraSuite and Avantes Avasoft 8. Spectra from the Ocean Optics and Andor Spectrometers were synchronized during analysis.

During the creation of our samples, luminescence from the jet of radio-frequency discharge products can be observed with all three spectrometers simultaneously in the glass Dewar. Typically the Andor Spectrometer uses the “step-and-glue" function. In this regime, the spectrometer will accumulate 100 scans, each with a 250 ms exposure time with the high resolution grating. Upon completing these scans, the grating is moved to the next portion of the spectral range, and the process is repeated until the entire desired range has been recorded. This method allows broad-range high-resolution spectra to be obtained over the range from 200-900 nm. The Avantes spectrometer generally is set to record continuously with the range of 950-1650 nm with an exposure time of 500 ms. The Ocean Optics spectrometer records continuously in the range from 200-1100 nm with an exposure time of 250 ms.

After sample accumulation, the decay of α-group emission is observed in the glass Dewar. Generally, the Avantes and Ocean-Optics spectrometers observed the decay on the same file with the same settings as the sample creation. The Andor spectrometer however, recorded a kinetic series with a 1 second exposure time on the third grating. The duration will depend on the observed sample, but a typical series length would be 150 seconds.

During the sample destruction, all three spectrometers can record simultaneously in both the Janis cryostat and the glass Dewar setups. The Andor spectrometer typically records a kinetic series of 120,000 spectra, each with exposure time of 3 ms, giving a total of 6 minutes of recording per series using the first grating in the ranges of 240-580 nm or 540-880 nm. However, studies

using a longer exposure time with the higher resolution 1st grating were performed on the γ-line emission of the nitrogen anion. The Ocean Optics and Avantes spectrometers generally record with a 250 ms integration time.

2.4 Automatic filling system

In both the combined optical and ESR spectroscopy set-ups LN_2 is used to cool the discharge tube. Initially this tube was filled manually, but this posed problems with waste, inconsistent cryogen levels, and the possibility for water to condense inside. When water from the air is allowed to condense inside, the dangerous condition of an ice plug can form, trapping evaporating nitrogen vapor inside the tube. This pressurized gas can forcibly eject the tube, destroying it as well as the discharge insert. Another issue occurs if the LN_2 is allowed to solidify. When the discharge is started, the solid nitrogen can sublimate creating a tremendous amount of vapor which can also destroy the tube. To alleviate these issues an automatic filling system was developed.

The system works by pressurizing a nitrogen Dewar with nitrogen gas. The nitrogen gas is provided from a gas line connected to an exterior tank. The gas flows from the tap through a regulator where the pressure is reduced to less than 5 PSI. Then it passes through an air hose to a 3-way normally closed solenoid valve. This 3-way normally closed solenoid valve will exhaust to the atmosphere when the valve is de-energized, and connect the inlet when energized. This allows the storage Dewar to continuously vent, keeping it at atmospheric pressure until pressure is needed to fill. Once energized, nitrogen gas will flow through the valve into the Dewar pressurizing it. The pressurized liquid nitrogen is forced from the storage Dewar through a transfer line into the quartz discharge tube. The pressure inside the Dewar was limited using an overpressure valve, which opens automatically when a set pressure is exceeded.

The solenoid valve is controlled by a circuit as seen in Fig. 2.7. There is an option to control with a Labview program which controls an output of the serial port. The control circuit takes this input and sends it to a solid-state relay which will energize the solenoid when the input is set high. When the input is low, the solenoid is de-energized. There is a fly-back diode in parallel with the solenoid to allow the current induced by Lenz's law to circulate until dissipated.

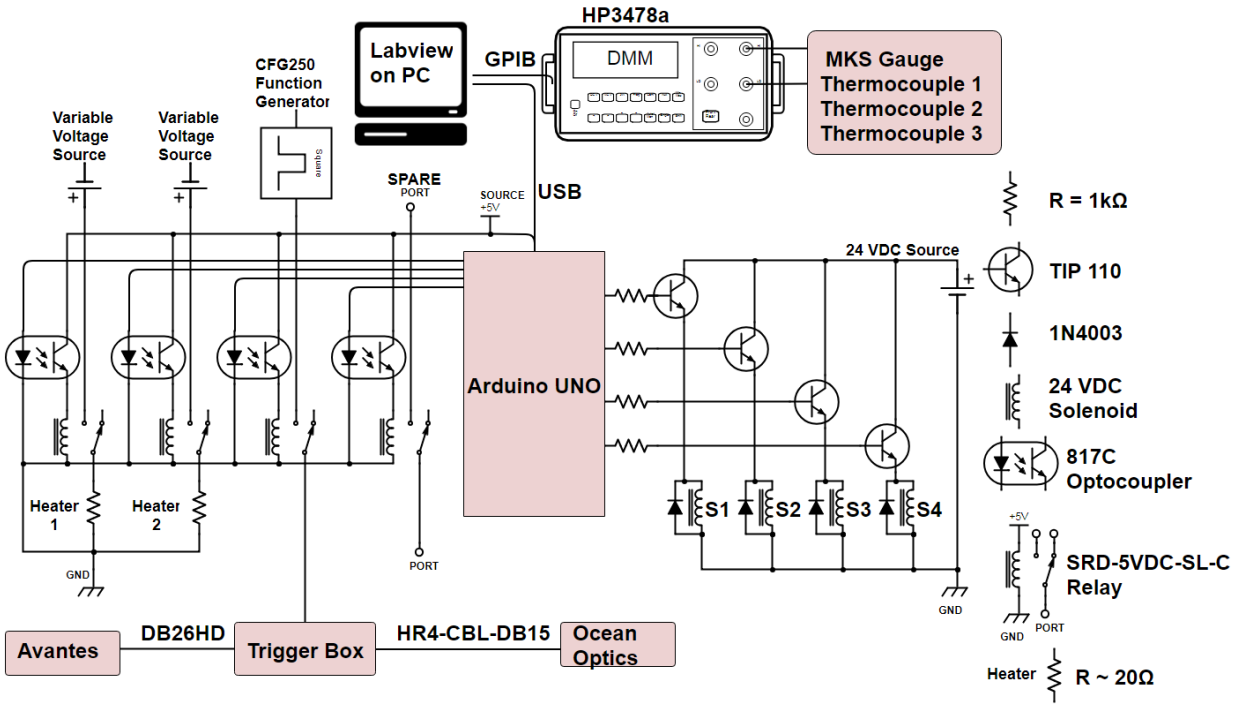

Figure 2.7: Automatic filling system circuit, optically-coupled physical relays are on the left, the Arduino development board is in the center, and solid-state relays are on the right.

The Labview program controls when the solenoid is to be energized. It does this by measuring the temperature at two locations inside of the quartz tube. One thermocouple is located at the bottom of the quartz tube, and the other is located near the top. The temperatures are measured using copper-constantan thermocouples which give approximately 25μV per degree K. Both thermocouples have one end placed in a reference bottle of LN_2 placed nearby. The voltages from the thermocouples are measured with HP 3478A digital multimeters which are connected to the controlling computer using GPIB.

The Labview program reads the values from the HP multimeters, converts them into temperatures which are relative to the reference, and decides whether or not to energize the solenoid. If the upper thermocouple becomes 10 K warmer than the bottom thermocouple, the solenoid will be energized for 60 seconds, filling the quartz tube.

The lowermost thermocouple is also used to control the PID heating system which consists of an Agilent power supply connected to an annular heater located at the bottom of the quartz

tube. The Labview program reads the temperature of the lowermost thermocouple and controls the output of the power supply to the heater to hold the temperature 1 K cooler than the reference. This prevents the cold helium vapor from freezing the LN_2 present in the bottom of the quartz discharge tube.

An Arduino UNO development board is controlled via USB by a PC running Labview using the LINX firmware developed by makerhub. This arrangement allows for 13 pins of TTL GPIO to be controlled via USB. The control box where the Arduino is mounted includes 4 solid state relays for controlling 24 VDC solenoid valves and 4 optically coupled physical relays capable of controlling AC or DC devices at voltages less than 120 VAC as shown in 2.7. Currently there are two 3-way solenoids responsible for filling the main LN_2 bath or the quartz discharge tube. One solenoid valve was used for flushing dry N_2 gas to remove any LN_2 or water from the quartz tube, and another solenoid valve was used for filling the main helium bath with clean He gas. A schematic of these connections is shown in Fig. 2.8.

In conjunction with a controlling Labview program, this control box allows the glass-Dewar optical set-up to be pre-cooled and operated autonomously for up to 8 hours. With this arrangement, the operator can fill the main bath and the two LN_2 storage Dewars the night before the experiment. Dry N_2 gas flushes the quartz tube before starting the experiment preventing the condensation of any water inside of the discharge tube. The level of LN_2 in the main nitrogen bath is maintained by the Labview and automatic filling systems. A thermocouple is installed inside the main bath. One end of this thermocouple is approximately 10 cm below the level of the foam cover, and another is at the bottom of the bath. When there is a $\sim$ 10 K temperature differential, the upper thermocouple probe is assumed to be out of LN_2 and the LN_2 bath is filled from the storage Dewar.

After the LN_2 bath is filled with LN_2, the main helium Dewar is filled with $\sim$ 775 Torr of UHP helium gas. This helium gas acts as a heat transfer gas which allows the experimental insert inside the helium Dewar to thermalize to liquid nitrogen temperature. While the apparatus is cooling, the helium Dewar is kept above atmospheric pressure. This prevents any contaminants from the air in

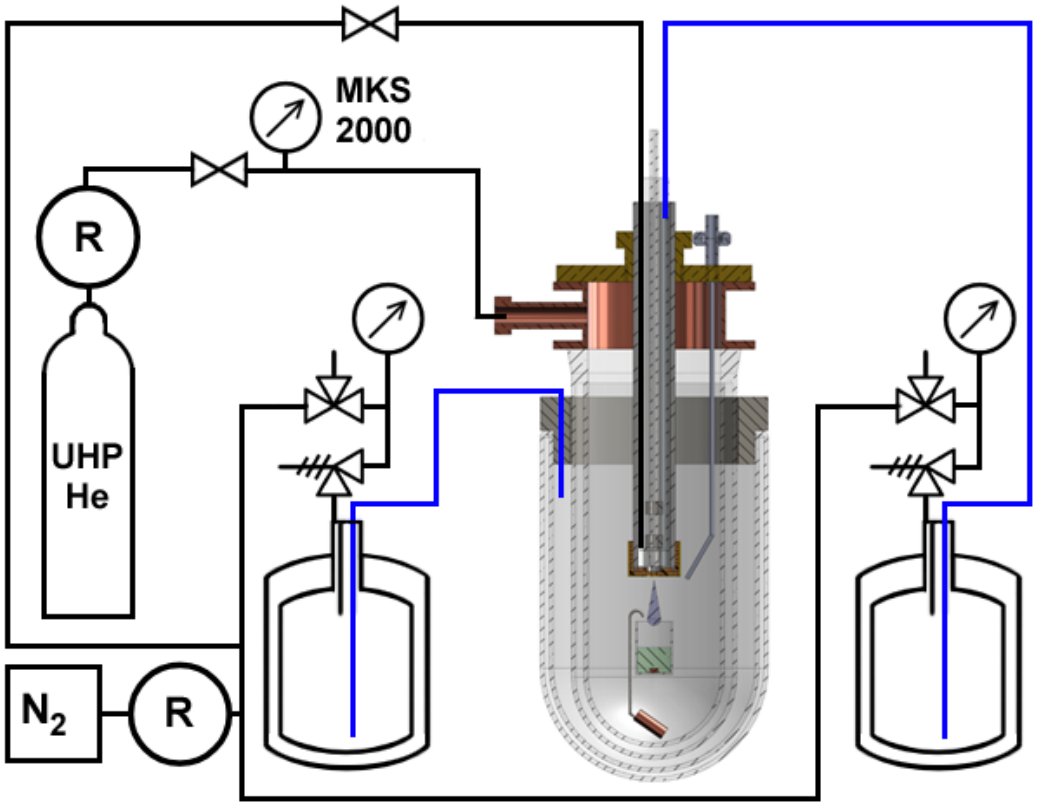

Figure 2.8: Automatic filling system diagram. Pressurized He and N_2 gas lines are shown in black and LN_2 lines are shown in blue.

the room to enter into the system. This pressure is maintained by a solenoid valve connected to a pressurized UHP He gas cylinder. This solenoid is controlled by the Labview program which reads

the pressure from a MKS-PDR 2000 capacitive manometer.

At a pre-determined time, the valve to the N_2 gas flushing will be closed, ceasing the flow of N_2 gas into the quartz discharge tube. Immediately following this, the 3-way valve will pressurize the LN_2 storage Dewar forcing LN_2 from the storage Dewar into the discharge tube. Two heaters will also be turned on, shown as heaters 1 and 2 on Fig. 2.7. These heaters are made of resistive wires connected to DC power supplies. The DC power supplies are connected to physical relays that are controlled by a TTL signal from the Arduino development board. The two heaters warm the quick connectors which seal around the outer diameter of the quartz discharge tube, and to the top of the quartz capillary where the stainless steel capillary is connected. These heaters help prevent the build-up of ice around these connections. If ice is allowed to build up around these connections, the nitrile O-ring can become frozen and brittle, causing leaks into our system.

The current configuration of this set-up requires approximately 6 hours to pre-cool the inner parts from room temperature to LN_2 temperature. The ability to automate the pre-cooling process saves the operator the wait time.

2.5 Pre-cooling

Before liquid helium can be transferred into the experimental setup, the system should be cooled as much as possible to minimize the evaporative losses. This is done by cooling the interior of the experimental apparatus to LN_2 temperatures.

2.5.1 Glass Dewar Pre-cooling

For the glass Dewar setup, pre-cooling is accomplished by filling the nitrogen bath and quartz discharge tube with LN_2. Once these volumes have been filled, the helium Dewar is flooded with ultra high purity (UHP) 5.0 helium gas from Praxair (99.999% purity). This gas is used as a transfer gas to cool the inner parts of the apparatus to LN_2 temperature. An automatic LN_2 filling system is used to maintain the level LN_2 in the discharge tube (see Section 2.4).

As the interior of the apparatus is cooled, helium gas is periodically added to keep the pressure inside greater than atmospheric pressure. This prevents contaminants from entering the system in

the event of a leak, and reduces the amount of time to cool the inner parts.

Care has to be taken to keep the nitrogen bath full to prevent the helium gas from diffusing from inside of the inner Dewar into the vacuum space. If enough helium diffuses through the Pyrex into the vacuum space the Dewar becomes "soft". A soft Dewar will have an unacceptable helium evaporation rate, and will have to be serviced. The Dewars that we had manufactured by Pope Scientific have a sealed glass nipple that can be opened by a glass blower. This port allows the vacuum space to be evacuated of any diffused helium gas.

The temperature is read using a factory calibrated Lakeshore Cryotronics GR-300-AA-0.3D Germanium thermometer connected to a Linear Research Incorporated LR-400 4-wire AC resistance bridge.

2.5.2 Metal Cryostat Pre-cooling

The Janis cryostat is pre-cooled by filling the liquid helium bath with LN_2. Once the bath is cooled to this temperature, the LN_2 is ejected by pressurizing the volume using ultra high purity (UHP) helium gas. The liquid ejected from the helium bath can then be added to the LN_2 bath. The main helium bath is pumped to a good vacuum (< 1 Torr) to ensure that all nitrogen liquid was ejected. If there is LN_2 remaining in the bottom of the bath, it will be impossible to transfer liquid helium due to the latent heat of the solidifying nitrogen.

2.6 Liquid helium transfer

Once the apparatus is cooled to LN_2 temperature, helium can be transferred from a transport Dewar into the system. This is done with a vacuum-jacketed cryogenic transfer line. The transport Dewar is placed on a lifting cart. The vent port of the transport Dewar is connected to a manifold which connects to the helium gas recovery system, and a cylinder of UHP helium gas. The main helium bath of the experimental apparatus is connected to the helium gas recovery system. The transport Dewar is lifted and the vacuum jacketed transfer line is inserted into both the transport Dewar and the experimental apparatus. Once the transfer line is inserted completely, the transport Dewar is pressurized with UHP helium gas. This forces the helium liquid from the transport Dewar

into the helium bath of the apparatus. When the desired amount of helium liquid is transferred, the cylinder of pressurized helium gas is closed, and the transport Dewar is vented to the recovery system. Once the pressure in the transport Dewar has equalized to atmospheric pressure, the Dewar is lowered and the transfer line is withdrawn.

2.7 Gas Handling System

The gas mixtures that are used to create our samples are prepared at room temperature in a gas handling system. This system consists of a manifold connecting gas storage tanks to gas mixing tanks, and a connection to an Edwards model 18 dual-stage rotary vane mechanical vacuum pump. A line connects this manifold to a Brooks 5850E mass flow controller which maintains a steady flux of 5×10^{19} atoms or molecules per second. A stainless steel capillary connects the flow controller to the cryogenic portion of the setup.

The hydrogen-nitrogen-helium gas mixtures are prepared using Linde Electronics & Specialty research grade helium gas (99.9999% purity). We also used research purity nitrogen and hydrogen gases (99.9999%) from Matheson and deuterium gas (99.6% D_2 and 0.4% HD) from Cambridge Isotope Laboratory Inc. The oxygen content in the gas mixtures ~ 1 ppm results from contamination in this helium gas. We increased the helium content of our gas mixtures to enhance the efficiency of dissociation of impurity molecules in the discharge.

2.8 Sample Creation

The main bath is disconnected from the helium recovery system and connected to the Edwards Model 80 vacuum pump. The main bath is allowed to pump down to several Torr and the fountain pump is turned on, filling the sample collection beaker with HeII.

The samples are created by passing gas mixtures through a radio frequency (RF) discharge zone and injecting them into a quartz beaker filled with HeII [24, 25].

The atomic source that produces the excited atoms and molecules is made up of a quartz tube with a concentric inner quartz capillary. The quartz discharge tube is inside of a double-walled stainless steel vacuum jacket which thermally insulates the atomic source from the cold helium

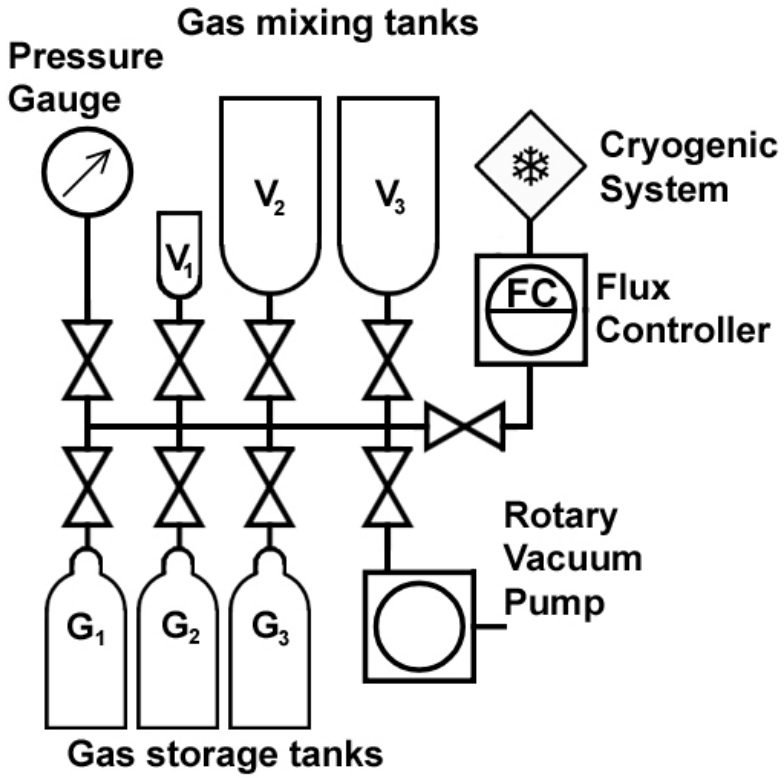

Figure 2.9: Diagram showing the scheme of the room temperature gas handling system.

vapor inside the main helium bath. At the bottom of the discharge tube there are two electrodes which surround the quartz capillary. The tube is filled with LN_2 which simultaneously cools the incoming gas mixture and the discharge electrodes. The RF discharge ($f \sim 50$ MHz, power ~ 75 W) is provided by a HP 8556B signal generator amplified by an E&I 3100L amplifier connected to electrodes surrounding the bottom of the quartz capillary. After passing through the discharge

zone, the dissociated impurity atoms and excited molecules along with helium gas exit the quartz capillary through an orifice diameter ~ 0.75 mm and enter the helium Dewar. The pressure gradient ~ 2 Torr between the discharge zone and cryostat creates a well-formed jet which is injected into a beaker of superfluid HeII placed 2.5 cm below the orifice. Impurity atoms and molecules are rapidly cooled in the gas jet by the dense helium vapor and coalesce into nanoclusters. The jet penetrates the surface of the HeII where the gas mixture containing dissociated impurity atoms and excited species forms a porous structure consisting of ensembles of nanoclusters. The helium level in the beaker is kept constant by a thermo-mechanical fountain pump which pumps HeII from the bottom of the main helium bath. During sample preparation a temperature of 1.5 K was maintained by pumping on the main bath with the Edwards model E2M80 vacuum pump. The temperature inside the beaker was measured using a factory-calibrated Lake Shore Cryotronics GR-300-AA-0.3D germanium thermometer.

2.8.1 Process of Drying the sample

After the sample has accumulated for 10 - 30 minutes, the flow of gas mixture is ceased, and the RF discharge is turned off. The fountain pump is then turned off, ceasing the flow of HeII into the sample collection beaker. Over the course of $\sim$ 15 - 20 minutes the liquid helium exits the beaker via film creep and evaporation, leaving a "dry" sample.

2.8.2 Destroying the sample

After the sample is dry, the pumping line is closed and the temperature inside of the sample beaker begins to increase from 1.2 to $\sim$15 K in $\sim$ 50 s, initiating destruction of the sample. As the temperature increases with time, the stabilized nitrogen atoms begin to diffuse through the sample, and recombine, resulting in luminescence of the sample. Thermoluminescence from the sample increases with temperature until T $\sim$ 10 K when the sample is completely destroyed in a series of bright flashes.

3. OPTICAL AND ELECTRON SPIN RESONANCE STUDIES OF DESTRUCTION OF POROUS STRUCTURES FORMED BY NITROGEN-RARE GAS NANOCLUSTERS IN BULK SUPERFLUID HELIUM*

3.1 Introduction

In this chapter we studied changes in the integrated spectra emitted during the destruction of nitrogen-neon-helium and nitrogen-argon-helium samples when the ratio of the nitrogen to rare gas atoms is changed from 1/20 to 1/1. It was found that when the ratio changed from 1/20 to 1/5, broad β-bands of NO molecules appeared in the spectra. This observation is a result of an accumulation of NO molecules [3] and an efficient recombination of N(^{2}D) with O(^{3}P) atoms as well as an energy transfer from metastable $N_2(A^3\Sigma_u)$ molecules to NO molecules at the end of the destruction. This effect is observed only for samples with local concentrations of stabilized N(^{4}S) atoms larger than 7×10^{18} cm^{-3} for nitrogen-neon-helium samples and larger than 1.3×10^{19} cm^{-3} for nitrogen-argon-helium samples. The presence of oxygen atoms in the system is a result of trace amounts of oxygen in the helium gas used for sample preparation.

3.1.1 Experimental Method

Experiments were performed in the metal optical helium cryostat. After sample preparation, ESR spectra of N(^{4}S) atoms stabilized in the samples were obtained at temperature $\sim$ 1.3 K and studies of sample thermoluminescence were also performed. Firstly, we studied thermoluminescence of the samples immersed in superfluid helium during warming up from 1.2 to 2.14 K. This annealing of the sample in HeII does not change the measured ESR signal of stabilized nitrogen atoms in the samples as is verified by registration of ESR signals of N(^{4}S) atoms before and after annealing.

Secondly, studies of thermoluminescence at higher temperatures were performed. As the tem-

*Material in this chapter was reprinted with permission from "Optical and Electron Spin Resonance Studies of Destruction of Porous Structures Formed by Nitrogen-Rare Gas Nanoclusters in Bulk Superfluid Helium", by P. T. McColgan, A. Meraki, R. E. Boltnev, D. M. Lee, and V. V. Khmelenko. Journal of Low Temperature Physics, DOI 10.1007/s10909-016-1707-5, Copyright 2017 by Springer.

perature increases, thermoluminescence of the sample was observed and recorded by the optical spectrometers and the concentrations of nitrogen atoms stabilized in the samples were monitored by the ESR spectrometer. This annealing compacts the sample so that more nitrogen atoms enter the sensitive region of the microwave cavity resulting in a growing ESR signal.

Finally, studies were performed when helium is evaporated from the sample cell. These consist of gradually warming the sample, using a PID controlled heater, as the helium vapor entered the sample cell chamber through a needle valve. This initiates faster warming of the sample in helium vapor, raising the temperature from 2.8 K to 20 K. The ESR measurements were performed at the following temperatures: T = 2.8, 3.5, 5, 10, and 20 K. During registration of ESR spectra the temperature was stabilized by a PID controller. ESR signals (normalized to temperature) continued growing as the temperature is increased to 3.5 K. During this warming up, we observed more intense thermoluminescence and the final destruction of the sample with bright flashes. The ESR measurements show a sharp decrease in the ESR signal from N atoms during the final destruction which occurs in the temperature range between 5 and 10 K for all samples studied.

3.2 Experimental Results

3.2.1 Dynamics of thermoluminescence during destruction of impurity-helium samples

An example of the dynamics of thermoluminescence during the destruction of a nitrogen-neon-helium sample is shown in Fig. 3.1. Each spectrum in Fig.3.1 is the sum of 100 spectra with integration time of 3 ms. Sample luminescence is characterized by a green glow of the nitrogen atoms (the α-group), which intensifies in time as the temperature inside the sample cell increases along with an intermittent appearance of β-group of oxygen atoms during flashes. Generally, V-K bands of molecular nitrogen are also observed before the final sample destruction when the sample explodes in a series of flashes, the spectra of which include the α- and α'-groups of N atoms, the β- and β''-groups of O atoms, and the V-K bands of nitrogen molecules, as well as the M- and β-bands of NO molecules. After the final bright flash, which occurs on the $\sim$107th second, the decay of luminescence of nitrogen atoms surviving in solid nitrogen micro-crystallites (α-group)

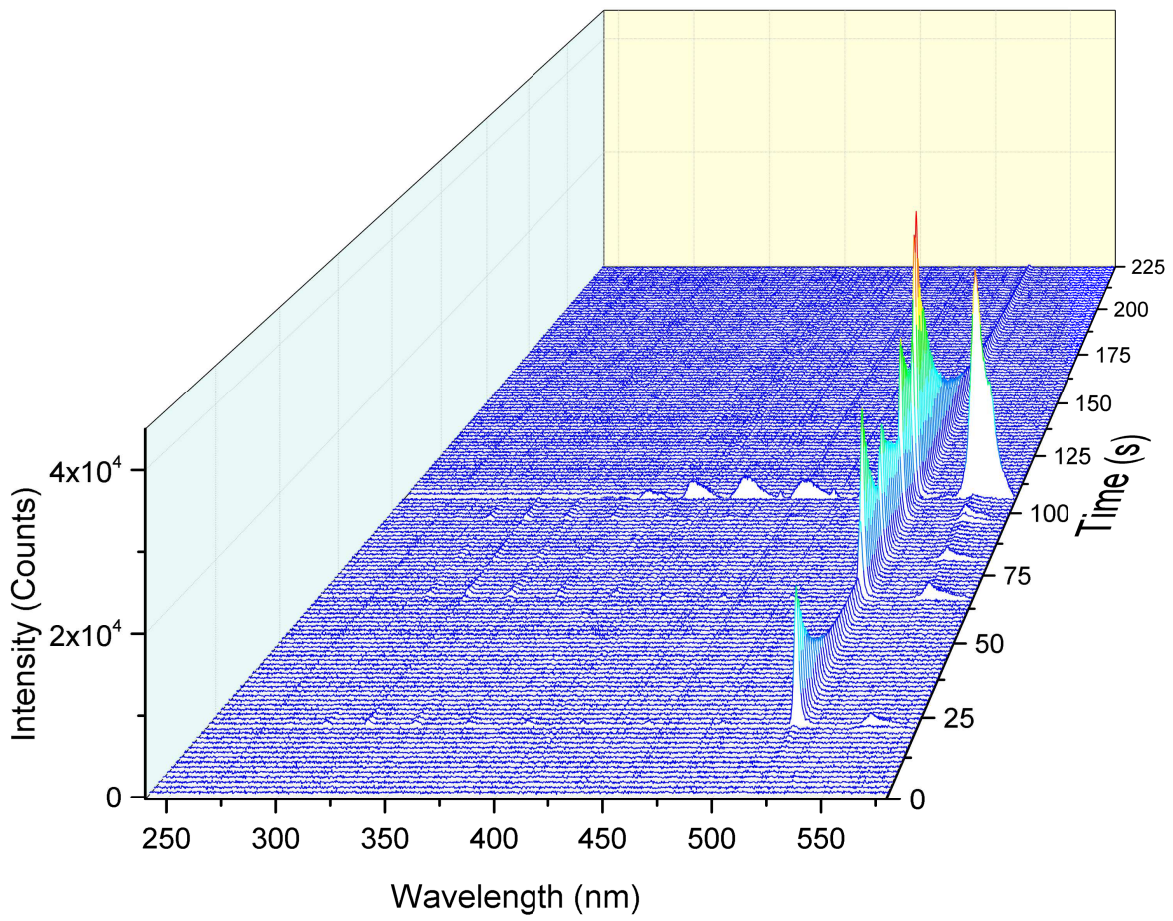

Figure 3.1: Dynamics of the thermoluminescence spectra during destruction of nitrogen-neon-helium sample recorded by the Andor Spectrometer. The sample was prepared from gas mixture $[N_2]$:[Ne]:[He] 1:1:100. The most prominent emission was from the α-group of nitrogen atoms, transition N(^{2}D$\rightarrow^4$S), and β-group of oxygen atoms, transition O(^{1}D$\rightarrow^1$S).

is observed.

Fig. 3.2 shows a comparison of the integrated spectra obtained during the destruction of samples prepared from nitrogen-argon-helium and nitrogen-neon-helium mixtures. The ratio of molecular nitrogen and rare gas for these mixtures is equal to 1/20 but the ratios of impurity (nitrogen + rare gas) to helium are different: 1:100 for the first gas mixture and 1:20 for the second. Spectra were obtained in the spectral range 240-580 nm. The identifications of the band and lines observed are also shown in Fig. 3.2. The most intense lines in both spectra are the α-group of N atoms, transition (^{2}D - ^{4}S), and the β-group of O atoms, transition (^{1}D - ^{1}S). The intensity of β-group emission

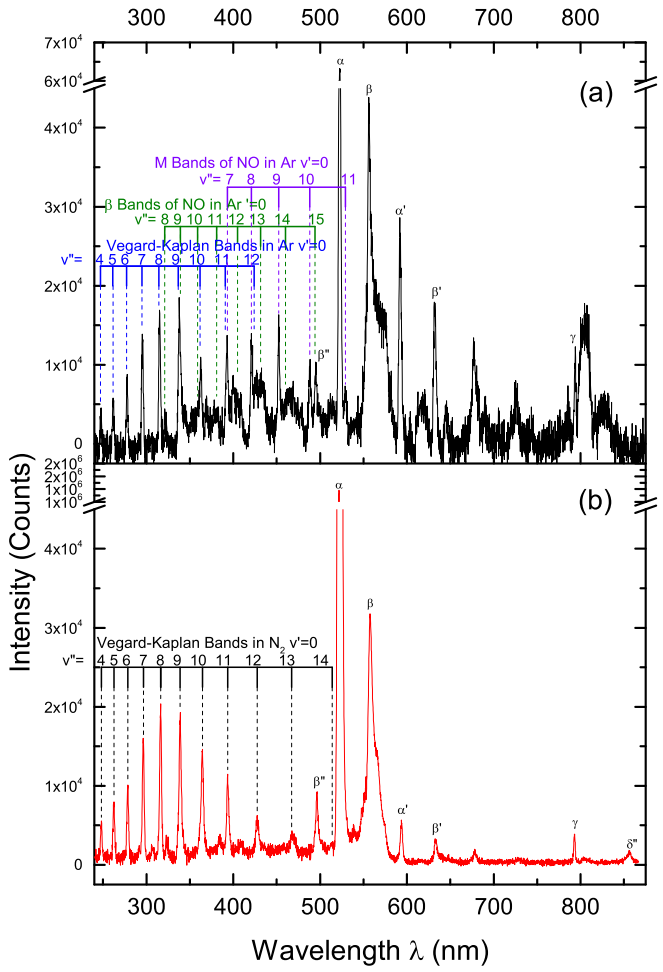

Figure 3.2: Comparison of integrated thermoluminescence spectra obtained during the destructions of samples prepared from a) nitrogen-argon-helium gas mixture [N_2]:[Ar]:[He] = 1:20:2000, and b) nitrogen-neon-helium gas mixture [N_2]:[Ne]:[He] = 1:20:400.

of O atoms is comparable to that of the α-group emission of N atoms because of the much higher ($\sim$ 10^5 times) probability of O(^{1}D - ^{1}S) transition than that of the N(^{2}D - ^{4}S) transition. Although the concentration of stabilized N atoms in the sample is more than three orders of magnitude larger than that of O atoms, the significantly greater probability of the transition of O atoms leads to an observation of emission from O atoms comparable to emission from N atoms. The V-K bands of N_2 molecules, corresponding to the ($A^3\Sigma_g^+ \rightarrow X^3\Sigma_u^+$) transitions, are also present in both spectra, but the surroundings for N_2 molecules are different: Ar atoms in nitrogen-argon-helium samples

and N_2 molecules in the nitrogen-neon-helium sample. This result shows differences in the formation of the nanoclusters for these different gas mixtures. In the case of the nitrogen-argon-helium sample the nitrogen atoms and molecules form a mixed nanocluster with argon atoms. However, in the case of nitrogen-neon-helium samples the nitrogen atoms and molecules formed the core of the nanocluster (due to their larger van der Waals interaction) which later is covered by a layer of Ne atoms. During destruction, the Ne layer is evaporated first, allowing processes of N atom recombination and the emission of excited species occur in the remaining molecular nitrogen core of the nanocluster. The α'- and δ''- groups of N atom, the β'- and β''- groups of O atom as well as the γ-line of N^- anion [5] are also present in the spectra. α'-, δ''-, β'-, and β''- are the lines, which correspond to simultaneous electronic transitions of atoms and vibrational transitions of neighboring N_2 molecules. The presence of these lines indicates that N_2 molecules are neighbors of emitting N(^{2}D) and O(^{1}D) atoms. The γ-line at 793 nm was only recently identified as the transition (^{1}D - ^{3}P) of a nitrogen anion N^- [5]. The excited states of the N^- anion are formed as a result of interaction of delocalized electrons and metastable nitrogen atoms N(^{2}D) during the process of sample destruction [5]. Additionally in the spectra of the nitrogen-argon-helium sample, weak M-bands and broad β- bands of NO molecules are present. M-bands correspond to the ($a^4\Pi$ - $X^2\Pi$) transitions and β-bands correspond to ($B^2\Pi$ - $X^2\Pi$) transitions of NO molecules.

In the following studies we will focus on investigating spectra in the spectral range 240-580 nm where a majority of the bands and lines are present and all significant changes occur.

3.2.2 Nitrogen-neon-helium samples

For preparation of nitrogen - neon - helium condensates, the gas mixture with ratios 1:20 and 1:50 of impurity to helium gas were used but the ratio between N_2 and Ne was changed from 1:20 to 1:1. After sample preparation, the ESR spectra of nitrogen atoms stabilized in nitrogen-neon-helium samples were obtained at 1.3 K. During warming up, the ESR spectra were measured at temperatures 2.8, 3.5, 5, 10 and 20 K. Fig. 3.3 shows ESR spectra of N(^{4}S) atoms stabilized in the samples formed from different nitrogen-neon-helium mixtures. Spectra were obtained for the samples which were compressed during evaporation of helium from the cell and correspond

Table 3.1: Average concentrations of nitrogen atoms determined by ESR spectroscopy in nitrogen - neon - helium samples

Gas mixture	Before sample destruction	After sample destruction
$[N_2]$:[Ne]:[He] = 1:20:400	2.6×10^{18} cm^{-3}	1.2×10^{17} cm^{-3}
$[N_2]$:[Ne]:[He] = 1:5:100	7.0×10^{18} cm^{-3}	9.6×10^{16} cm^{-3}
$[N_2]$:[Ne]:[He] = 1:1:100	1.25×10^{19} cm^{-3}	8.8×10^{16} cm^{-3}

to the maximum concentration of nitrogen atoms for each of the samples. Although maximal concentrations were obtained at different temperatures for different samples, all signals presented in Fig. 3.3 were normalized to the temperature 1.3 K. We can see that as the content of nitrogen molecules in the gas mixture is increased, the ESR signals from nitrogen atoms stabilized in the samples became larger and the line widths are increasing due to stronger dipole-dipole interactions.

The maximum average concentration of nitrogen atoms obtained from our ESR measurement for nitrogen-neon-helium samples as well as the concentration of atoms remaining in the ESR cavity after destruction of the samples are listed in Table 3.1. Increasing the ratio of N_2/Ne from 1/20 to 1/1 in the gas mixture used for sample preparation led to increasing the average concentration of stabilized nitrogen atoms in the samples from 2.6×10^{18} cm^{-3} to 1.25×10^{19} cm^{-3} before destruction. The highest concentration was achieved in the sample prepared from the gas mixture $[N_2]$:[Ne]:[He] = 1:1:100 with the largest content of N_2 molecules. The difference in residual concentrations of N atoms after sample destruction is not understood. This question needs additional studies.

Figure 3.4 shows the comparison of the integrated thermoluminescence spectra during destruction of nitrogen-neon-helium condensates. The most intense lines in the spectra are the α-group of N atoms and the β-group of O atoms. Also, V-K bands of N_2 molecules and M- and β-bands of NO molecules, as well as the β''-group of O atoms are present in the spectra. However, they are much weaker than those of the α- and β-groups. We observe that as the ratio N_2/Ne is increased, broad β-bands of NO molecules appear. In the spectra taken of the sample prepared from the gas mixture $[N_2]$:[Ne]:[He] = 1:20:400 we found the V-K molecular nitrogen bands along with the atomic

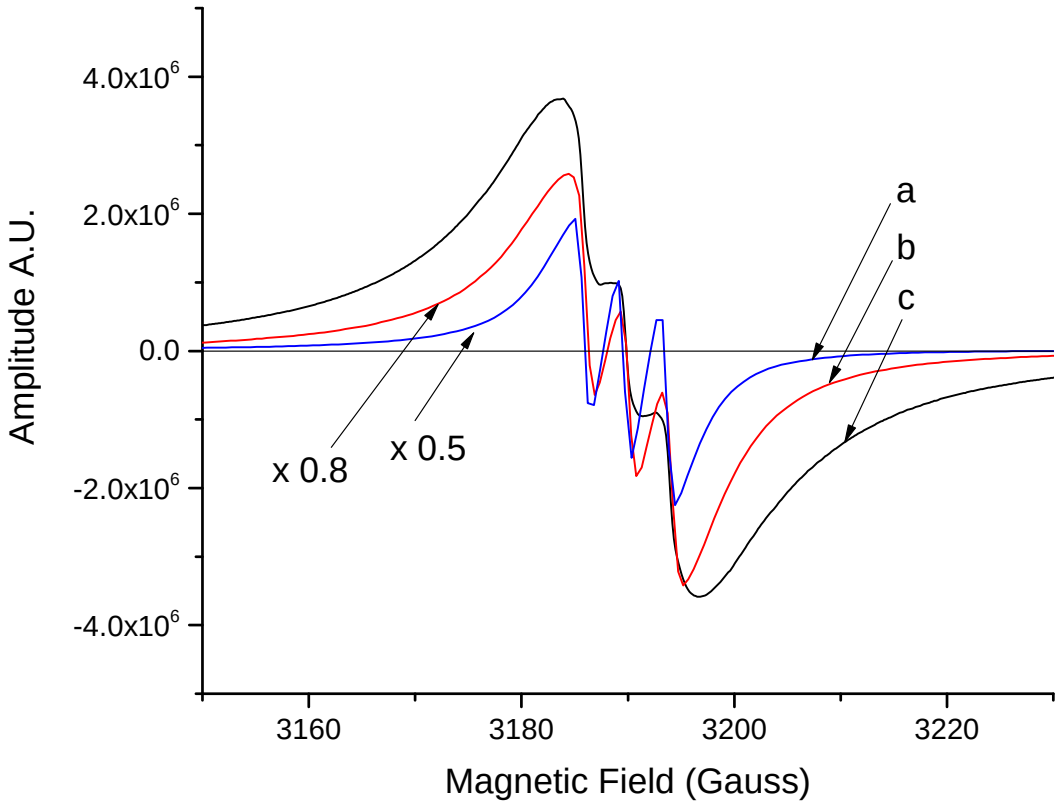

Figure 3.3: Comparison of ESR spectra of N(^{4}S) atoms stabilized in the samples prepared from the following nitrogen-neon-helium gas mixtures: a) [N_2]:[Ne]:[He] = 1:20:400, b) [N_2]:[Ne]:[He] = 1:5:100, and c) [N_2]:[Ne]:[He] = 1:1:100.

nitrogen α-group and atomic oxygen β-groups. The positions of V-K bands correspond to excited N_2 molecules surrounded by nitrogen molecules. In the spectra of the sample prepared from the [N_2]:[Ne]:[He] = 1:5:100 gas mixture, weak M-bands and intense broad β-bands of NO molecules are present as well as the V-K bands corresponding to ($A^3\Sigma_u^+$, $v' = 1 \rightarrow X^3\Sigma_u^+, v'' = 5 - 9$) transitions in N_2, which were not seen in the spectrum obtained from the previous sample (see Fig. 3.4b). The M-bands and β-bands were emitted by NO molecules surrounded by neon atoms [61], but the V-K bands were emitted by excited N_2 molecules surrounded by molecular nitrogen. The spectrum of the sample prepared from gas mixture [N_2]:[Ne]:[He] = 1:1:100 is dominated by the

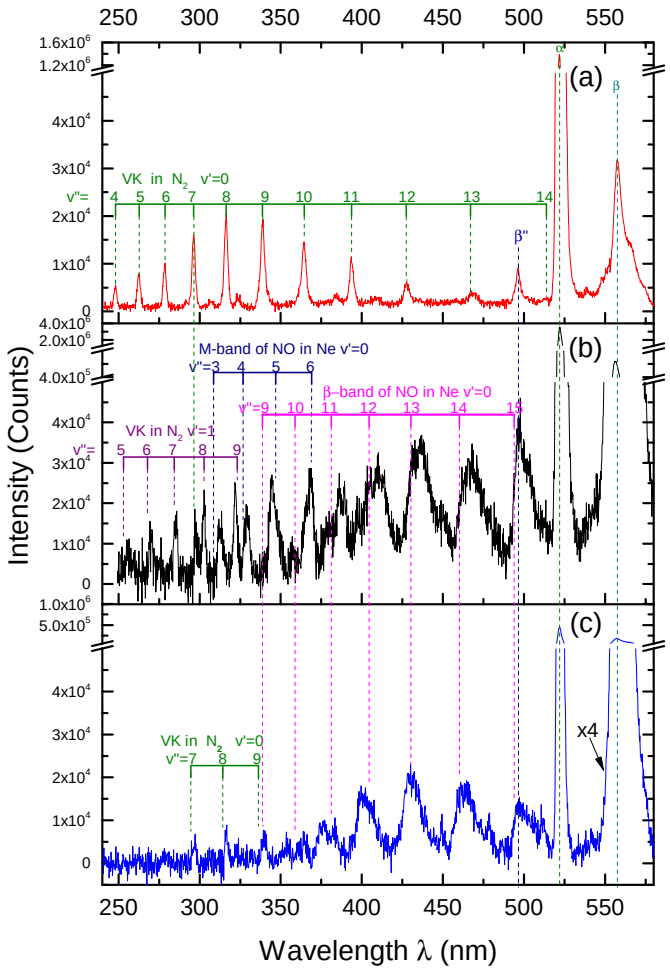

Figure 3.4: Comparison of integrated spectra obtained during the destruction of samples prepared from the following nitrogen-neon-helium gas mixtures: a) $[N_2]$:[Ne]:[He] = 1:20:400, b) $[N_2]$:[Ne]:[He] = 1:5:100, and c) $[N_2]$:[Ne]:[He] = 1:1:100.

β-bands of NO molecules in a neon environment (See Fig. 3.4c).

3.2.3 Nitrogen-argon-helium samples

For preparation of nitrogen-argon-helium samples, the gas mixtures with a 1/100 ratio of rare gas to helium gas was used, but the ratio between N_2 and Ar was changed in the range from 1/20 to 1/1. After sample preparation, the ESR spectra of nitrogen atoms stabilized in nitrogen-argon-helium samples were obtained at the temperature of 1.3K. ESR measurements were also

Table 3.2: Average concentrations of nitrogen atoms determined by ESR spectroscopy of nitrogen-argon-helium samples

Gas mixture	Before sample destruction	After sample destruction
$[N_2]$:[Ar]:[He] = 1:20:2000	1.9×10^{18} cm^{-3}	7.6×10^{15} cm^{-3}
$[N_2]$:[Ar]:[He] = 1:5:600	1.3×10^{19} cm^{-3}	8.2×10^{16} cm^{-3}
$[N_2]$:[Ar]:[He] = 1:1:200	3.6×10^{19} cm^{-3}	4.9×10^{16} cm^{-3}

performed at the different stages of warming at temperatures 2.8, 3.5, 5, 10 and 20 K. Figure 3.5 shows ESR spectra of N(^{4}S) atoms stabilized in the samples prepared from different nitrogen-argon-helium gas mixtures. The spectra correspond to the largest ESR signals for each of the samples obtained in the process of warming up. As the concentration of nitrogen in the gas mixture is increased, the average concentration of nitrogen atoms stabilized in the sample also increases. This is characterized by an increasing amplitude and appearance of broad wings of the ESR spectra. Broad wings appear due to increasing local concentration of N atoms [36] in the samples with higher nitrogen content. The maximum average concentrations of nitrogen atoms determined from ESR measurements as well as estimates of concentrations of atoms surviving after destruction are listed in Table 2. As the concentration of molecular nitrogen is increased following the N_2/Ar ratio 1:20 to 1:1, the concentration of stabilized nitrogen atoms before destruction increases from 1.9×10^{18} cm^{-3} to 3.6×10^{19} cm^{-3} as seen in Table 3.2.

Figure 3.6 shows integrated spectra taken during destruction of the samples prepared from different nitrogen-argon-helium gas mixtures. Increasing the content of N_2 molecules in the gas mixture leads to increasing thermoluminescence intensity of the samples during destruction. As in the case of nitrogen-neon-helium samples, the most intense lines during destruction of nitrogen-argon-helium samples are the β-group of O atoms and the α-group of N atoms. Also the V-K bands of N_2 molecules are present in all spectra. The positions of V-K bands in the observed integrated spectra during destruction of nitrogen-argon-helium samples are listed in Table 3.3. Also in Table 3.3, the positions of V-K bands in an N_2 matrix and in an Ar matrix observed in the previous work [62] are shown for comparison. From the comparison of the V-K band positions obtained in this

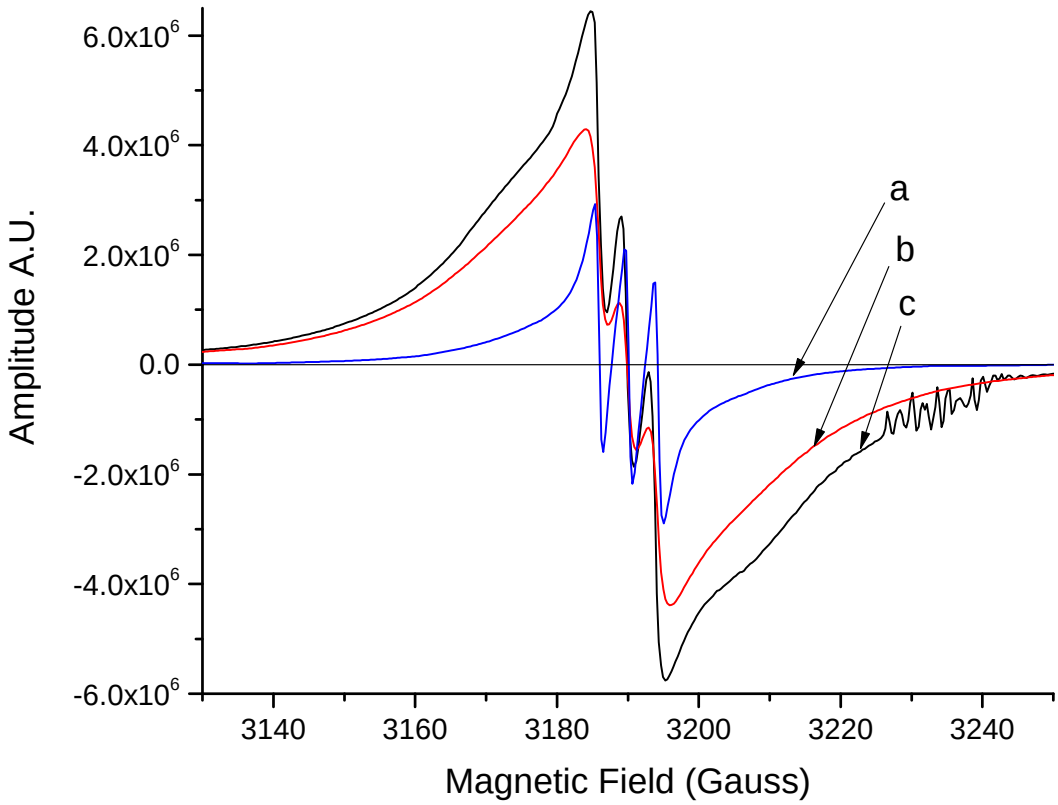

Figure 3.5: Comparison of ESR spectra of N(^{4}S) atoms stabilized in samples prepared from the following nitrogen-argon-helium gas mixtures: a) [N_2]:[Ar]:[He] = 1:20:2000, b) [N_2]:[Ar]:[He] = 1:5:600, and c) [N_2]:[Ar]:[He] = 1:1:200

work and obtained earlier in nitrogen and argon matrices, we can conclude that in the samples prepared from gas mixture with N_2/Ar ratio equal to 1/20, the V-K bands are found to be similar to those in an argon matrix, whereas, in samples prepared from gas mixtures with a greater content of nitrogen (ratios N_2/Ar equal to 1/5 and 1/1) the V-K bands are similar to those in a nitrogen matrix.

Another feature of the spectra is the presence of M-bands and β-bands of NO molecules. It should be noted that the behavior of these bands are different. The intensities of M-bands are highest for the sample prepared from the gas mixture with the ratio of N_2/Ar equal to 1/20, and are reduced upon increasing the content of N_2 in the gas mixture. In contrast, the intensities of

β-bands of NO molecules are minimal for the lowest content of N_2 molecules and increase with the increasing content of N_2 in the gas mixture. The β-bands are broad and the positions of the bands are sometimes shifted from the position of the β-bands of NO molecules for the Ar matrix.

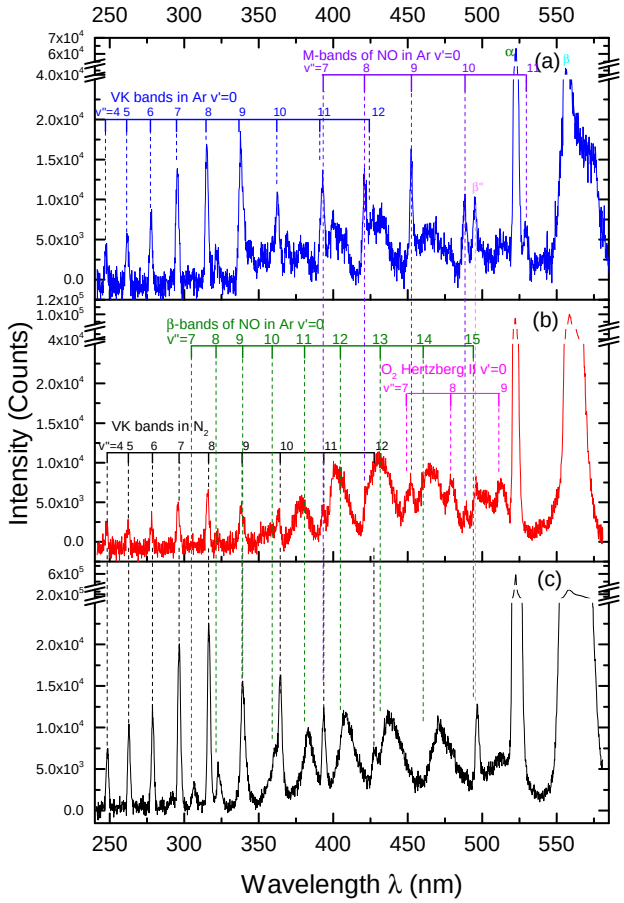

Figure 3.6: Comparison of integrated spectra obtained during the destruction of samples prepared from the following nitrogen-argon-helium gas mixtures: a) $[N_2]$:[Ar]:[He] = 1:20:2000, b) $[N_2]$:[Ar]:[He] = 1:5:600, and c) $[N_2]$:[Ar]:[He] = 1:1:200.

Table 3.3: Positions (in nm) of Vegard-Kaplan bands observed during destruction of nitrogen-argon-helium samples

ν"	1:1:200	1:5:200	1:20:1200	in N_2 [62]	in Ar [62]
ν" $= 4$	248.1	247.3	248.0	248.2	247.1
ν" $= 5$	262.5	262.3	261.5	262.6	261.4
ν" $= 6$	278.6	278.0	278.0	278.6	277.2
ν" $= 7$	296.2	296.0	295.4	296.4	294.8
ν" $= 8$	316.3	316.2	315.1	316.3	314.6
ν" $= 9$	339.0	338.4	337.8	338.8	336.8
ν" $= 10$	364.5	364.1	362.4	364.4	362.0
ν" $= 11$	393.6	392.5	392.4	393.6	390.9
ν" $= 12$	427.6		421.0	427.4	424.2
ν" $= 13$	467.5			467.0	463.1

3.2.4 Comparison of the spectra for samples formed from different nitrogen-rare gas-helium gas mixtures.

Fig. 3.7 shows integrated spectra obtained during destruction of the samples prepared from gas mixtures N_2: Rare gas (RG): He where RG = Ar, Ne, and Kr. The ratio for N_2/RG is equal to 1/5 for all gas mixtures. In all spectra, V-K bands of N_2 molecules and M-bands of NO molecules are present. Surprisingly, the emission of N_2 molecules occurs from N_2 layers, whereas the emission of NO molecules comes from the corresponding RG layers (Ar, Ne or Kr). The striking difference in the spectra of nitrogen-krypton-helium samples presented in Fig. 3.7c is the domination of the M-bands and the complete absence of β-bands of NO molecules. In contrast, in the spectra of the nitrogen-neon-helium and nitrogen-argon-helium samples, the M-bands are weak, but β bands of NO molecules are intense and broad (see Fig. 3.7a and 3.7b).

3.3 Discussion

We studied ensembles of molecular nitrogen-rare gas nanoclusters containing stabilized nitrogen atoms. Concentrations of nitrogen atoms stabilized in the samples were determined by ESR measurements. By changing the ratio of molecular nitrogen to rare gas from 1/20 to 1/1 in condensing gas mixtures, the average concentration of stabilized N atoms can be changed from 2.6×10^{18}

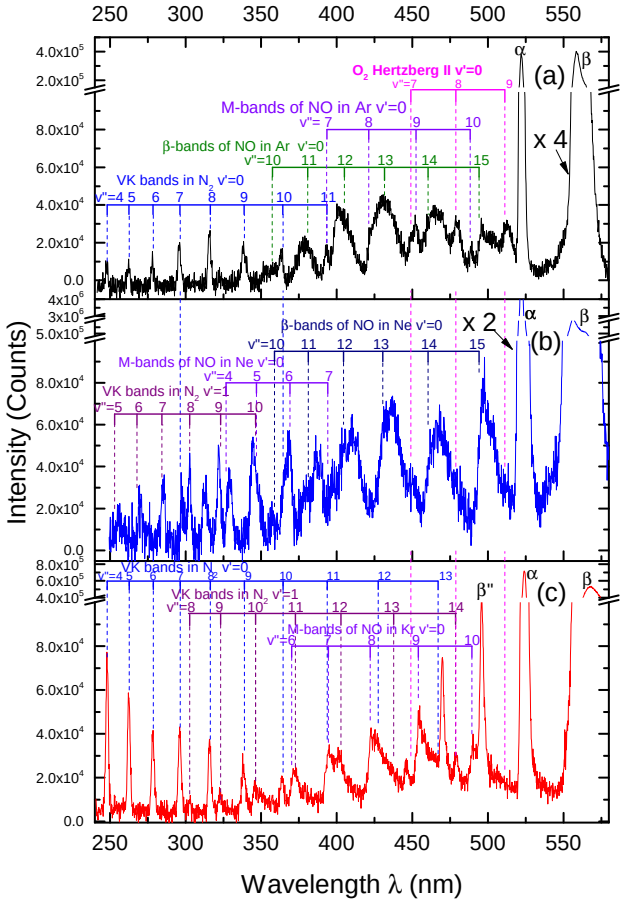

Figure 3.7: Comparison of integrated spectra obtained during the destructions of samples prepared from different nitrogen-rare gas-helium mixtures: a) $[N_2]$:[Ar]:[He] = 1:5:600, b) $[N_2]$:[Ne]:[He] = 1:5:600, and c) $[N_2]$:[Kr]:[He] = 1:5:1200.

cm^{-3} to 1.25×10^{19} cm^{-3} in nitrogen-neon-helium samples and from 1.9×10^{18} cm^{-3} to 3.6×10^{19} cm^{-3} in nitrogen-argon-helium samples. As one can see, an addition of neon or argon atoms does not substantially influence the efficiency of N atom stabilization in contrast with the results on heavier krypton atoms, which increase the stabilization efficiency of nitrogen [36] and hydrogen [38, 63] atoms in impurity-helium condensates. During the process of warming up, recombination of stabilized nitrogen atoms was initiated and the thermoluminescence spectra were studied. The mechanism of thermoluminescence is the following: Recombination of N(^{4}S) atoms produces $N_2(A^3\Sigma_u^+)$ molecules. The excitations from metastable molecules can easily be transferred through

the N_2 solid matrix and excite stabilized N(^{4}S) and O(^{3}P) atoms which result in α-group emission of N atoms and β-group emission of O atoms. Decreasing the N_2/RG ratio in the gas mixture should lead to formation of nanoclusters with increasing numbers of RG atoms. This results in reducing the efficiency of transferring excitations through the nanoclusters. This should enhance the emission of V-K band of N_2 molecules. This effect is clearly observed for nitrogen-neon-helium samples (see Fig. 3.4). For the ratio N_2/Ne = 1/20 the strongest V-K bands were observed and, as expected, the increase of N_2/Ne ratio led to better energy transfer by excitation from $N_2(A^3\Sigma_u)$ molecules to other species such as N and O atoms and NO molecules.

In the case of nitrogen-argon-helium samples increasing the N_2/Ar ratio also led to increasing the intensity of N and O atoms as well as NO molecule emissions, although the V-K bands of N_2 molecules were still present in the spectra.

The main effect observed in this work is the enhancement of the emission of β-bands of NO molecules with an increase of the N_2/RG ratio. In the experiments we observed NO β-bands corresponding to transitions from the lowest vibrational level of $B^2\Pi$ state. There are two possible processes for excitation of this state: the energy transfer from $N_2(A^3\Sigma_u)$ molecules and recombination of nitrogen atoms in the metastable ^{2}D-state with oxygen atoms in the ground ^{3}P-state. Both mechanisms become more efficient during the final stages of destruction at higher temperatures. This behavior is consistent with the previous investigations of NO molecules in solid N_2 and solid rare gases [64, 65, 66, 67].

The broad features, which we assigned to the β-group of O atoms, probably corresponds to emission of rare gas oxide excimers NeO, ArO and KrO [68, 69, 70]. More detailed studies of their emission are underway. The broad feature near 632 nm in the nitrogen-neon-helium spectra can be assigned to the spin-forbidden transition O(^{1}D-^{3}P) in a Ne matrix (see Fig. 3.2a) which was observed for the first time in [68].

3.4 Conclusions

1. In these experiments we observed optical luminescence spectra during the destruction of samples prepared from different nitrogen-rare gas-helium mixtures. The α-group of nitro-

gen, β-group and β''-group of oxygen as well as V-K bands of N_2 and M- and β-bands of NO molecules were present in every sample tested. We found that as the relative concentration of nitrogen to rare-gas increased, the prevalence of β-bands of NO molecules increased. In addition to having a greater intensity, the centers of these bands tended to shift. The NO-β-bands tended to blue-shift for samples prepared from gas mixtures containing neon with increasing molecular nitrogen concentration, and red-shift for argon containing gas mixtures with increasing molecular nitrogen concentration.

2. The thermoluminescence observed during the destruction of nitrogen-neon-helium and nitrogen-argon-helium samples substantially differs compared to that of nitrogen-krypton-helium-samples. In nitrogen-krypton-helium samples the M-bands ($a^4\Pi$, $v' = 0 \rightarrow X^2\Pi$, $v'' =$ 4-11) of NO molecules were observed, in contrast to nitrogen-neon-helium and nitrogen-argon-helium samples where the β-bands ($B^2\Pi$, $v'=0 \rightarrow X^2\Pi$, v'' = 10-15) dominate for NO molecules.

3. The average concentrations of nitrogen atoms are directly related to the content of nitrogen molecules in the gas mixture from which the impurity-helium samples are prepared.

4. LUMINESCENCE OF MOLECULAR NITROGEN NANOCLUSTERS CONTAINING STABILIZED NITROGEN, OXYGEN, HYDROGEN, AND DEUTERIUM ATOMS.*

4.1 Introduction

Chemical and physical processes occurring in solid nitrogen have stimulated a broad range of research including studies of ices present in the interstellar medium [71], as well as studies of high-energy density materials (HEDM). A promising method in the search for high energy density systems has achieved local concentrations as high as 2×10^{21} cm^{-3} of stabilized nitrogen atoms in aerogel-like ensembles of nitrogen nanoclusters submerged in superfluid helium [36, 39, 40, 41]. In this method the products of a radio-frequency (RF) discharge in nitrogen-helium gas mixtures were injected into bulk superfluid helium, resulting in the production of ensembles of molecular nitrogen nanoclusters containing very high concentrations of stabilized nitrogen atoms [24, 25]. This method also holds promise for the study of low temperature chemical reactions in ensembles of nanoclusters. For example, exchange tunneling reactions between atoms and molecules of hydrogen isotopes were studied in nanoclusters immersed in superfluid helium [1, 72, 73, 74]. Another possibility is the investigation of chemical reactions of a variety of heavier atoms and molecules during the warming of ensembles of nanoclusters containing stabilized atoms. Earlier investigations of chemical reactions during warming were performed in ensembles of molecular nitrogen and nitrogen-rare gas nanoclusters containing stabilized N and O atoms [19, 21, 23, 26]. Rapid release of stored chemical energy in the samples resulted in intense thermoluminescence. In the optical spectra of thermoluminescence the bands of N and O atoms as well as N_2, NO and O_2 molecules were observed. During investigations of the dynamics of spectra accompanying the destruction of these samples, it was found that during the process of annealing by raising the sample temperature, the emission of N, O atoms and the Vegard-Kaplan (V-K) bands of N_2 molecule were present. At the end of the destruction process bright flashes were observed, and in the spectra

*Material in this chapter was reprinted with permission from "Luminescence of Molecular Nitrogen Nanoclusters Containing Stabilized Atoms", by P. T. McColgan, A. Meraki, R. E. Boltnev, D. M. Lee, and V. V. Khmelenko. Journal of Physical Chemistry A. DOI 10.1021/acs.jpca.7b09661, Copyright 2017 by American Chemical Society.

of these flashes, intense bands of O atoms and NO and O_2 molecules were present [3]. It was found that small changes in the oxygen content in the nanoclusters drastically influenced the optical spectra obtained[3]. This earlier work provided examples of observations of chemical reactions in collections of nanoclusters containing stabilized nitrogen and oxygen atoms.

In the experiment presented in this chapter, we added hydrogen or deuterium molecules into the gas mixtures used for preparing the samples in bulk superfluid helium. Firstly, we expected that the addition of a small quantity of hydrogen isotopes would increase the efficiency of dissociation of atoms in the RF discharge zone, creating samples with the highest energy content [13]. During destruction of these samples, new nitrogen compounds such as polynitrogen molecules might be formed. The synthesis of high energy density materials is a significant problem, and a promising direction is to synthesize polymeric nitrogen. A large energetic release from polynitrogen molecule decomposition provides a strong motivation to study polynitrogen as a clean high energy density material. Such materials decompose into environmentally clean N_2, and produce enormous amounts of energy per unit mass without harmful waste [75]. Theoretical calculations have evaluated the structure and stability of numerous isomers of possible N_n molecules with n ranging from 3 to 60, but only some of the isomers are good candidates for HEDM. Neutral and ionic species N_3, N_3^+, N_3^-, N_4^+, were detected and studied in solid nitrogen films [18, 76, 77, 78, 79, 80]. A cation N_5^+ has been synthesized as a part of a compound [81, 82]. There are some detailed reviews of experimental and theoretical work on polynitrogen compounds in the literature [83, 84]. Experimental evidence was obtained for the existence of tetranitrogen (tetrazete), N_4, in the gas and solid phases [85, 86, 87, 88]. Matrix isolated tetranitrogen was obtained by condensing products of an electrical discharge on a cold window [87], or by bombarding solid nitrogen by electrons [88]. In the former case an intense broad band at λ = 360 nm was observed, which was assigned to the emission of $N_4(D_{2h})$ tetranitrogen. There are several approaches for the creating the N_4 species. The formation of N_4^+ cations followed by a neutralization reaction with electrons has been experimentally realized [85, 86, 87, 88]. However the association of two metastable $N_2(A^3\Sigma_u^+)$ molecules was suggested as an alternative mechanism for the formation of N_4 polynitrogen [6].

The conditions during our experiments are ideal for testing this suggestion. In our experiments, molecular nitrogen nanoclusters with high concentrations of stabilized N(^{4}S) atoms were formed. During destruction of the ensembles of nanoclusters, N(^{4}S) atoms recombine and create a large quantity of metastable $N_2(A\Sigma_u^+)$ molecules. Interactions of pairs of these molecules during the explosive destruction of the samples can lead to the formation of N_4 polymers which could be identified by the light emitted at λ = 360 nm [88].

Secondly, the addition of hydrogen or deuterium in the nitrogen-helium gas mixture provides the possibility of observing radicals containing H or D atoms such as the NH (ND) radicals. Eight emission systems of the NH radical have been found in the range from vacuum UV at 160 nm to near IR at $\sim$1.2 μm [10, 89]. The most intense transition is the triplet system $A^3\Pi \rightarrow X^3\Sigma^-$ with a maximum around 336 nm. This band is a chief characteristic of the NH radical [9, 13, 90, 91, 92, 93, 94, 95, 96]. The singlet systems $c^1\Pi \rightarrow a^1\Delta$ at λ = 324 nm [97, 98], $c^1\Pi \rightarrow b^1\Sigma^+$ at λ = 450 nm [99, 100], and $d^1\Sigma^+ \rightarrow b^1\Sigma^+$ at λ = 162 nm [89, 101] have been observed in gas phase spectra. The weak, forbidden transitions $a^1\Delta \rightarrow X^3\Sigma^-$ at λ = 795 nm [10, 102] and $b^1\Sigma^+ \rightarrow X^3\Sigma^-$ at λ = 471 nm [10, 103] were observed in the emission spectra of NH (ND) in noble-gas matrices. Recently, the transition between the two lowest metastable states $b^1\Sigma^+ \rightarrow a^1\Delta$ was detected at 1.17 μm in the emission spectra of matrix isolated NH [10]. In our experiments, the spectra were throughly examined in these spectral regions to observe the bands of NH (ND) radicals.

In this chapter we present studies of the dynamics of optical spectra during the destruction of ensembles of molecular nitrogen nanoclusters containing stabilized nitrogen, oxygen and also hydrogen or deuterium atoms. We found that in the spectra of the samples prepared from deuterium-nitrogen-helium gas mixtures the bands at λ = 336, 360, and 471 nm are present in addition to bands observed during destruction of nanoclusters containing only N and O atoms. The intensity of all bands in the spectra were influenced by the presence of admixtures of hydrogen isotopes. We conclude that the band at λ = 360 nm belongs to the emission of the N_4 compound, supporting the results obtained in Ref.[30]. Possible mechanisms for the formation of the N_4 compounds are discussed. The emission at λ = 336 nm was assigned to the $A^3\Pi$,$v' = 0 \rightarrow X^3\Sigma^-$,$v'' = 0$ transition

of ND radicals. The assignment of 473 nm band is still controversial. Two species, ND radicals and N^- anions [5] may be responsible for this emission.

4.2 Experimental Results

4.2.1 Influence of hydrogen on thermoluminescence spectra of ensembles of nitrogen nanoclusters

First we studied the destruction process of samples prepared from the gas mixture H_2:N_2:He 1:330:33,000. Figures 4.1 and 4.2 show the dynamics of luminescence during the destruction of samples prepared from gas mixture H_2:N_2:He = 1:330:33,000 in the wavelength range 240 to 580 nm and 540 - 880 nm, respectively. Figure 4.1a shows the dynamics of the emission of α-group of N atoms, Vegard-Kaplan (V-K) bands of N_2 molecules and β- and β''- groups of O atoms [3] which were observed from the beginning of sample thermoluminescence. The intensities of these features increase with temperature. The spectrum of emission observed during the early stage of destruction, with identification of bands is shown Fig. 4.1b. At the end of the destruction during bright flashes, the intense β-group and the band with maximum at λ = 360 nm were most intense. The dynamics of thermoluminescence at the final stage destruction are shown in Fig. 4.1c. During the time period of 60 ms the correlation between the emission of the β-group and the band with a maximum at λ = 360 nm were observed. The spectrum of the most intense flash with identification of the bands is presented in Fig 4.1d. The weak α-group of nitrogen atoms and β''-group of oxygen atoms are also present in this spectrum.

Figure 4.2a shows the dynamics of the emission of the β-group of O atoms, α'-group and δ''-group of N atoms, and the γ-line of N^- anions [5]. The intensity of all lines increased with temperature. The spectrum of the emission at the beginning of the destruction with the identification of all observed bands is shown in Fig. 4.2b. The dynamics of the thermoluminescence during the last 900 ms of sample destruction is shown in Fig. 4.2c with better time resolution. At the end of the destruction, the intense β-group of O atoms and γ-line of N^- anions, as well as weaker δ''-group of N atoms, and β'-group of O atoms were observed. The spectrum with identified bands

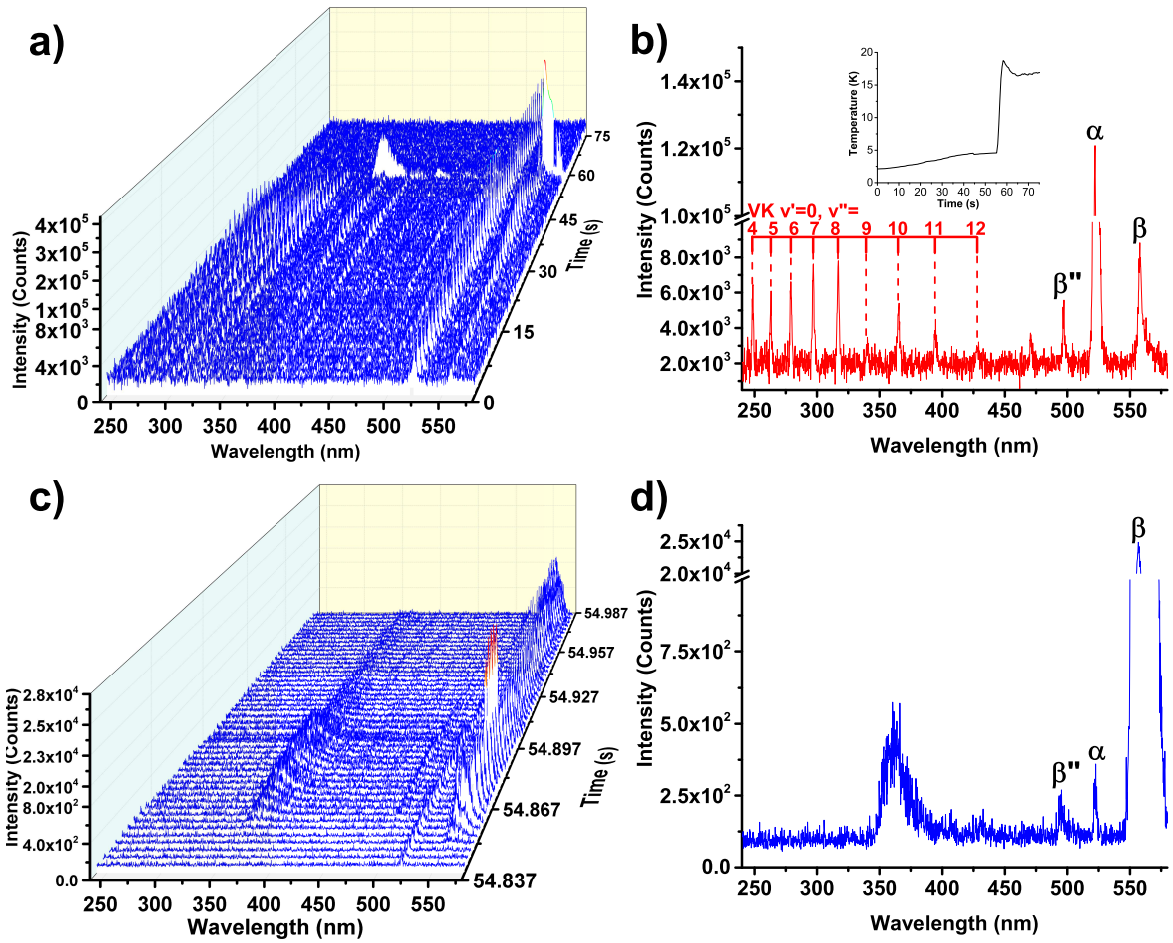

Figure 4.1: Spectra taken in the range 240-580 nm by the Andor Spectrometer during destruction of the sample prepared from gas mixture $[H_2]$:$[N_2]$:[He] 1:330:33000. a) Dynamics of luminescence spectra for the entire destruction process. Each spectrum was accumulated during a period of 1.5 s. b) Spectrum taken during destruction at t = 37.5 s with band identifications. Temperature dependence on time during sample destruction is shown in the inset. c) Dynamics of luminescence spectra during the final period of destruction (150 ms) of the sample with exposure time 3 ms. d) Spectrum taken at the end of sample destruction corresponds to t = 54.891 s with band identifications.

corresponding to largest flashes at the end of destruction is shown in Fig. 4.2d. The most striking change in the spectra compared to those obtained for nitrogen-helium samples [3, 21, 26] was the appearance of a broad band with maximum at λ = 360 nm. The position and origin of the atomic and molecular bands in the spectra presented in Figs. 4.1 and 4.2 are listed in columns 2 of Tables 4.1, 4.3, 4.4, 4.5. The presence of α', β', β'', and δ' groups of N and O atoms in the spectra

indicates that N_2 molecules are neighbors of these atoms [3, 104].

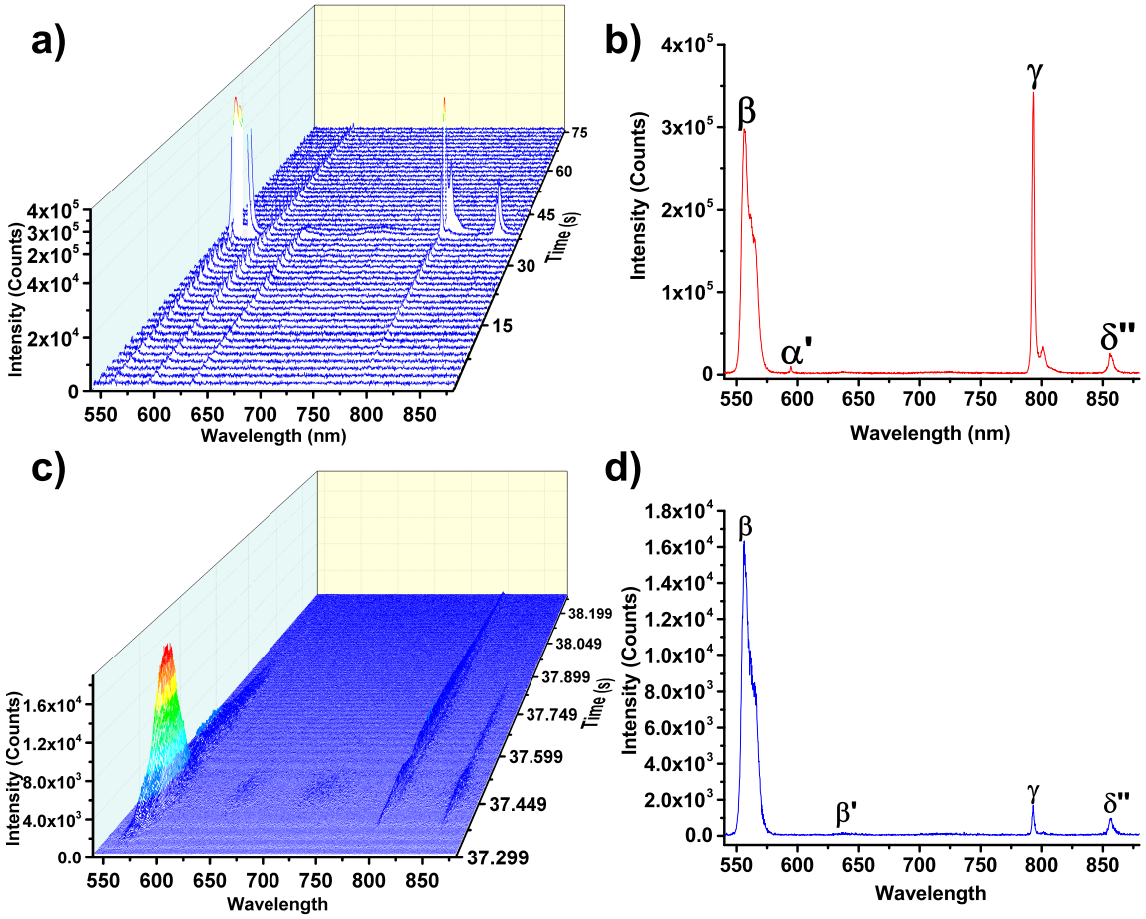

Figure 4.2: Spectra taken in the range 540-880 nm with the Andor Spectrometer during destruction of the sample prepared from gas mixture $[H_2]$:$[N_2]$:[He] = 1:330:33000 a) Dynamics of the luminescence spectra during the entire destruction process. Each spectrum has an exposure time of 1.5 s. b) Spectrum taken during destruction at t= 37.5 s with identification of all bands observed with exposure time 1.5 s. c) Dynamics of the luminescence spectra during the final period of sample destruction with exposure time 3 ms. d) Spectrum taken at the end of sample destruction at t = 37.491 s with band identifications.

As a next step, we observed the influence of the presence of molecular hydrogen in the initial gas mixtures on the appearance of the band at λ = 360 nm. Thus spectra were studied during destruction of the samples prepared from different H_2:N_2:He gas mixtures. The ratio between

Table 4.1: Positions (nm) of the Vegard-Kaplan bands $N_2(A^3\Sigma_u^+\ v' = 0 \rightarrow X^1\Sigma_g\ v'')$ observed during the destruction of samples prepared from different gas mixtures

Band v′,v″	in N_2 Matrix [105]	$[H_2]$:$[N_2]$:[He] 1:330:33,000	$[D_2]$:$[N_2]$:[He] 1:2,000:100,000	$[D_2]$:$[N_2]$:[Ar]:[He] 1:500:4,500:225,000	$[D_2]$:$[N_2]$:[Ne]:[He] 1:500:5,000:100,000
0,4	248.4	248.6	250.08	248.2	248.9
0,5	263.0	263.2	263.22	263	263.7
0,6	278.9	279.1	278.69	278.6	279.5
0,7	296.8	296.8	296.49	296.4	297.1
0,8	316.8	317.2	318.12	315.9	317.2
0,9	339.3	-	337.9	338.3	340.1
0,10	365.2	365.5	365.65	-	365.5
0,11	393.5	394.4	394.3	394.9	394.6
0,12	427.1	-	429.99	-	-

H_2/N_2 in these mixtures was changed from 1/200 to 1/500.

Table 4.2: Integrals of the intensities of bands (arb. units) observed during the entire destruction process (Int) and during the largest flash (Flash) for samples prepared from different hydrogen-nitrogen-helium gas mixtures

Band	$[H_2]$:$[N_2]$:[He] 1:200:20,000		[H]:$[N_2]$:[He] 1:330:33,000		[H]:$[N_2]$:[He] 1:500:50,000	
	Int	Flash	Int	Flash	Int	Flash
α	1.92×10^5	1.73×10^3	1.74×10^6	2.06×10^4	9.02×10^5	6.62×10^3
β	1.41×10^5	2.10×10^4	9.03×10^5	3.44×10^5	4.73×10^5	3.01×10^4
γ	1.13×10^5	4.01×10^3	4.38×10^5	7.53×10^4	2.82×10^5	5.42×10^3
$\lambda = 360$ nm	-	5.49×10^4	-	1.75×10^5	-	4.06×10^4
V-K $v' = 0, v'' = 7$	3.39×10^5	9.76×10^3	1.62×10^6	6.00×10^3	1.00×10^6	1.22×10^4

Figure 4.3 shows the integrated spectra of the emission observed with the Ocean Optics spectrometer during the destruction of samples prepared from different H_2:N_2:He gas mixtures. Lines and bands observed include the α-group and α'-group of N atoms, the γ-line of N^- anions, the Vegard-Kaplan (V-K) bands of N_2 molecules ($v' = 0$, $v'' = 2$-12), and the β-group of O atoms.

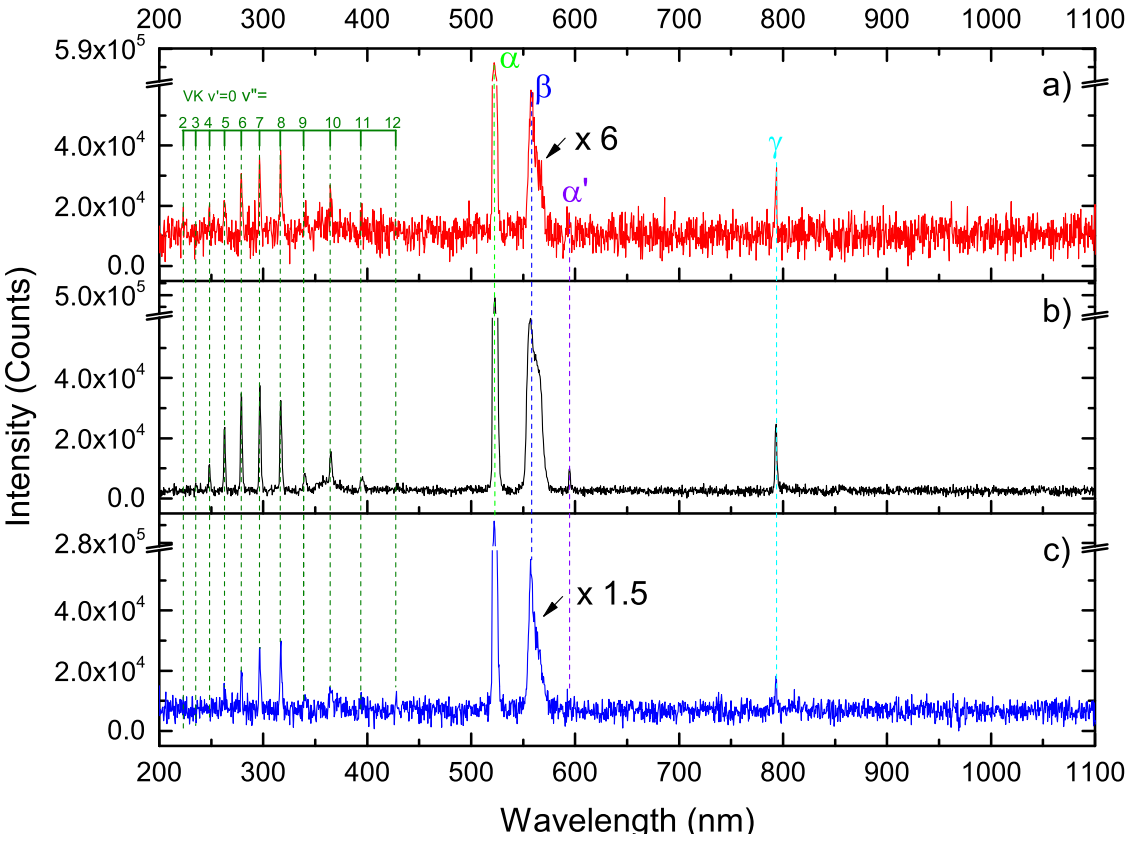

Figure 4.3: Integrated spectra observed with the Ocean Optics spectrometer during the entire destruction process for samples created from different H_2:N_2:He gas mixtures: a) [H_2]:[N_2]:[He] = 1:200:20,000. b) [H_2]:[N_2]:[He] = 1:330:33,000. c) [H_2]:[N_2]:[He] = 1:500:50,000.

This figure demonstrates the influence of the concentration of H_2 in the sample gas mixture on the intensity of the observed lines in the spectra. The integrals of intensities of bands shown in Figs. 4.3 and 4.4 are listed in Table 4.2. The maximum intensities of the lines were observed for the gas mixture with the ratio H_2/N_2 = 1/330 as shown in Table 4.2. The intensities of bands from the sample prepared from gas mixture with H_2/N_2 ratio equal to 1/200 are 4-9 times smaller and the intensities of the bands of the sample prepared from gas mixture with ratio H_2/N_2 = 1/500 were twice smaller.

Figure 4.4 shows spectra of the emission of the largest flashes observed with the Ocean Optics spectrometer accompanying the destruction of samples prepared from gas mixtures with different H_2:N_2:He ratios. Lines and bands observed include the α- , δ-, and δ'' - groups of N atoms, the

Table 4.3: Positions of lines of N and O atoms, and nitrogen anion observed during the destruction of samples prepared from different gas mixtures.

	in N_2 Matrix[14]	$[H_2]$:$[N_2]$:[He] 1:300:30,000	$[D_2]$:$[N_2]$:[He] 1:2,000:100,000	$[D_2]$:$[N_2]$:[Ar]:[He] 1:500:4,500:225,000	$[D_2]$:$[N_2]$:[Ne]:[He] 1:500:5,000:100,000
α	522.8	522	522.3	523.7	523.3
α'	594.4	594.5	-	592.1	594.5
δ''	857	-	-	-	857.2
β	554.9	557.8	557.4	559.1	557.6
β'	636.7	633.2	-	632.7	-
β''	494	-	-	-	-
γ	791	793	794.0	794.2	793.8

Table 4.4: Positions of "new" lines emitted during the destruction of samples prepared from different gas mixtures with the addition of hydrogen and deuterium molecules.

in N_2 Matrix	$[H_2]$:$[N_2]$:[He] 1:330:33,000	$[D_2]$:$[N_2]$:[He] 1:2,000:100,000	$[D_2]$:$[N_2]$:[Ar]:[He] 1:500:4,500:225,000	$[D_2]$:$[N_2]$:[Ne]:[He] 1:500:5,000:100,000
336 (ND)[9]	-	337.8	336.6	337.7
471 (ND)[9]	-	472.9	473.9	472.4
360 (N_4^+)[88]	361.9	363.3	361.5	365.1

γ-line of N^- anions[5], the Vegard-Kaplan (V-K) bands of N_2 molecules, the β-group of O atoms, and the M-bands of the NO molecule. It is also interesting to note that for all samples made from gas mixtures with small admixtures of molecular hydrogen, the broad feature at λ = 360 nm was clearly observed only in the spectra of the largest flashes. This figure demonstrates the same tendency between the concentration of H_2 in the gas mixture used for sample preparation and the intensity of the lines in the emitted spectra as was demonstrated in Fig. 4.3. The most intense luminescence was observed for the sample prepared from the gas mixture with ratio H_2/N_2 $\sim$1/330 as shown in Table 4.2 and Fig. 4.4. In contrast to the integrated spectra, in the spectra of the largest flashes, V-K bands are substantially suppressed, but a new rather intense band with maximum at λ = 360 nm appears. The intensity of the band at λ = 360 nm for gas mixture with H_2/N_2 ratio 1/330

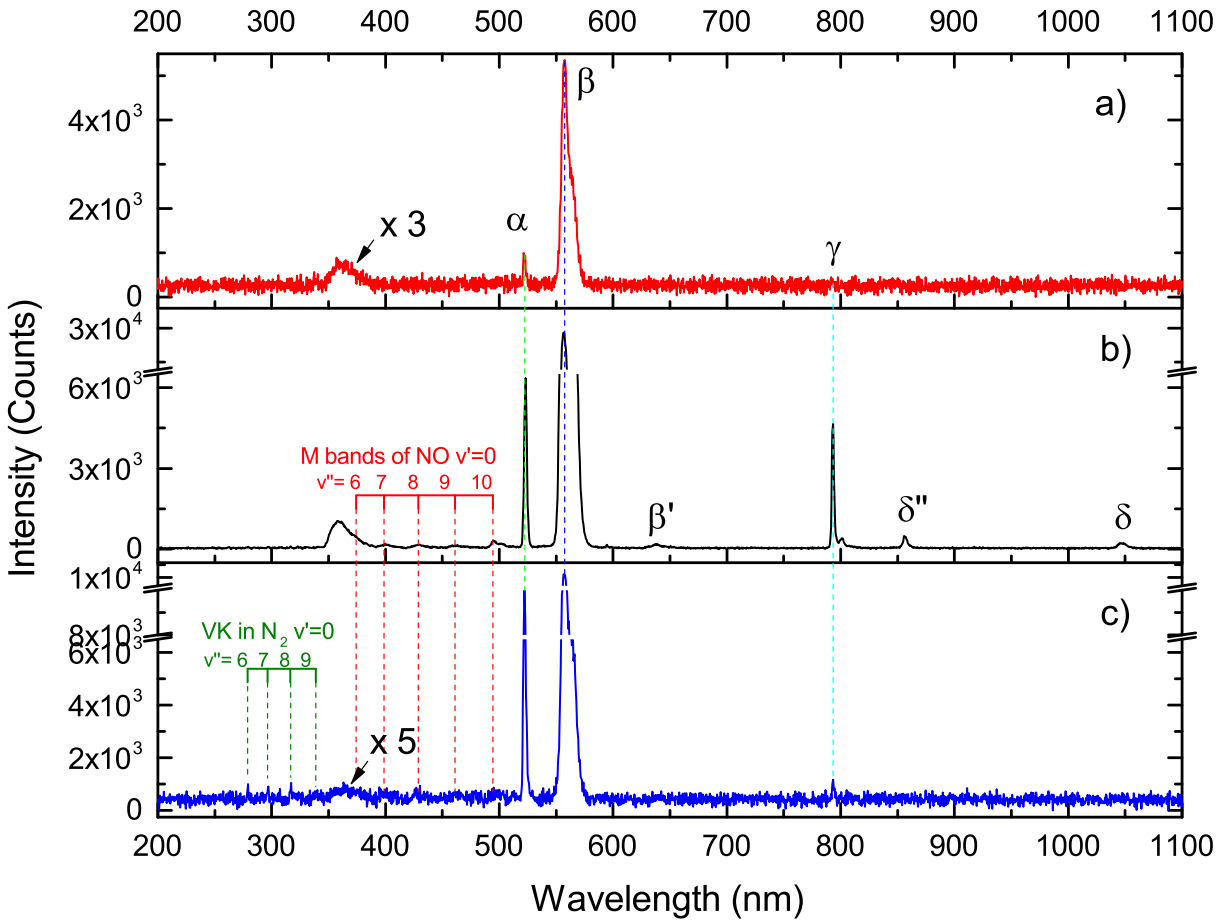

Figure 4.4: Spectra of the largest flashes during the destruction of samples formed by different hydrogen-nitrogen-helium gas mixtures: a) $[H_2]$:$[N_2]$:[He] = 1:200:20,000 b) $[H_2]$:$[N_2]$:[He] = 1:330:33,000 c) $[H_2]$:$[N_2]$:[He] = 1:500:50,000. Spectra were taken with the Ocean Optics spectrometer with exposure time 500 ms.

was three times greater than for the gas mixture with H_2/N_2 ratio 1/200 and four times greater than for gas mixture with H_2/N_2 ratio 1/500.

4.2.2 Influence of deuterium on thermoluminescence spectra of ensembles of nitrogen nanoclusters

To understand the origin of the band at λ = 360 nm we performed experiments to study the influence of the addition of D_2 molecules to N_2-He gas mixtures used for sample preparation on the spectra obtained during sample destruction. The isotope shift effect can help in the identification

of bands corresponding to species containing hydrogen isotopes.

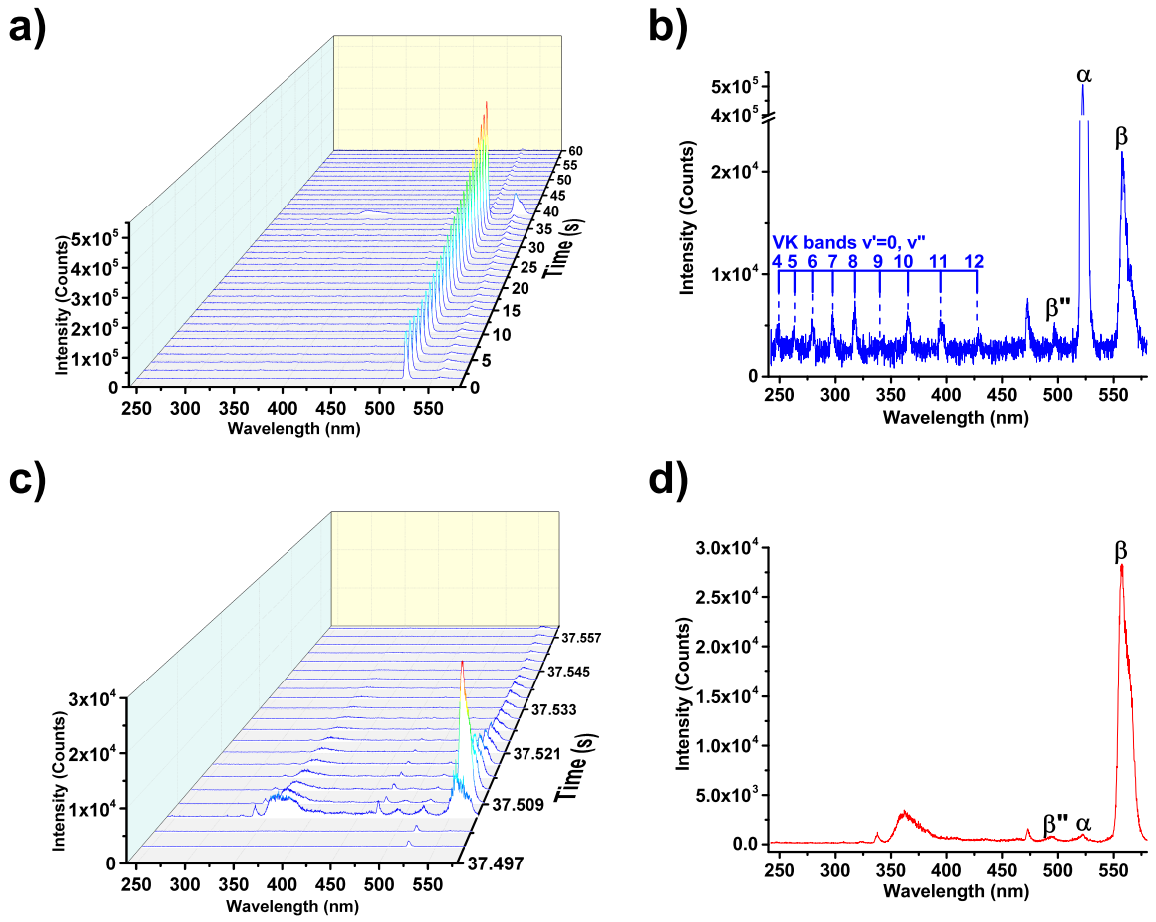

Figure 4.5: Spectra taken in the range 240-580 nm with the Andor Spectrometer. Spectra were observed during the destruction of the sample prepared from gas mixture $[D_2]$:$[N_2]$:[He] = 1:2,000:100,000: a) Luminescence dynamics for the entire destruction process. Each spectrum has an exposure time 1.5 s. b) Spectrum taken at t = 34.5 s with 1.5 s exposure time with band identifications. c) Dynamics during the final stage (60 ms) of the sample destruction. Each spectrum has exposure time 3 ms d) Spectrum taken at the end of destruction at t = 37.509 s with 3 ms exposure time with band identifications.

Figure 4.5a shows the dynamics of the emission of the α-group of N atoms, the Vegard-Kaplan (V-K) bands of N_2 molecules and the β-group of O which were observed in the thermoluminescence of the sample prepared from the gas mixture D_2:N_2:He = 1:2,000:100,000. The intensities

of the bands mentioned above increase with temperature. The spectrum of the emission is shown in Fig. 4.5b near the end of destruction where the emission from the V-K band is most intense. This spectrum also includes the strong α-group of N atoms, and the β-group of O atoms as well as other weaker lines including the β''-group from oxygen, and the line at λ = 473 nm. The dynamics of thermoluminescence at the end of destruction is shown in Fig. 4.5c. During the time period of 60 ms, the intensity of emission of the β-group correlates with the intensity of the band at λ = 360 nm. The spectrum of this emission is shown in Fig 4.5d. The strong β-group of O atoms and the band at λ = 360 nm along with the weaker α-group of N atoms, and bands at 337 nm and 473 nm are also present in this spectrum. The positions and origins of atomic and molecular bands in the spectra presented in Fig. 4.5 are listed in column 3 in Tables 4.1-4.5. It is interesting to note that the appearance of the bands at λ = 336 nm and at λ = 473 nm in the samples prepared with the addition of D_2 molecules is in contrast with the case of hydrogen containing samples, where these bands have not been observed.

Table 4.5: Positions (nm) of NO-M bands ($a^4\Pi$, $v' = 0 \rightarrow X^2\Pi$, v'') and NO β-bands ($B^2\Pi$, $v' = 0 \rightarrow X^2\Pi$, v'') observed during the destruction of samples prepared from different gas mixtures

v',v''	N_2 Matrix[67]	[H]:[$^{14}N_2$]:[He] 1:300:30,000	[D_2]:[N_2]:[He] 1:2,000:100,000	[D_2]:[N_2]:[Ar]:[He] 1:500:4,500:225,000	[D_2]:[N_2]:[Ne]:[He] 1:500:5,000:100,000
NO-M bands					
0,7	399.41	394.8	398.8	401.6	395.2
0,8	428.71	429.0	429.4	430.9	429.9
0,9	462.00	464.1	463.6	-	-
0,10	494.4[3]	496.8	494.2	494.6	496.6
NO-β bands					
0,8	322.40	323.5	-	-	324.4
0,9	340.40	340.7	-	-	339.4
0,10	359.30	-	-	-	-
0,11	383.75[3]	384.0	-	-	384.0

We also studied the influence of the concentration of D_2 molecules in the N_2:He gas mixture

used for sample preparation on the intensity of the bands in the spectra obtained during the destruction of the samples. Figure 4.6 shows the integrated spectra of the emission observed with the Ocean Optics spectrometer during the destruction of different D_2:N_2:He samples. Lines and bands observed include the α- and α'- groups of N atoms, the γ-line of N^- anions, the V-K bands of N_2 molecules (v′ = 0, v″ = 2-13), and the β-group of O atoms. This graph demonstrates that there exists an optimal concentration of D_2 in the gas mixture used for sample preparation that produces a maximum intensity for all lines of luminescence during sample destruction. This optimum concentration of D_2 corresponds to the spectra shown in Fig. 4.6b. The integrals of intensities of the bands shown in Figs. 4.6 and 4.7 are listed in Table 4.6.

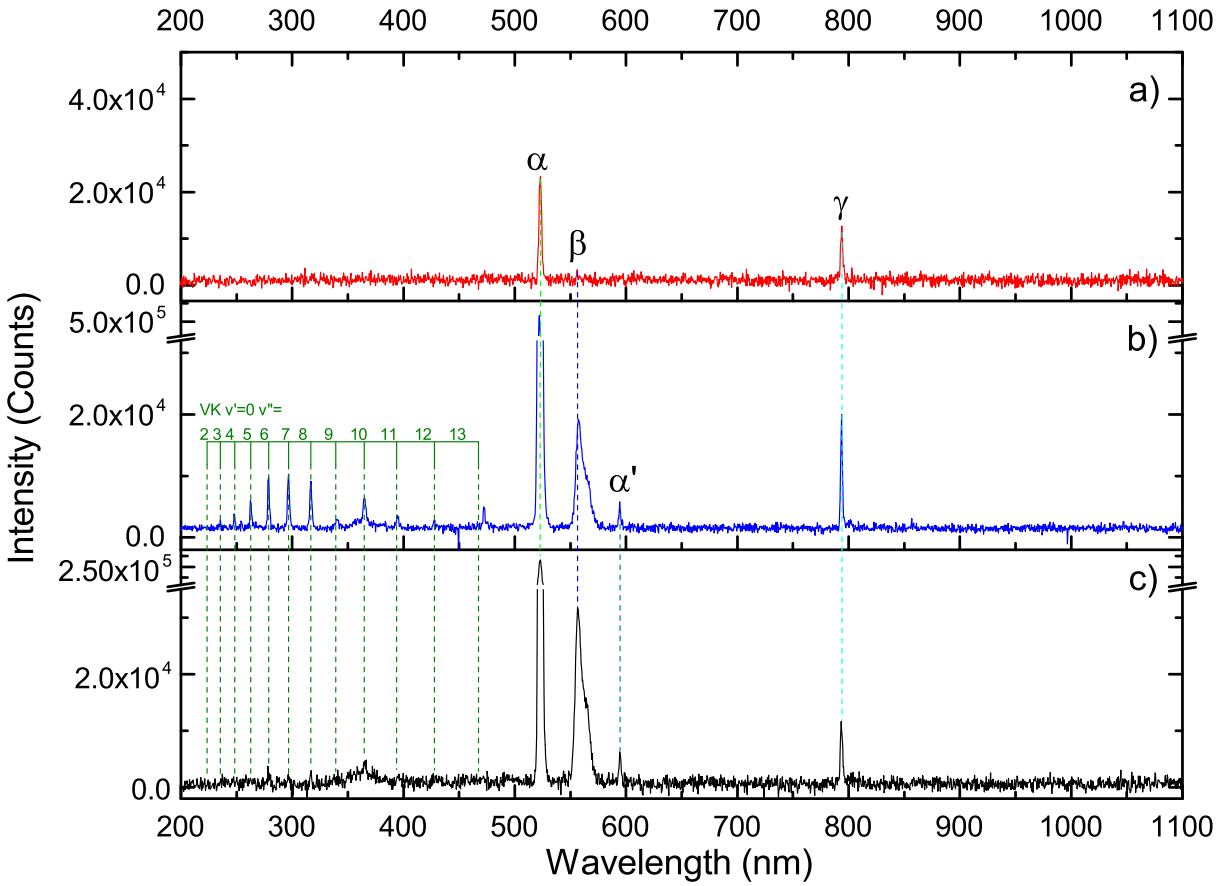

Figure 4.6: Integrated spectra taken with the Ocean Optics spectrometer during the destruction of samples created from different deuterium-nitrogen-helium gas mixtures: a) [D_2]:[N_2]:[He] = 1:750:50,000, b) [D_2]:[N_2]:[He] = 1:2,000:100,000, and c) [D_2]:[N_2]:[He] = 1:10,000:500,000

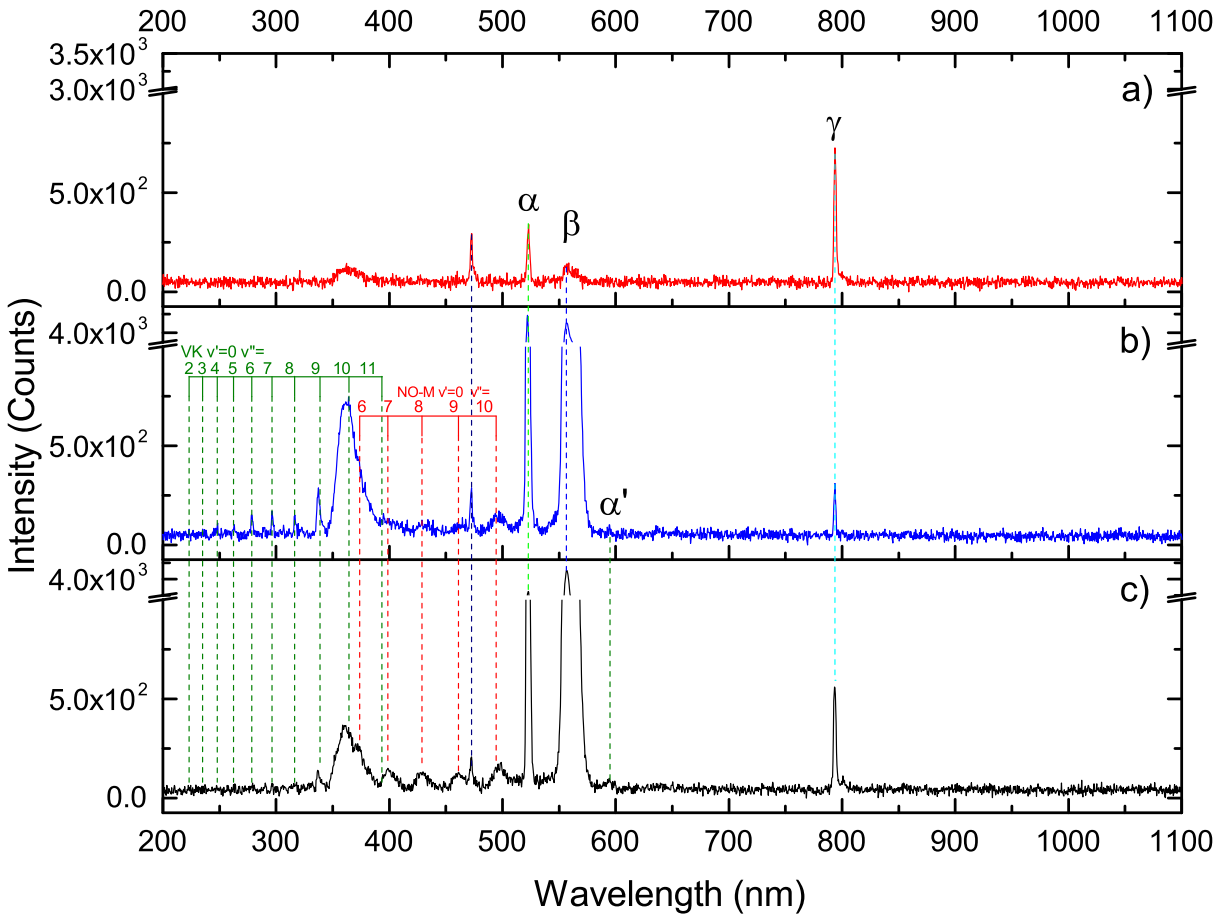

Figure 4.7: Spectra taken with the Ocean Optics spectrometer of the largest flashes during the destruction of samples created from different deuterium-nitrogen-helium gas mixtures: a) $[D_2]$:$[N_2]$:[He] = 1:750:50,000, b) $[D_2]$:$[N_2]$:[He] = 1:2,000:100,000, and c) $[D_2]$:$[N_2]$:[He] = 1:10,000:500,000.

Figure 4.7 shows spectra of the emission observed with the Ocean Optics spectrometer for the largest flashes during destruction of samples prepared from different D_2:N_2:He gas mixtures. Lines and bands observed include the broad band at λ = 360 nm, the α-group of N atoms, the γ-line of N^- anions, the weak Vegard-Kaplan (V-K) bands of N_2 molecules ($v' = 0$, $v'' = 2$-11), the strong β-group of O atoms, and the M-bands of NO molecules ($v' = 0$, $v'' = 6$-10). This graph demonstrates the similar relation between the concentration of D_2 in the gas mixture used for sample preparation and the intensity of the luminescence observed during sample destruction as shown in Fig. 4.6. The optimum concentration of D_2 for observation of the most intense bands corresponds to the

Table 4.6: Integrals of the intensities of bands (arb. units) observed during the entire destruction process (Int) and during the largest flash (Flash) for samples prepared from different deuterium-nitrogen-helium gas mixtures

Band	$[D_2]$:$[N_2]$:[He] 1:750:50,000		$[D_2]$:$[N_2]$:[He] 1:2000:100,000		$[D_2]$:$[N_2]$:[He] 1:10,000:500,000	
	Int	Flash	Int	Flash	Int	Flash
α	8.47×10^4	1.41×10^3	1.58×10^6	1.76×10^4	1.16×10^6	1.19×10^4
β	4.12×10^4	2.58×10^3	2.41×10^5	5.81×10^4	3.58×10^5	5.05×10^4
γ	2.24×10^5	1.24×10^4	2.86×10^5	5.07×10^3	2.01×10^5	1.11×10^4
$\lambda = 360$ nm	-	2.58×10^4	-	1.25×10^5	-	6.77×10^4
V-K $v' = 0$, $v'' = 7$	1.23×10^5	5.13×10^3	5.47×10^5	9.48×10^3	1.15×10^5	4.86×10^3

$[D_2]$:$[N_2]$:[He] = 1:2,000:100,000 gas mixture as can be seen from Table 4.6. The spectrum of the sample created from this gas mixture is shown in Fig. 4.7b. It is also interesting to note that in all spectra of largest flashes of the samples prepared from D_2:N_2:He gas mixtures, the intense broad feature at λ = 360 nm was observed.

4.2.3 Destruction of samples prepared from Argon and Neon containing mixtures

To observe possible matrix effects on the positions of the atomic and molecular bands, we also studied samples prepared from deuterium-nitrogen-helium gas mixtures with the addition of rare gases Ne and Ar.

Figure 4.8a shows the dynamics of the emission of the sample prepared from gas mixture D_2:N_2:Ar:He = 1:500:4,500:225,000. The α-group of N atoms, the V-K bands of N_2 molecules and the β-group of O atoms were observed from the beginning of sample thermoluminescence. The intensities of these features increase with temperature. The spectrum of the sample emission with identification of bands is shown in Fig. 4.8b. The spectrum was observed near the end of destruction where the emission from the V-K band is most intense. This spectrum also includes the strong α-group of N atoms, the β-group of O atoms, and in addition other weaker lines at λ = 473 and the β''-group of oxygen. The dynamics of thermoluminescence during the brightest flashes is shown in Fig. 4.8 c. During the time period of 60 ms the emission of α-group, the β'-

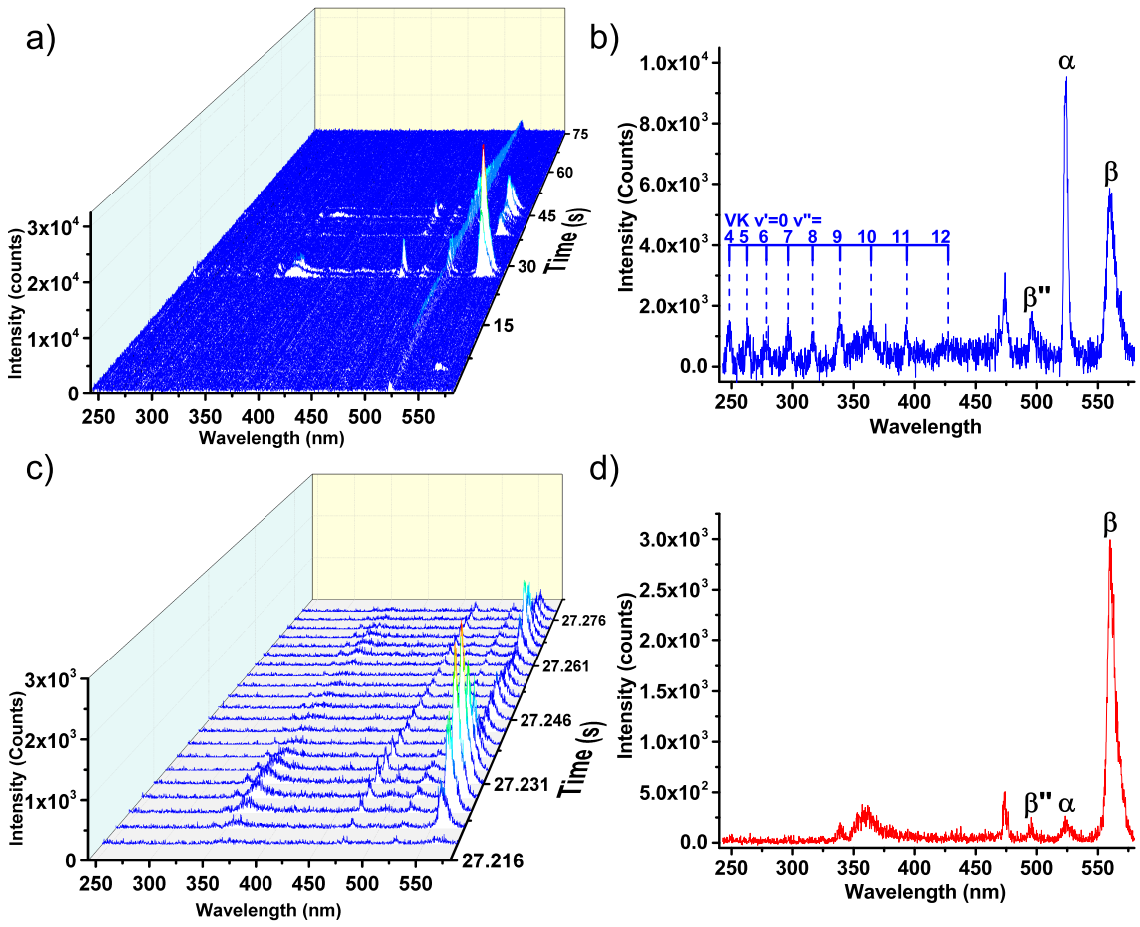

Figure 4.8: Spectra taken in the range 240-580 nm with the Andor Spectrometer. Spectra were observed during the destruction of the sample prepared from gas mixture: $[D_2]$:$[N_2]$:[Ar]:[He] = 1:500:4,500:225,000: a) Dynamics of spectra during the entire destruction process with exposure time 1.5 s. b) Spectrum taken at t = 44.1 s with 1.5 s exposure time with identification of all observed bands. c) Dynamics of spectra taken with exposure time 3 ms during the final stages of the sample destruction. d) Spectrum taken at t = 27.231 s with 3 ms exposure time with identification of observed bands.

and β''-groups and bands at λ = 336 nm, and λ = 473 nm as well as the broad feature at λ = 360 nm were observed. The spectrum of this emission with band identifications is shown in Fig. 4.8d.

Figure 4.9 shows a comparison of spectra taken during the destruction of samples created from deuterium-nitrogen-helium gas mixtures as well as those formed with the addition of rare gases Ne and Ar. Features observed in this spectra include the strong α-group of N atoms and the β-group of O atoms, the V-K bands of N_2 molecules ($v' = 0$, $v'' = 4$-11), the M bands of NO molecules (v'

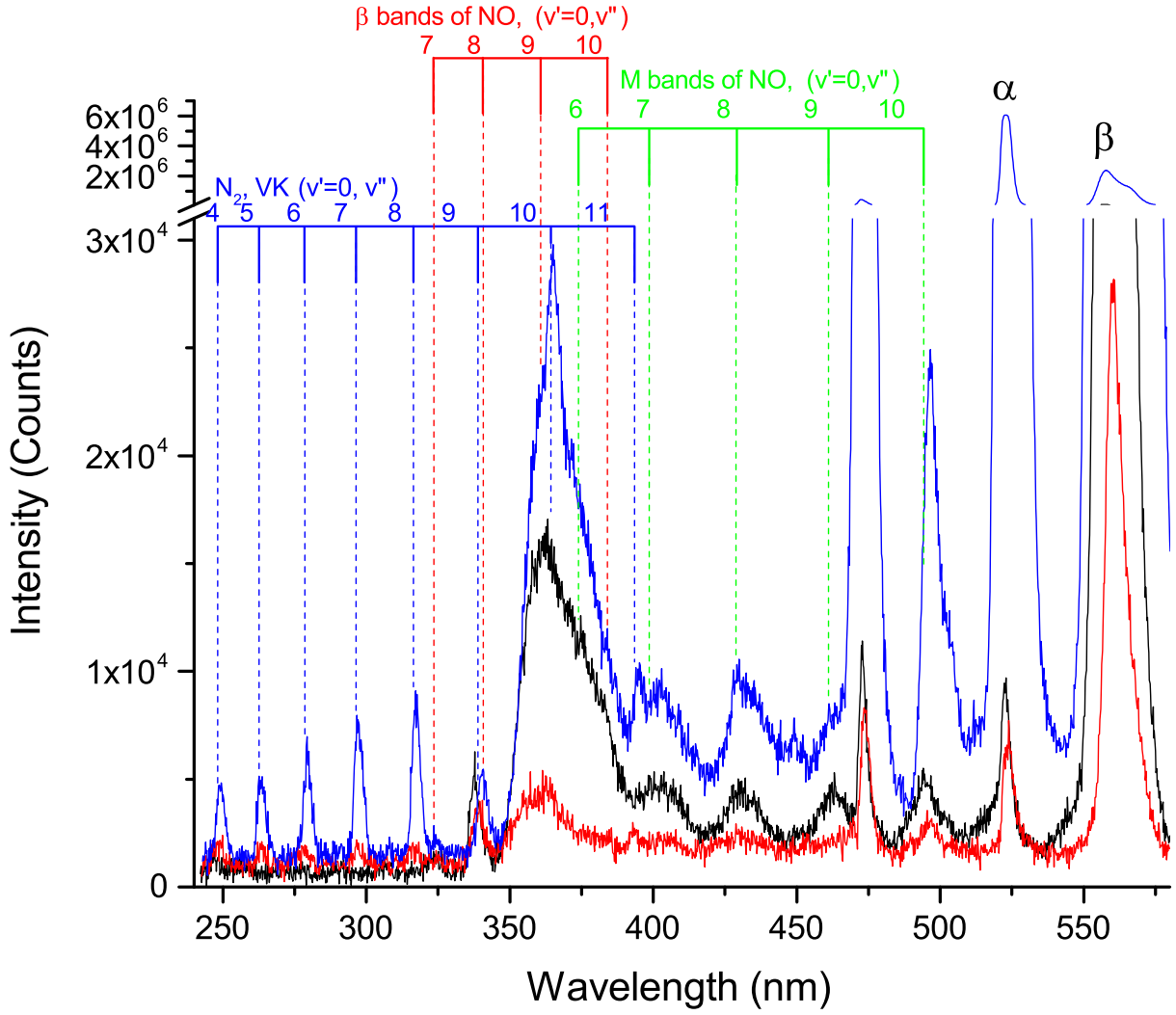

Figure 4.9: Spectra of the largest flash observed by the Andor Spectrometer with spectral resolution of 0.53 nm during the destruction of samples prepared from different gas mixtures: $[D_2]$:$[N_2]$:[Ne]:[He] = 1:500:5,000:100,000 (blue), $[D_2]$:$[N_2]$:[Ar]:[He] = 1:500:4,500:225,000 (red), and $[D_2]$:$[N_2]$:[He] = 1:2,000:100,000 (black).

= 0, v″ = 6-10), along with the broad band with maximum at λ = 360 nm, and the bands at λ = 336 nm and at λ = 473 nm. The most intense flash was from the sample prepared from the gas mixture containing neon. The positions and origins of atomic and molecular bands in the spectra presented in Figs 4.5 and 4.9 are listed in columns 3-5 of Tables 4.1, 4.3, 4.4, and 4.5.

4.3 Discussion

The addition of hydrogen or deuterium molecules into the gas mixtures used for sample preparation can lead to the appearance of luminescence from some new species formed in chemical reactions during the destruction of these samples. It was found that a relatively small change of the hydrogen and deuterium impurity content drastically influenced the spectra obtained (see Figs. 4.3, 4.4, and 4.6, 4.7). Indeed, in the spectra obtained during the destruction of samples prepared from deuterium-nitrogen-helium gas mixtures, we observed new intense bands at λ = 336, 360, and 473 nm. For samples prepared from hydrogen-nitrogen-helium gas mixtures we observed only one new intense band at λ = 360 nm in addition to the bands observed in the spectra obtained from samples prepared from "pure" nitrogen-helium gas mixtures[3, 26].

Possible candidates for emission of these bands may be species containing H and D atoms such as the radicals NH and ND. The energy levels and transitions of the NH radical are presented in Fig. 4.10. The transitions $A^3\Pi_i \rightarrow X^3\Sigma^-$ and $b^1\Sigma^+ \rightarrow X^3\Sigma^-$ of ND can be responsible for emission at λ = 336 and 473 nm, respectively. The position of the ND bands in different matrices is shown in Table 4.7. The observed positions of the new lines at λ = 336 and 473 nm shown in Table 4.4 are close to the positions of ND radical lines in the rare gas matrices (see Table 4.7). Assignment of emission at λ = 473 nm to the $b^1\Sigma^+$, $v' = 0 \rightarrow X^3\Sigma^-$, v'' = 0 transition of ND radicals are also supported by a decrease of the emission of δ-, and δ'' - groups of N atoms in the spectra when the band at λ = 473 nm is present (see Fig. 4.7). The $b^1\Sigma^+$-state of the ND radical is formed in the recombination of N(^{2}P) and D(^{2}S) atoms (see Fig. 4.10). As a result of this reaction the N(^{2}P) atoms were removed from the system and thus the δ-, and δ'' emissions are absent. In the emission from hydrogen-nitrogen-helium samples the band at λ = 473 nm is absent, but the emission of the δ-, and δ'' groups are present (see Fig. 4.4), providing evidence that N(^{2}P) atoms have undergone radiative decay and thus did not participate in the reactions with H(^{2}S) atoms in this case.

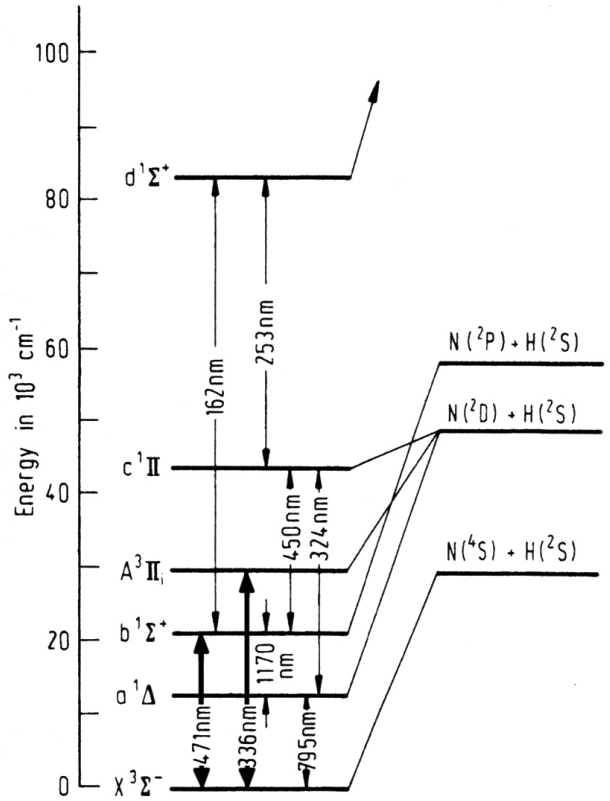

Figure 4.10: Energy diagram for NH radicals [4]. The transitions observed in this work are shown as thicker arrows.

Table 4.7: Positions (nm) of NH and ND transition $A^3\Pi_i$,v′ $= 0 \rightarrow X^3\Sigma^-$, v″ = 0 and $b^1\Sigma^+$, v′ $= 0 \rightarrow X^3\Sigma^-$, v″ = 0 in different rare-gas matrices[9, 10].

Radical	Matrix	$A^3\Pi_i$, v′ $= 0 \rightarrow X^3\Sigma^-$, v″=0	$b^1\Sigma^+$, v′ $= 0 \rightarrow X^3\Sigma^-$, v″=0
NH	Ne	335.92[9]	
	Ar	337.76[9]	472.99 [10]
	Kr	338.95[9]	
ND	Ne	335.57[9]	
	Ar	337.76[9]	473.26 [10]
	Kr	338.73[9]	

An alternative interpretation for the line at λ = 473 nm may be the transition $^1S_0 \rightarrow ^3P_1$ of N^- anion [5]. Fig. 4.11 shows the energy diagram for the three lowest energy levels of the N^-

anion. If the line at λ = 473 nm belongs to the $N^-(^1S_0 \rightarrow ^3P_1)$ transition we can calculate the line corresponding to the $N^-(^1S_0 \rightarrow ^1D_2)$ transition, because we know the position of the line corresponding to the $N^-(^1D_2 \rightarrow ^3P_{1,2})$ transition (γ-line)[5]. The position of the $N^-(^1S_0 \rightarrow ^3D_2)$ transition should be at λ = 1167 nm. The position of this line should be resolved even if the line corresponding to the NH (ND) transition $b^1\Sigma^+$, $v' = 0 \rightarrow a^1\Delta^+$, $v'' = 0$, which was observed in an Ar matrix at λ = 1173.58 nm (1170.47 nm), is present in the spectra [10].

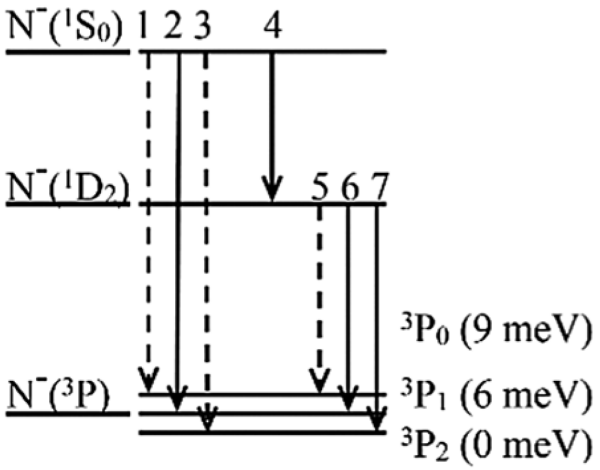

Figure 4.11: Energy diagram for N^- anions [5].

Experiments with registration of lines from the samples in the NIR region should resolve this problem. We can conclude that for the identification of the emission at λ = 473 nm there are two possible candidates, the ND radical (transition $b^1\Sigma^+$,$v' = 0 \rightarrow X^3\Sigma^-$, v'' = 0), or the N^- anion (transition $^1S_0 \rightarrow ^3P_1$). Both of these candidates have the same precursor N(^{2}P) atom.

From the comparison of the observed bands at λ = 336 nm with the results of emission from ND($A^3\Pi_i$,$v' = 0 \rightarrow X^3\Sigma^-$,$v''$ = 0) obtained in rare gas matrices (see Table. 4.7) we can assign this emission to the $A^3\Pi_i \rightarrow X^3\Sigma^-$ transition of the ND radical. The $A^3\Pi_i$-state of ND radical is the result of the recombination of N(^{2}D) and D(^{2}S) atoms. Indeed we observed a correlation between intensities of emissions at λ = 336 nm and that of the α-group of N atoms, which supports the

assignment for this emission.

Another candidate for emission of the band at 336 nm might be the N_2 molecule transition $C^3\Pi_g$, $v' = 0 \rightarrow B^3\Pi_g$,$v'' = 0$. In the gas phase this band is located at λ = 337 nm [88], but there is no evidence for observation of this band in solid nitrogen.

The most interesting result obtained in this work is the observation of the rather intense broad band with the maximum at λ = 360 nm for hydrogen-nitrogen-helium and deuterium-nitrogen-helium samples. After analysis of our previous results we found that we observed only very weak bands at 360 nm during the destruction of nitrogen nanoclusters containing only stabilized nitrogen atoms and small $(10^{-3} - 10^{-4})$ admixtures of oxygen atoms [3, 21]. The addition of H_2 or D_2 molecules in the gas mixture used for sample preparation resulted in a large enhancement of the intensity of the band appearing at λ = 360 nm in the luminescence spectra in the final stage of sample destruction (see Figs. 4.4, 4.7, 4.9). We found that the maximum intensity of the 360 nm band corresponds to some optimum quantity of H_2 or D_2 present in the make-up gas mixture. An important observation is that the addition of rare gases in the make-up gas mixture does NOT significantly influence the position of this band (see Fig. 4.9).

In the literature there are two explanations for the emission bands at λ = 360 nm. The first observation of this broad band was obtained when solid nitrogen was irradiated by 400 eV electrons, and the band was assigned to an unidentified impurity [106]. Later this luminescence band was studied during the excitation of solid nitrogen films by 500 eV electrons [88]. The band was assigned to the emission of polynitrogen N_4^* which was formed as a result of a neutralization reaction of N_4^+ with electrons in solid nitrogen. The scenario of "hole self-trapping" for N_2^+ ions with the formation of N_4^+ in a nitrogen matrix was quite recently proposed [18, 107] because of the localized character of positive charge carriers in solid N_2 [108]. This suggestion is in good accordance with both the study of gas-phase equilibria of solvation reactions of N_2^+ with N_2 molecules which revealed electrostatic bonding in the core clusters N_4^+ [109] and the laser-induced dissociation experiments showing N_4^+ as the ionic core for the even ion clusters $N_2^+ - (N_2)_n$ [110].

Another interpretation of the 360 nm band corresponding to the transition ND ($A^3\Pi$, $v' = 0 \rightarrow$

$X^3\Sigma^-$, v$'' = 1$) was suggested from the analysis of the luminescence spectra of the 0.1% N_2 doped solid deuterium irradiated by electrons [111]. Emission of NH (ND) radicals was also studied in different solid rare gases. It was found that the position of the (0-1) NH($A^3\Pi \rightarrow X^3\Sigma^-$) transition is shifted by a few nanometers for different solid rare gases and that the band had a resolved structure [9]. We rule out this interpretation because of the unusual broad shape of the observed band at λ = 360 nm and the absence of the more intense emission of the (0-0) NH($A^3\Pi \rightarrow X^3\Sigma^-$) transition.

In our experiments the spectra of the 360 band were not significantly influenced by the addition of rare gases or by the replacement of hydrogen isotopes in the nitrogen nanoclusters. This would also give a preference for the interpretation of the observed band at 360 nm in our experiments as an emission of N_4 polynitrogen. However, the question remains open as to why this emission was enhanced when the impurities of H_2 or D_2 were present in the molecular nitrogen nanoclusters. A possible explanation of this behavior is the change of the efficiency of formation of N atoms in the discharge zone with the addition of H_2 and D_2 molecules. It has been known for many years that the presence of water vapor in nitrogen discharges increases the production of N atoms via dissociation of N_2 molecules[13].

For the conditions of our experiments, the formation mechanism of N_4 polynitrogen predicted in earlier theoretical work[6] can be realized. It was shown that the barrier for N_4 compound formation from two nitrogen molecules in the excited metastable $A^3\Sigma_u^+$ states is very small (~ 0.25 eV) [6]. Intense recombination of N(^{4}S) atoms during the explosive destruction of the samples results in high concentrations of metastable $N_2(A^3\Sigma_u^+)$ molecules [3] which can participate in bimolecular reactions to form N_4 compounds. The potential curves for different electronic configurations of $N_4(D_{2h})$ polynitrogen is shown in Fig.4.12. The bound state of the N_4 compound in the potential curve of two interacting triplet molecules is located at a distance R = 1.83 Å between molecules (see Fig. 4.12). The lower potential curve of the N_4 compound for the interaction of two N_2 molecules in the ground state at this distance has a repulsive character. Therefore, the emission from the bound triplet-triplet $2A_g$ state of N_4 to the singlet-singlet $1A_g$ state involving the dissoci-

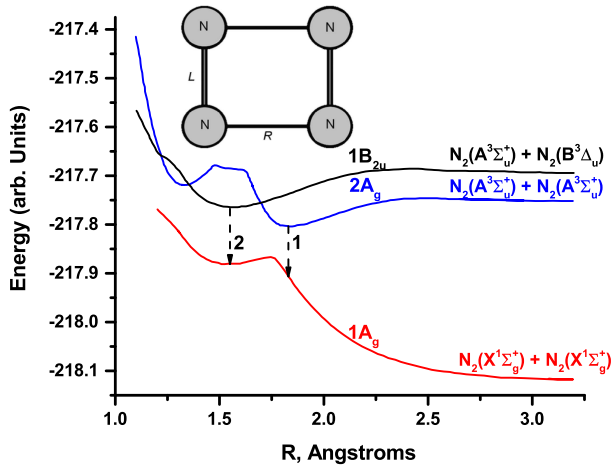

Figure 4.12: Dependence of the system energy on the distance between N_2 molecules R. Each curve corresponds to the indicated symmetry of the wave function. The interatomic distance inside the N_2 molecule was L = 1.274Å. Inset shows an N_4 cluster of D_{2h} symmetry[6].

ation of the compound into two molecules (transition 1 in Fig. 4.12) should be broad and without any structure just as for the case of excimer molecules. The predicted energy of the emitted photon is $\sim$ 3.1 eV. Both of these predictions are in good agreement with the broad non-structured emission with a maximum at λ = 360 nm (E $\sim$ 3.44 eV) observed in our experiments. According to this analysis we can thus assign the observed emission at $\lambda \sim$ 360 nm to the $2A_g \rightarrow 1A_g$ transition of $N_4(D_{2h})$ compound [6]. After emission the compound dissociates into two N_2 molecules in the ground state.

In the case of formation of N_4 compounds as a result of the interaction of $N_2(A^3\Sigma_u^+)$ and $N_2(B^3\Delta_u)$, the potential curve has a minimum at R = 1.55Å. At this distance there is also a minimum in the potential curve of N_4 resulting from the interaction of two N_2 $(X^1\Sigma_g^+)$ molecules in the ground state (see Fig.4.12). This means that after emission of the photon with energy of $\sim$ 3 eV (transition 2 in Fig.4.12) the N_4 compound will remain in the metastable state providing the possibility for the formation of a high-energy density material.

Further experimental and theoretical work would be desirable to realize high energy density materials from N_4 polynitrogen.

4.4 Conclusions

1. The process of stabilizing high concentrations of ground state atoms in molecular nitrogen nanoclusters provides a unique opportunity to study low temperature reactions and to produce a variety of unusual species in excited states.

2. A weak broad band at 360 nm is observed during the destruction of ensembles of molecular nitrogen nanoclusters containing stabilized nitrogen and small admixtures of oxygen atoms. This band was enhanced in the spectra of samples prepared from gas mixtures that contained hydrogen or deuterium.

3. Since this band is not changed significantly in rare gas matrices, we suggest that the N_4^* polynitrogen molecule is responsible for the emission of the band at 360 nm. The exact shape and location of the 360 nm band is not altered by hydrogen isotope substitution. These N_4 polynitrogen compounds are formed during the process of sample destruction accompanied by fast chemical reactions of nitrogen atoms and molecules.

4. The observed emission at λ = 336 nm was assigned to the ND radical, $A^3\Pi$, $v' = 0 \rightarrow X^3\Sigma^-$, $v'' = 0$ transition.

5. The observed emission at λ = 473 nm may be assigned to the ND radical, $b^1\Sigma^+$, $v' = 0 \rightarrow X^3\Sigma^-$, v'' = 0 transition, but the alternative assignment to the N^- anion $^1S_0 \rightarrow ^3P_1$ transition, can also be considered.

5. LUMINESCENCE OF ND RADICALS DURING THE DESTRUCTION OF MOLECULAR NITROGEN NANOCLUSTERS.*

5.1 Introduction

In the previous chapter we described experiments in which small admixtures of hydrogen or deuterium were added into gas mixtures used for preparation of nitrogen-helium condensates in superfluid helium [112]. A new intense broad band at $\lambda \sim 360$ nm was observed in these experiments. This band was assigned to the $2A_g \rightarrow 1A_g$ transition of $N_4(D_{2H})$ polymeric nitrogen. Additionally, in the experiments with the introduction of deuterium, the bands at λ = 336 and 473 nm were observed and were tentatively assigned to the ($A^3\Pi_i \rightarrow X^3\Sigma^-$) and ($b^1\Sigma^+ \rightarrow X^3\Sigma^-$) transitions of the ND radical [112]. The transition ($A^3\Pi_i \rightarrow X^3\Sigma^-$) at λ = 471 had previously been observed in the emission spectra of the NH(ND) radicals in noble-gas matrices [9, 10, 95, 103]. However in the same experiment we observed the γ-line emission at 793 nm, which corresponds to the $^1D_2 \rightarrow {}^3P_2$ transition of N^- anions [5]. The presence of N^- anions during the destruction of the samples raised the possibility of observing other transitions of this species. Therefore the transition $^1S_0 \rightarrow {}^3P_{1,2}$ of N^- anions may be an alternative interpretation for the line at λ = 473 nm. If we assign the line at λ = 473 nm to the N^- ($^1S_0 \rightarrow {}^3P_{1,2}$) transition, and knowing the wavelengths of another transition N^- anion ($^1D_2 \rightarrow {}^3P_{1,2}$) [5], it is possible to calculate the wavelength of the transition $N^-(^1S_0 \rightarrow {}^1D_2)$. The calculated wavelength for $N^-(^1S_0 \rightarrow {}^1D_2)$ transition is equal to λ = 1167 nm. The position of this line is very close to the position of the band corresponding to the transition $b^1\Sigma^+$, v′ = 0 $\rightarrow$ $a^1\Delta^+$, v″ = 0 of the NH(ND) radical which was observed at λ = 1170.47 nm in an argon matrix [10].

To resolve the problem regarding the possibility of two alternative assignments of the emission at λ = 473 nm, we performed experiments with simultaneous registration of the spectra of emission in the ultra-violet (UV), visual (VIS), and near infrared (NIR) regions during the destruction of pure

*Material in this chapter was reprinted with permission from "Luminescence of ND radicals during the destruction of molecular nitrogen nanoclusters", by P. T. McColgan, S. Sheludiakov, R. E. Boltnev, D. M. Lee, and V. V. Khmelenko. Chemical Physics, DOI 10.1016/j.chemphys.2018.08.040, Copyright 2019 by Elsevier.

nitrogen-helium samples and samples containing nitrogen and deuterium atoms. Analysis of these spectra provides convincing evidence for the assignment of the bands at λ = 336, 473, and 1170 nm to the ND radical.

5.2 Experimental Results

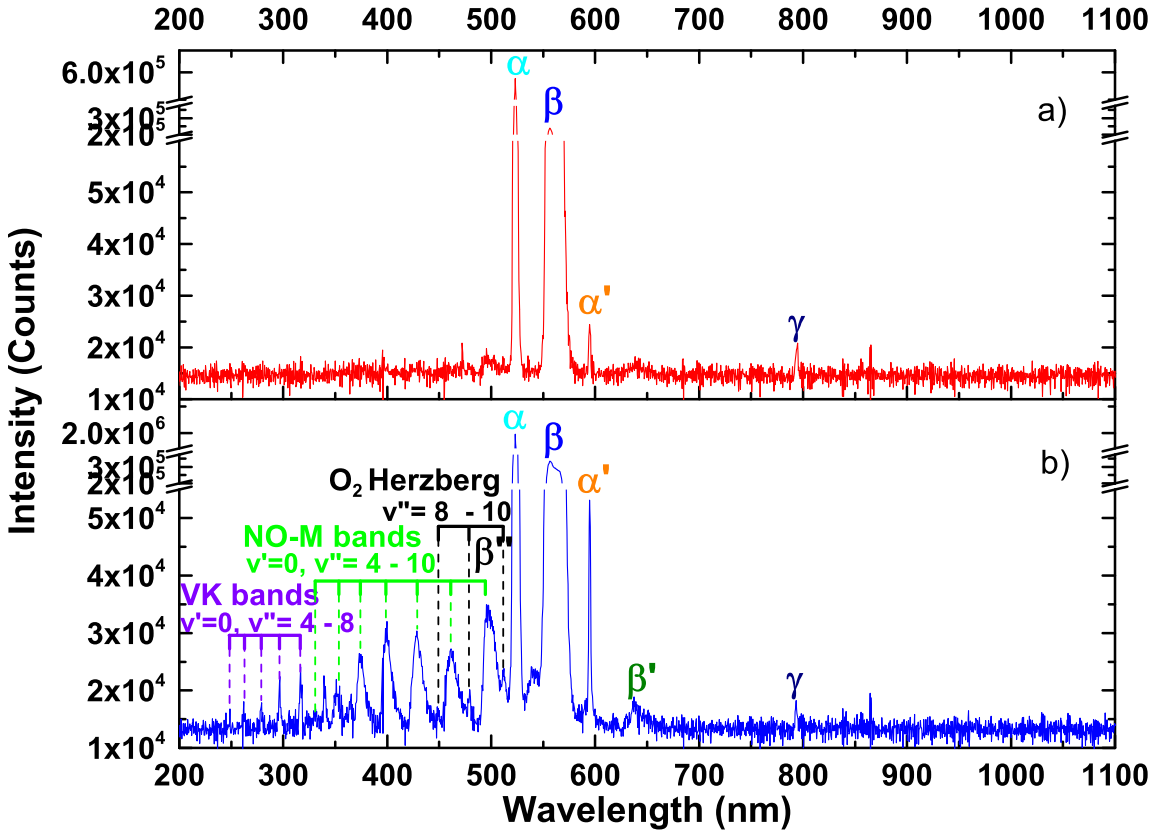

Figure 5.1: Integrated spectra taken in the range 200-1100 nm by the Ocean Optics spectrometer during destruction of the samples prepared from different gas mixtures a) $[D_2]$:$[N_2]$:[He] = 1:2000:100,000 (red), b) N_2:He 1:100 (blue). Each spectrum was accumulated during a period of 75 s.

We studied spectra during the destruction of two samples prepared from gas mixtures: $[N_2]$:[He] = 1:100 and $[D_2]$:$[N_2]$:[He] = 1:2000:100000. Usually the process of sample destruction lasted $\sim$ 65-70 s. Fig 5.1 shows integrated spectra obtained during the destruction in the UV and visual

spectral ranges. Addition of deuterium in nitrogen-helium gas mixtures leads to a substantial reduction in the intensities of all bands previously observed from nitrogen-helium samples (see Fig. 5.1). In the integrated spectra of the nitrogen-helium sample the α, α'-groups of N atoms, β, β', and β''-groups of O atoms, γ-line of N^- anions, Vegard-Kaplan (V-K) bands of N_2 molecules, M-bands of NO molecules and the second Herzberg bands of O_2 molecules are present [3]. Only a few bands such as the α, α'-groups of N atoms and the β-group of O atoms, and γ-line of N^- anions [5] remain in the integrated spectra of the deuterium-nitrogen-helium sample.

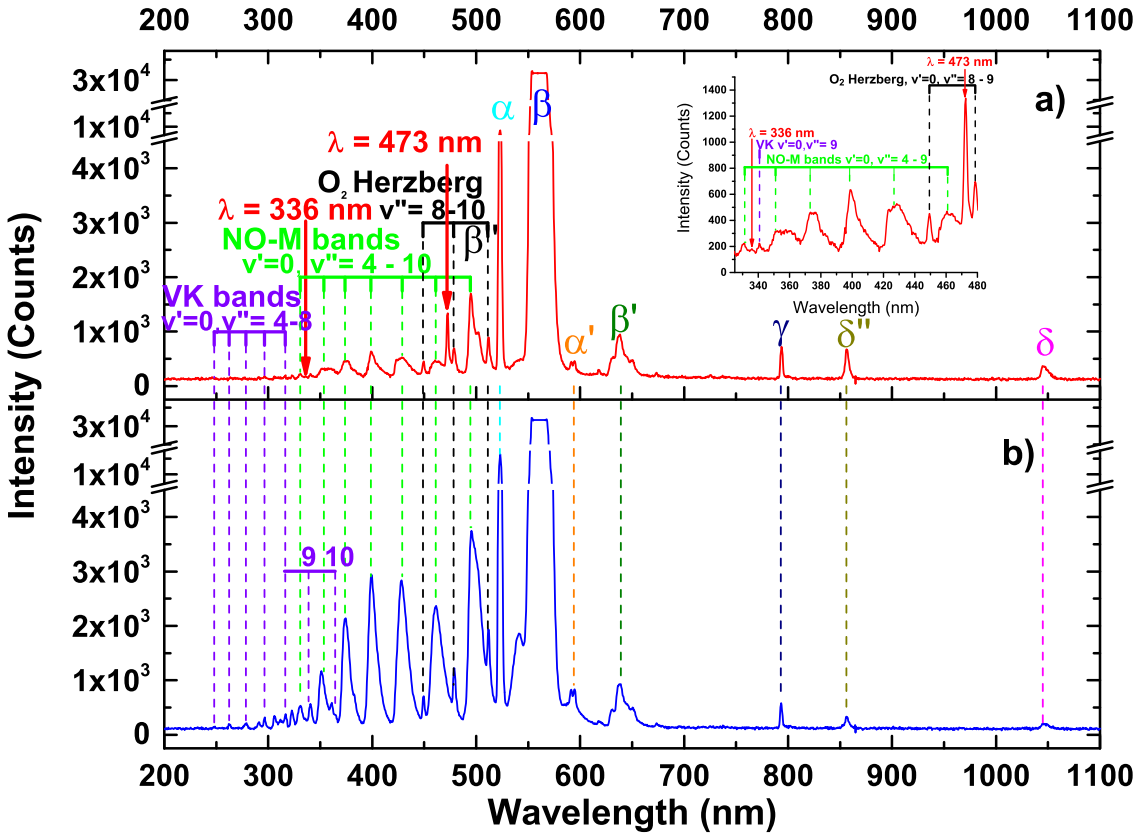

Figure 5.2: Spectra taken by the Ocean Optics Spectrometer during the most intense flashes during the destruction of the samples prepared from different gas mixtures: a) $[D_2]$:$[N_2]$:[He] = 1:2000:100,000 (red), b) N_2:He 1:100 (blue). Each spectrum was accumulated during a period of 0.5 s. Features at λ = 336 and 473 nm are shown in the inset

However, the spectra of the largest flashes obtained during the destructions of both of these

samples have more common features (see Fig. 5.2). All of the previously mentioned bands observed in the integrated spectra of the nitrogen helium sample are present in the spectra of the largest flashes of both samples. Also the δ, δ''-groups of N atoms appeared in the spectra of both samples. Additional bands at λ = 336 and λ = 473 have appeared in the spectra of the deuterium-nitrogen-helium sample (see Fig. 5.2a). These bands preliminarily were assigned to the emission of ND radicals, corresponding to transitions $A^3\Pi_i \rightarrow X^3\Sigma^-$ and $b^1\Sigma^+ \rightarrow X^3\Sigma^-$, respectively [112].

To understand when the emission of ND radicals appears during the destruction of the samples, we studied the dynamics of the spectra. Experiments were performed with simultaneous registration of the spectra in the range 200-1100 nm with the Ocean Optics spectrometer and in the range 900-1650 nm by the Avantes spectrometer. In Fig. 5.3 we combined the spectra obtained by both spectrometers. Fig. 5.3a shows the dynamics of the luminescence spectra in the range 200-1650 nm during the destruction of the deuterium-nitrogen-helium sample. From this figure we can conclude that in the spectra of most of the flashes, only α and δ-groups of N atoms and β-group of O atoms and the bands at $\lambda \sim 1170$ nm are present. However during the largest flashes the maximum number of molecular and atomic bands as well as the bands of the ND radical at $\lambda \sim$ 336, 473, and 1170 nm are present, as can be seen in Fig. 5.3b. This was the first time in which the emission of the band at λ = 1170 nm was observed (shown in Fig. 5.3a and 5.3b) during the destruction of molecular nitrogen nanoclusters containing stabilized nitrogen and deuterium atoms.

To obtain further support that the emissions of the bands at λ = 336, 473, and 1170 belong to the ND radical, we performed similar studies of a nitrogen-helium sample prepared from gas mixture $[N_2]$:[He] = 1:100. Figure 5.4a shows the dynamics of the luminescence spectra during the destruction of the nitrogen-helium sample in the spectral range 200 - 1100 nm. From this figure we can see that intensity of the α-group of N atoms increased with time and at the end of the destruction in the large flashes, many atomic and molecular bands are present. In bright flashes the δ-group of N atoms, β-group of O atoms, and NO bands are present. The spectra of the largest flash from the nitrogen-helium sample is shown in Fig. 5.4b. There are *no* bands from the ND radical in this spectrum. As can be seen from the spectra of the largest flash shown in Fig. 5.4a,

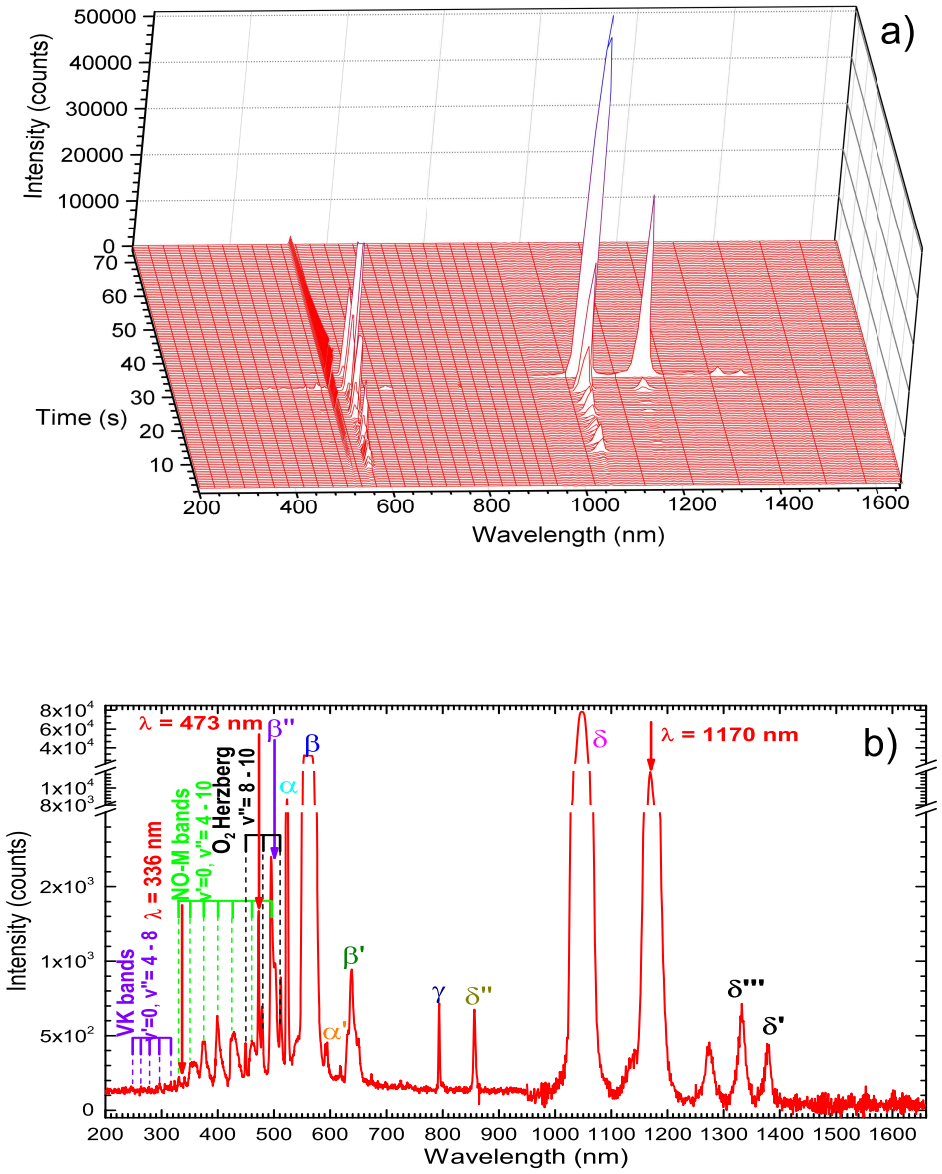

Figure 5.3: Spectra obtained during the destruction of the sample prepared from the gas mixture $[D_2]:[N_2]:[He] = 1:2000:100{,}000$. a) Dynamics of the luminescence spectra. b) Spectrum of the brightest flash with identifications. Spectra were obtained by the Ocean Optics spectrometer in the range 200-1100 nm, and by Avantes spectrometer in the range 900-1650 nm. Each spectrum was accumulated during a period of 500 ms.

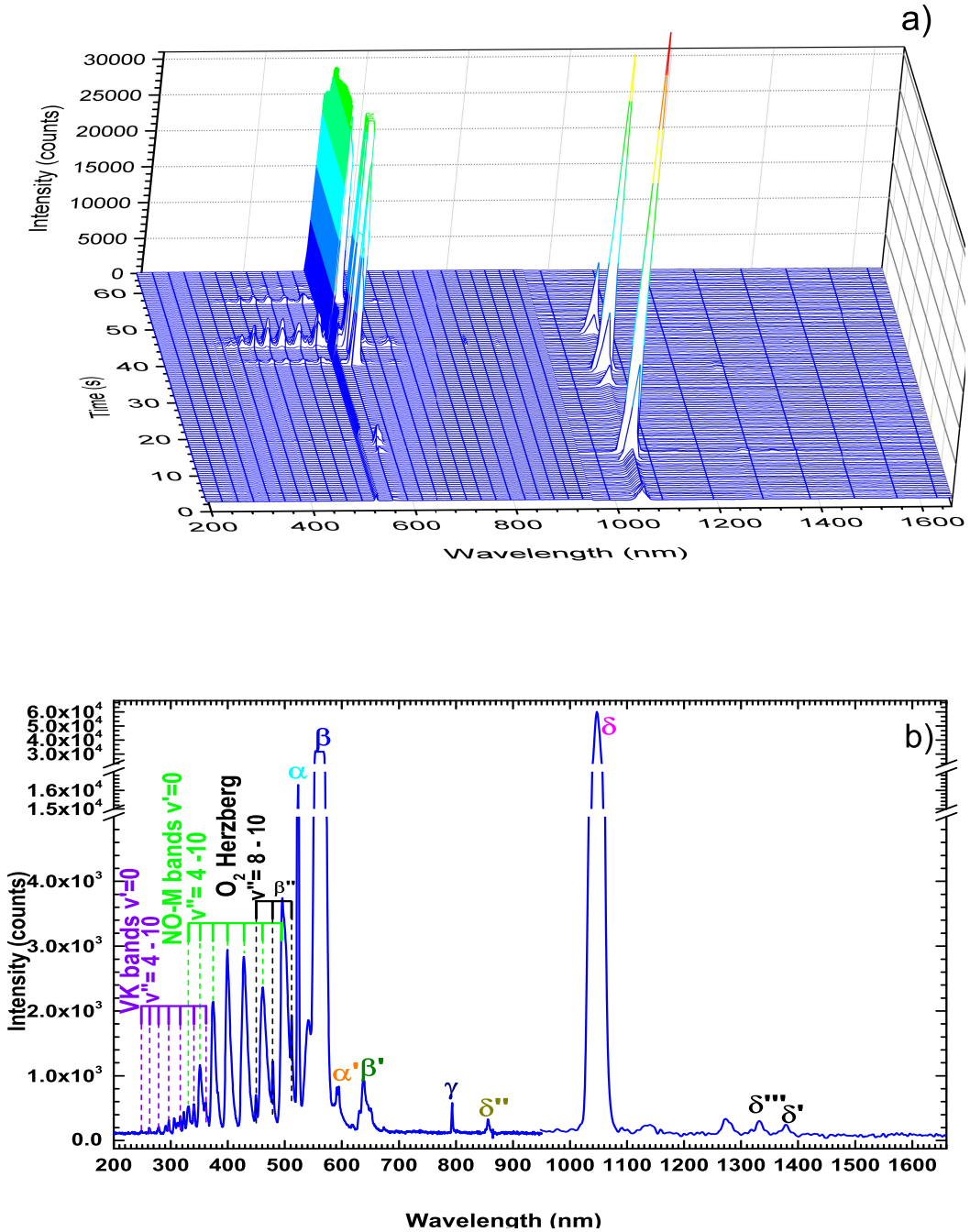

Figure 5.4: Spectra obtained during the destruction of the sample prepared from the gas mixture N_2:He = 1:100. a) Dynamics of the luminescence spectra. b) Spectrum of the brightest flash. Spectra were obtained by the Ocean Optics spectrometer in the range 200-1100 nm, and by Avantes spectrometer in the range 900-1650 nm. Each spectrum was accumulated during a period of 500 ms.

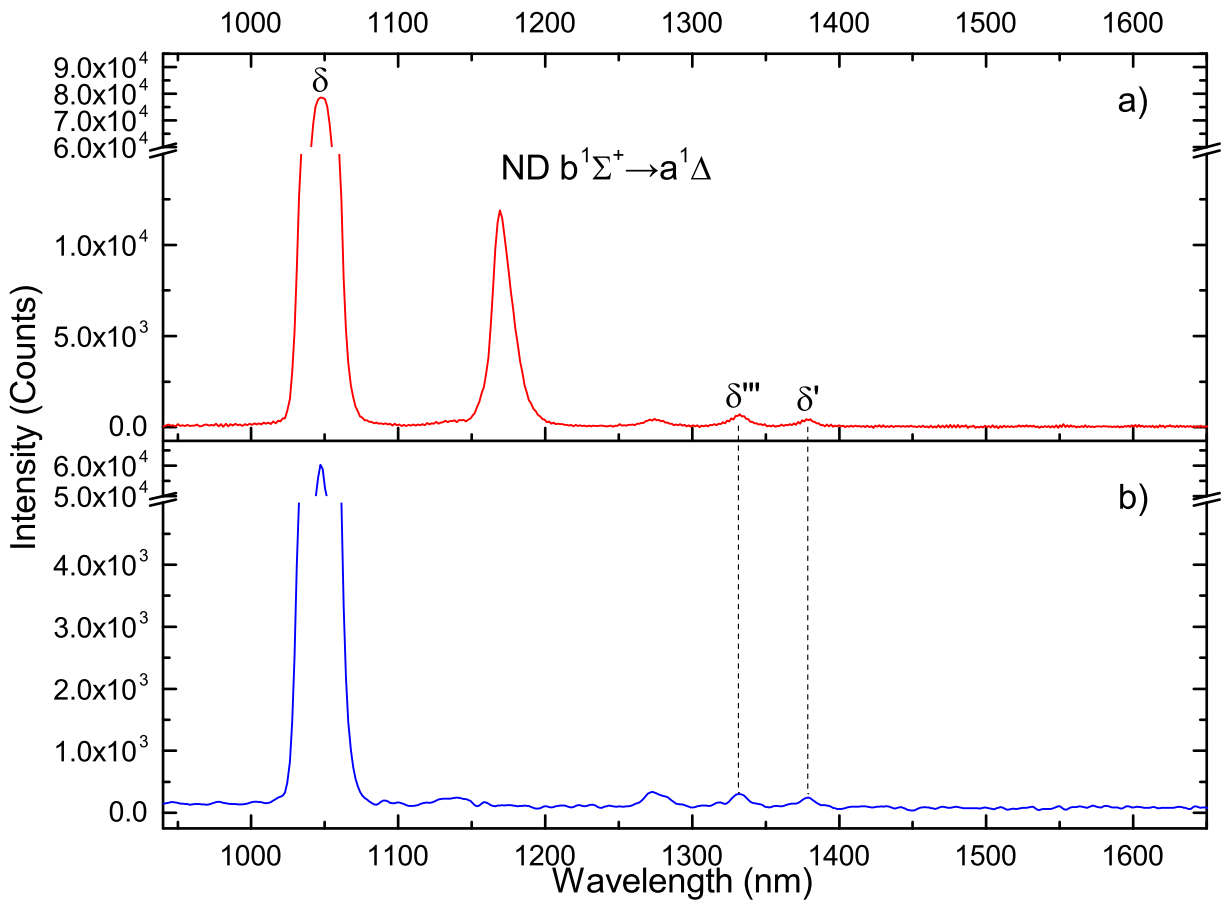

Figure 5.5: Comparison of the spectra taken in the range 940-1650 nm by the Avantes Avaspec Spectrometer during destruction of the samples prepared from different gas mixtures a) $[D_2]$:$[N_2]$:[He] 1:2000:100,000 (red), b) N_2:He 1:100 (blue). Each spectrum was accumulated during a period of 0.5 s.

there are only bands, corresponding to δ, δ', and δ'''-groups of N atoms, present in the NIR region of this spectrum. Therefore we can conclude that in the absence of deuterium in the gas mixture used for sample preparation the bands at λ = 336, 473, and 1170 are also absent. This provides additional evidence for the assignment of these bands to emission of the ND radical. Figure 5.5 shows the comparison of the spectra in the region 950 - 1650 nm for deuterium-nitrogen-helium and nitrogen-helium samples obtained during their destruction. There is no emission near λ = 1170 nm in the spectrum of the nitrogen-helium sample. At the same time the emission of N^- anion at λ= 793 (γ-line) is present in the spectrum of the nitrogen-helium sample (Fig. 5.4b). This allows

us to conclude that the band at λ = 1170 nm belongs to the ND radical. In Figs. 5.6a and 5.6b the time dependences of the emission intensities of the α and δ-groups of N atoms and the bands at λ = 336 nm, 473 nm and 1170 nm are shown.

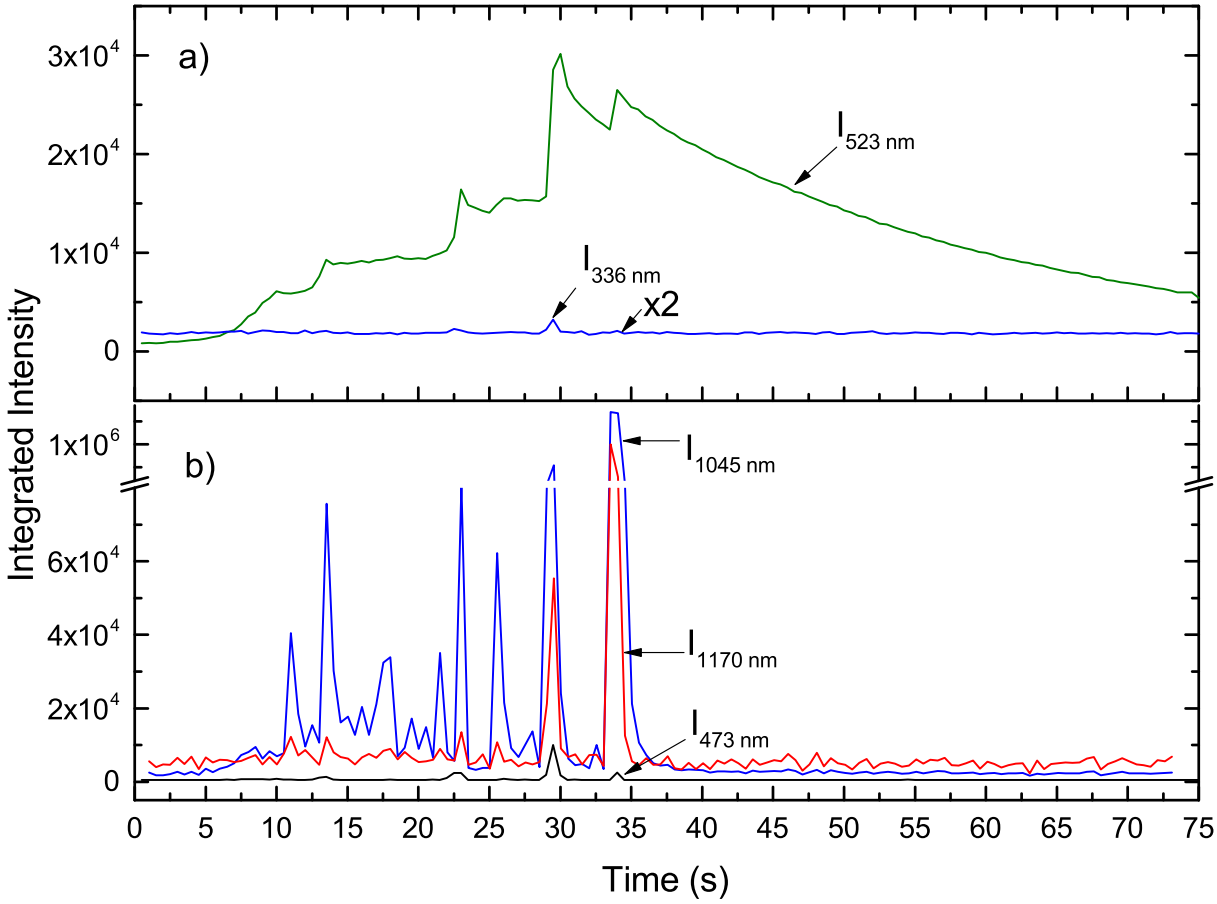

Figure 5.6: a) Comparison of integrated intensities behavior in time of the α-group emission of N atoms (green line) and the emission of ND radicals at λ = 336 (blue line). b) Comparison of integrated intensities behavior in time of the δ-group emission of N atoms (blue line) and the emission at λ = 473 (black line) and 1170 nm (red line) of ND radicals.

5.3 Discussion

Previously, the thermoluminescence during the destruction of molecular nitrogen nanoclusters containing nitrogen and oxygen atoms was studied. The well-known α, α'-groups of N atoms, the

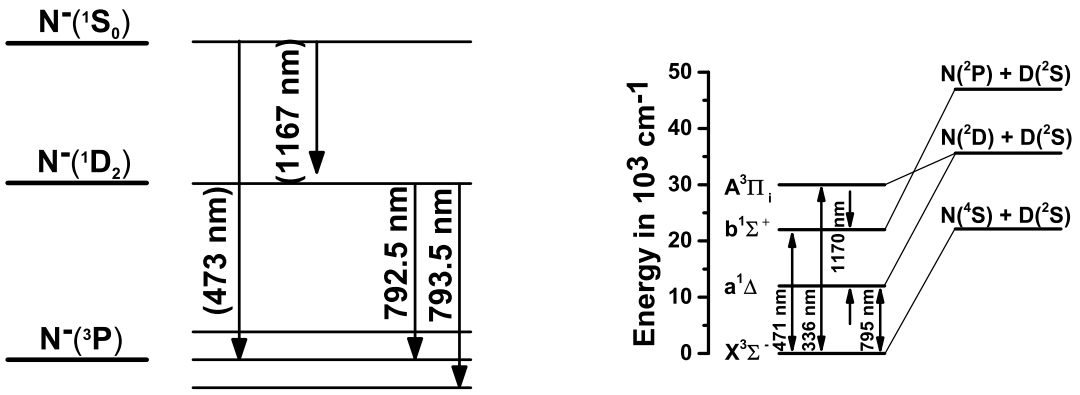

Figure 5.7: a) Energy diagram for N^- anions. [7, 8] b) Energy diagram for NH radicals.[4]

β, β', β''-groups of O atoms, the V-K bands of N_2 molecules, the M- and β-bands of NO molecules and the second Herzberg bands of O_2 molecules were observed in these studies [3, 21, 22, 23]. The addition of hydrogen or deuterium in nitrogen-helium gas mixtures used for sample preparation led to the appearance of the band at λ = 360 nm of polymeric nitrogen N_4 and two bands at $\lambda \sim$ 336 and 473 nm, which were preliminarily assigned to the emission of the ND radical in the thermoluminescence spectra during sample destruction [112]. The only remaining problem was with the accuracy of the assignment of the band at λ = 473 nm to the $b^1\Sigma^+ \rightarrow X^3\Sigma_-$ transition of the ND radical, because the alternative interpretation for this band could perhaps be the $^1S_0$-$^3P_{1,2}$ transition of N^- anion (see Fig 5.7a).

Figure 5.7a shows the energy diagram for the three lowest energy terms of the N^- anion. The transition ($^1S_0 \rightarrow {}^3P_1$) had never been observed previously for the N^- anion. If this assignment would be correct, we can find the position of the third transition, $^1S_0$ - $^1D_2$, of the N^- anion shown in Fig. 5.7a because the characteristics of the γ-line (at λ = 793 nm) corresponding to the $^1D_2$ - $^3P_{1,2}$ transition of N^- anion is well known [5]. The result of the calculation for the $^1S_0$ - $^1D_2$ transition of the N^- anion provides a value λ = 1167 nm. This simple analysis motivates us to perform experiments with simultaneous registration of thermoluminescence spectra during the destructions of deuterium-nitrogen-helium samples in the UV, visual and near infrared, and compare these

spectra with that obtained for "pure" nitrogen-helium samples for which the observation of the N^- anion bands might be expected.

Figures 5.1a and 5.1b show that there are *no* bands at λ = 336 and 473 nm in the integrated spectra of thermoluminescence of the two samples studied. Both these bands together with the band at λ = 1170 nm are present in the spectra of the most intense flashes during the destruction of deuterium-nitrogen-helium samples (see Fig. 5.3b). Therefore we assigned these three bands to the emission of the ND radical. Figure 5.7b shows the energy diagram for the NH(ND) radicals. Bands at λ = 336, 471 and 1170 nm were assigned to the transitions $A^3\Pi_i \rightarrow X^3\Sigma^-$, $b^1\Sigma^+ \rightarrow X^3\Sigma^-$ and $b^1\Sigma^+ \rightarrow a^1\Delta$, respectively, of ND radicals. The formation mechanism for excited states of ND radicals could be a result of recombination reactions of nitrogen atoms in excited states N(^{2}D) and N(^{2}P) with deuterium atoms in the ground state.

$$N(^2D) + D(^2S) \rightarrow ND(A^3\Pi_i) \tag{5.1}$$

$$N(^2P) + D(^2S) \rightarrow ND(b^1\Sigma^+) \tag{5.2}$$

The presence of substantial quantities of N(^{2}D) and N(^{2}P) atoms in nanoclusters is supported by the observation of intense emission of α- and δ-groups where the lifetime of α-group is $\sim$ 30 s and the lifetime of δ-group is $\sim$ 1 ms in solid molecular nitrogen [104].

As a consequence of these reactions, the emissions from $A^3\Pi_i$ state which corresponds to the bands at λ = 336 nm should correlate with the emission of α-group of nitrogen atoms, transition ^{2}D - ^{4}S. The emission from $b^1\Sigma^+$ state of ND radical which corresponds to the bands at λ = 473 nm and 1170 nm should correlate with the emission of the δ-group of nitrogen atoms, transition ^{2}P - ^{2}D. Figures 5.6a and 5.6b show that intensities of ND radical bands do correlate with the intensities of the corresponding α and δ-group emissions of nitrogen atoms only in the largest flashes.

5.4 Conclusions

1. Comparison of the spectra obtained during the destruction of nitrogen-helium and deuterium-nitrogen-helium samples provided evidence for assignment of the bands observed in the luminescence of deuterium-nitrogen-helium samples at λ = 336, 471, and 1170 to the emission of ND radicals with corresponding transitions $A^3\Pi_i^+ \rightarrow X^3\Sigma^-$, $b^1\Sigma^+ \rightarrow X^3\Sigma^-$, $b^1\Sigma^+ \rightarrow a^1\Delta$.

2. These ND bands were observed during the final stages of destruction of the samples. The processes of recombination of excited metastable nitrogen atoms with deuterium atoms in ground state are responsible for the appearance of excited states of the ND radical.

6. ROTATIONALLY INDUCED LUMINESCENCE OF NANOCLUSTERS IMMERSED IN SUPERFLUID HELIUM.

6.1 Introduction

In this chapter we study the influence of vortex density in HeII on the intensity of luminescence accompanied by the process of injection of molecular nitrogen nanoclusters into a rotating beaker containing HeII. During these measurements, the nanoclusters continued to enter into the bulk HeII inside the rotating beaker. Nitrogen atoms stabilized on the surfaces of nanoclusters [36] provide an excellent opportunity for visualization of the process of capturing nanoclusters into vortex cores. When two nanoclusters are captured into a vortex core they can collide and two nitrogen atoms residing on the surfaces of these nanoclusters can then recombine, starting processes that lead to luminescence of nitrogen atoms in nanoclusters. We observed the influence of rotation speed of the beaker with HeII on the intensity of luminescence from the ensembles of nanoclusters.

We found that increasing the rotation speed of the beaker containing HeII led to an increase of luminescence of the injected nanoclusters. We explained this effect by an efficient capturing of nanoclusters in quantum vortex cores when the density of vortices was increased. Increasing the density of vortices by increasing the rotational speed of the beaker containing HeII results in more chemical reactions of pairs of nitrogen atoms on the surfaces of neighboring nanoclusters in vortex cores, leading to increasing intensity of luminescence.

6.2 Experimental Method

We recorded the luminescence during the injection of the products of a discharge in nitrogen-helium gas mixtures into bulk superfluid helium contained in the cylindrical quartz beaker (see Fig. 6.1). During these recordings the beaker was rotated at various speeds. The rotation speeds were equal to 3, 4, and 7.5 rad/s. These speeds were similar to those used for measurements of the attenuation of second sound in uniformly rotating HeII [59]. For each rotation speed the recording of luminescence lasted for 5 minutes. We performed investigations for three different

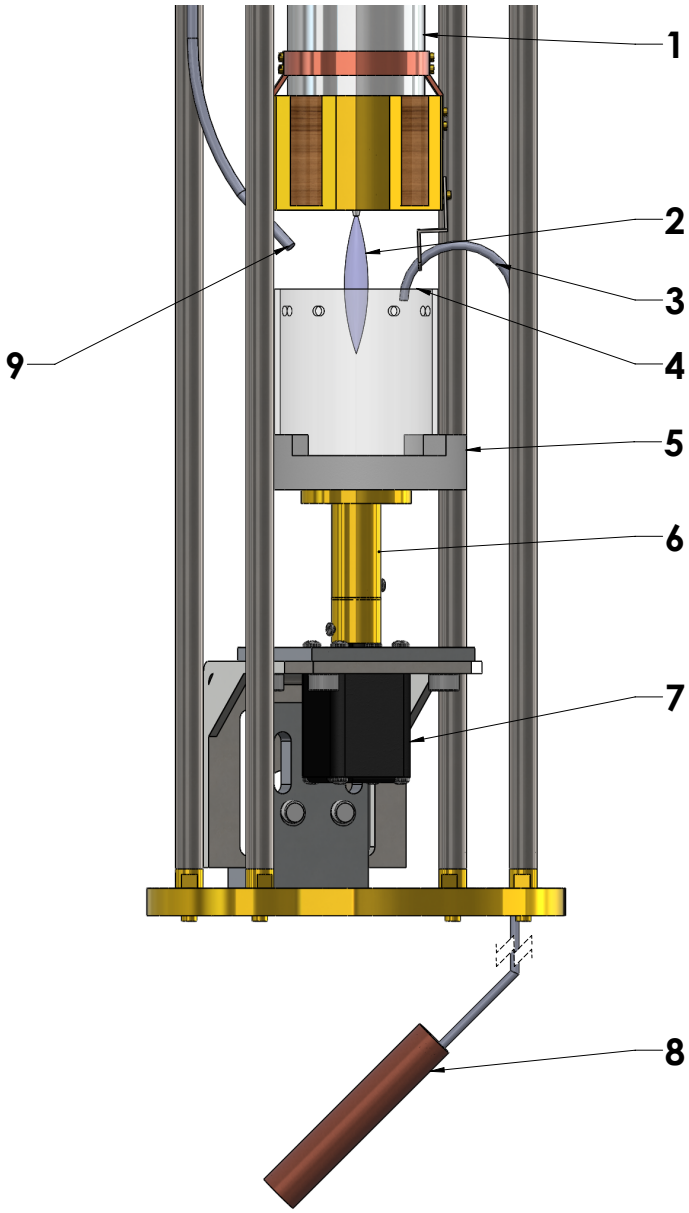

Figure 6.1: Rotating beaker assembly. 1: Atomic source, 2: Nitrogen-helium jet, 3: Fountain pump line, 4: Quartz beaker, 5: Teflon beaker holder, 6: Brass flange, 7: NEMA 8 stepper motor, 8: Fountain pump body, 9: Optical fiber.

nitrogen-helium gas mixtures: N_2:He = 1:400, 1:200, and 1:100.

6.3 Experimental Results

We recorded the luminescence spectra and their intensity during the injection of nanoclusters into bulk superfluid helium while the beaker with helium was rotating uniformly. The spectra were

obtained over a broad range. The Ocean Optics spectrometer provided spectra in the 200-1100 nm range, the Andor spectrometer in the 240-580 nm range, and the Avantes spectrometer in the 950-1650 nm range.

Figure 6.2 shows the spectra obtained by the Andor spectrometer during the condensation of gas mixture N_2:He = 1:200 for three different rotational speeds of the beaker filled with HeII. From the comparison of these spectra one can see that the intensities of emission assigned to the molecular nitrogen bands and helium atomic lines which were collected from the gas phase jet are almost the same for all three rotation speeds of the beaker.

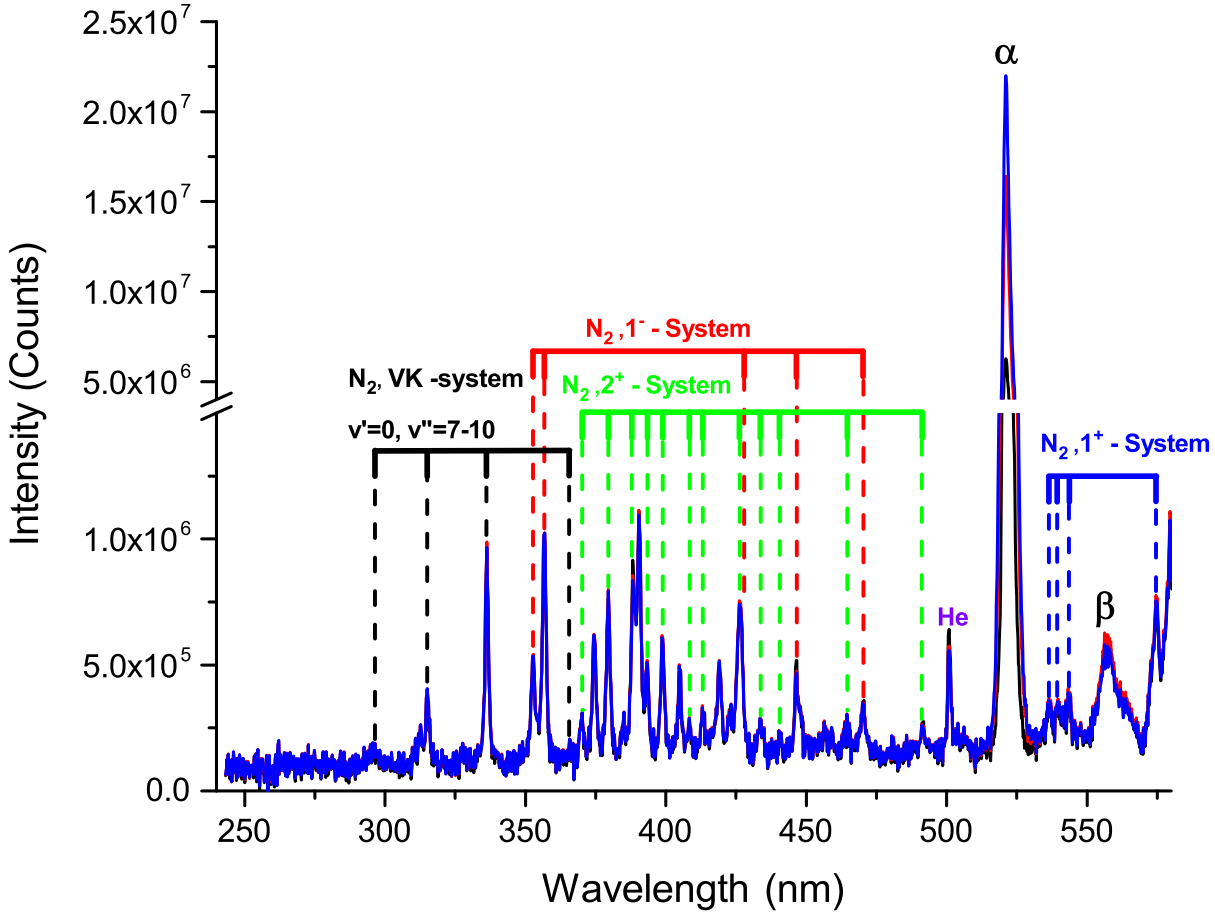

Figure 6.2: Spectra observed with the Andor spectrometer during condensation of the gas mixture N_2:He = 1:200 into a beaker filled with HeII for different rotational speeds: a) 3 rad/s (black), b) 4 rad/s (red), c) 7.5 rad/s (blue). Each spectrum was obtained by integration of the emission during a 5 minute time interval.

In contrast, the α-group emission of nitrogen atoms in nanoclusters immersed into superfluid helium depends on the rotation speed of the beaker with HeII. Increasing the rotation speed of the beaker from 3 rad/s to 7.5 rad/s resulted in a substantial increase of the α-group emission. Figure 6.3 shows a comparison of intensities of α-group emission during the injection of two different gas mixtures (N_2:He = 1:100 and 1:200) for three different rotational speeds of the beaker filled with liquid helium. These spectra were obtained by the Andor spectrometer using the first grating with a resolution of 0.53 nm.

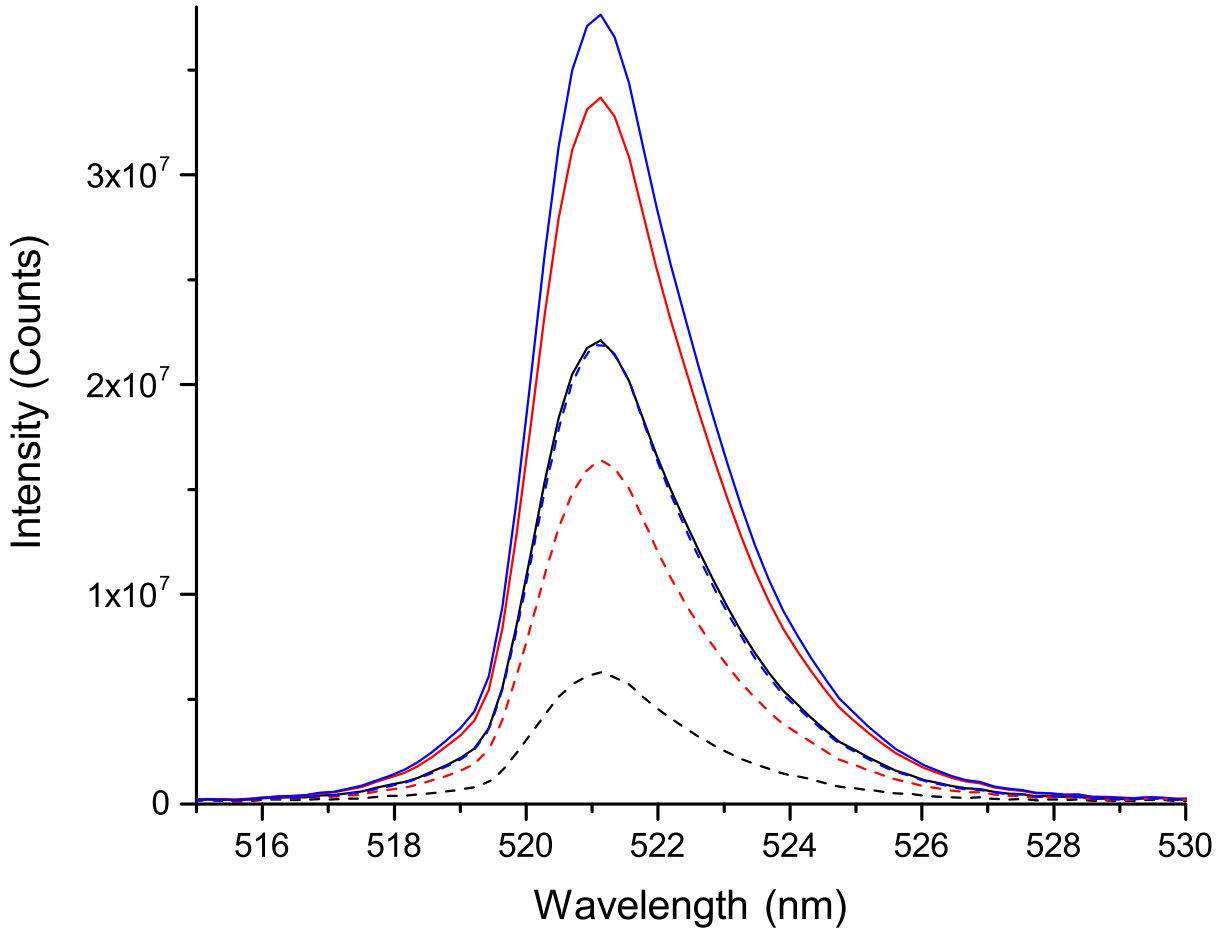

Figure 6.3: Comparison of α-group emission observed during condensation of gas mixtures N_2:He = 1:100 (solid line) and 1:200 (dashed line) for different rotational speeds: 3 rad/s (black), 4 rad/s (red), 7.5 rad/s (blue). Each spectrum was obtained by integration of the emission during a 5 minute time interval.

We performed similar investigations for the gas mixture N_2:He = 1:400. Fig. 6.4 shows the dependence of the integrated intensity of the α-group of N atoms in nanoclusters immersed into HeII on the rotation speed of the beaker for three different gas mixtures used for injection of nanoclusters. It is clearly seen that increasing the rotational speed of the beaker led to an increase of the integrated luminescence for each gas mixtures used in the experiments. Also, it was found that increasing the flux of nitrogen clusters into bulk HeII resulted in increasing the intensity of the α-group for each value of rotation speed of the beaker.

The spectra observed in the NIR range by the Avantes spectrometer shows a result similar to that obtained in the UV-VIS ranges, namely, the emission from the gas-phase jet was essentially unaltered by the rotation of the beaker with HeII as seen in Fig. 6.5. The most dramatic effect of rotating HeII was observed for the emission of the δ-group of N atoms stabilized in the N_2 nanoclusters as shown in Fig. 6.5. Figure 6.6a shows a comparison of the intensities of the overlapping N atom δ-group and $N_2(B^3\Pi_g,\ v' = 0 \rightarrow A^3\Sigma_u^+,\ v'' = 0)$ emissions during the injection of two different gas mixtures (N_2:He 1:100 and 1:200) for three different rotational speeds of the beaker. Similar investigations were made for gas mixture N_2:He 1:400. We performed deconvolution for these overlapping bands. An example of the analysis is shown in Fig. 6.6b for the spectra recorded during the injection of N_2:He 1:100 gas mixture into the beaker rotating with the angular speed 4 rad/s. A similar deconvolution was made for all spectra shown in Fig. 6.6a to obtain the dependence of the integrated intensity of δ-group emission on the rotation speed of the beaker. Figure 6.7 shows the dependence of the integrated intensity of N atoms δ-group in nanoclusters immersed in HeII on the rotational speed of the beaker with HeII for three different gas mixtures used for injection of nanoclusters. For gas mixture 1:400 an almost linear growth of the δ-group intensity with increasing rotational speed of HeII was observed. For more concentrated gas mixtures N_2:He = 1:100 and 1:200 increasing of the integrated intensity of δ-group was observed only with increasing the rotation speed of the beaker from 3 to 4 rad/s. Further increase of the rotational speed of the beaker with HeII to 7.5 rad/s resulted in a small decrease of the intensity of δ-group emission.

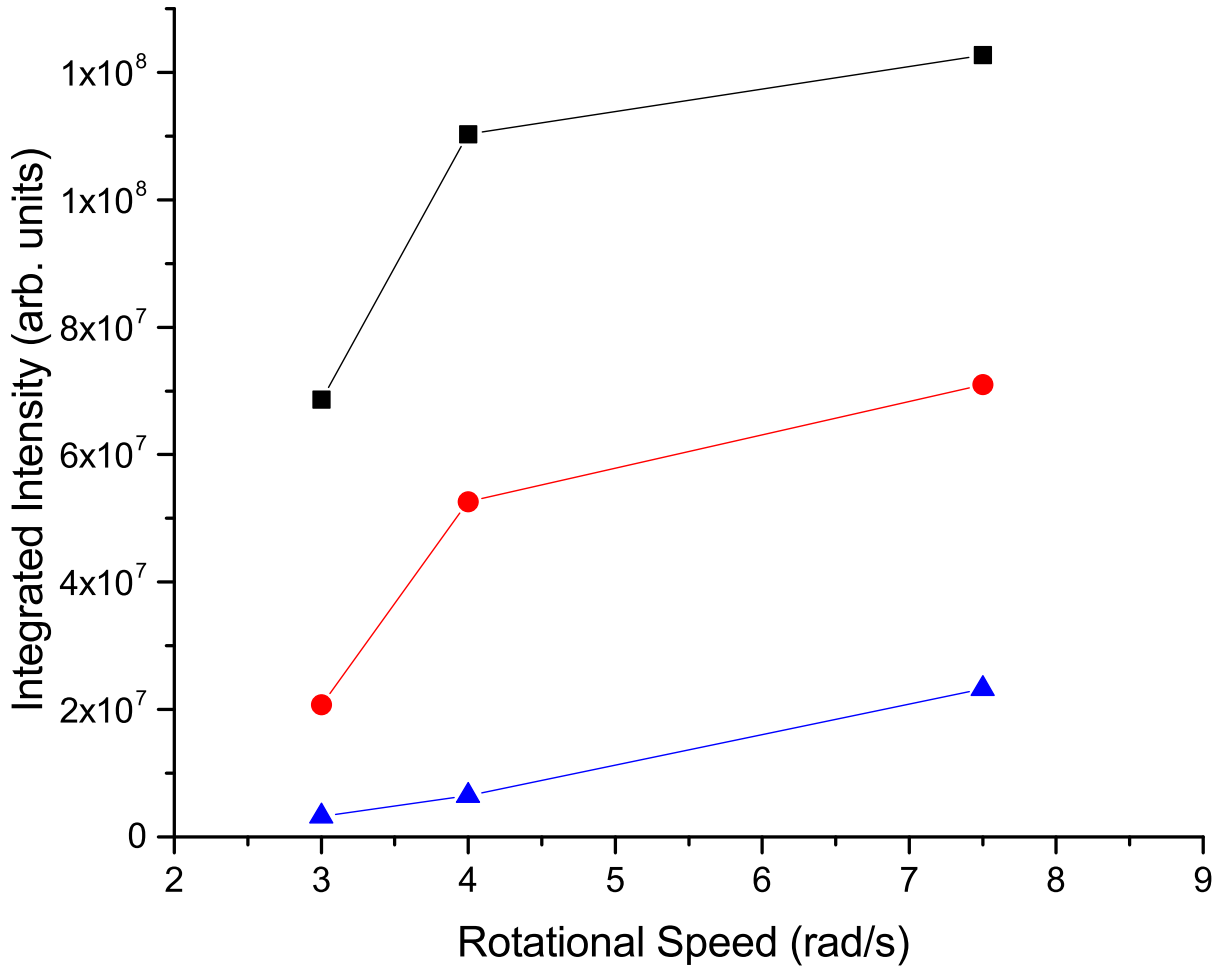

Figure 6.4: Dependence of integrated intensity of N atom α-group observed during the injection of nitrogen-helium gas mixtures N_2:He = 1:100 (black squares), 1:200 (red circles) and 1:400 (blue triangles) into a rotating beaker with HeII on the rotation speed of the beaker.

6.4 Discussion

Superfluid helium is characterized by two unique features; anomalously high heat conductance and formation of quantized vortices. The efficient heat removal property of HeII was efficiently used in the method of injection of products of our discharge in nitrogen-helium gas mixtures into bulk HeII [24]. This approach allows us to achieve the highest concentrations of stabilized nitrogen atoms [35, 39, 40]. Nitrogen atoms are stabilized on molecular nitrogen nanoclusters which form an aerogel-like porous structure inside HeII [28]. Nanoclusters are formed during the process of

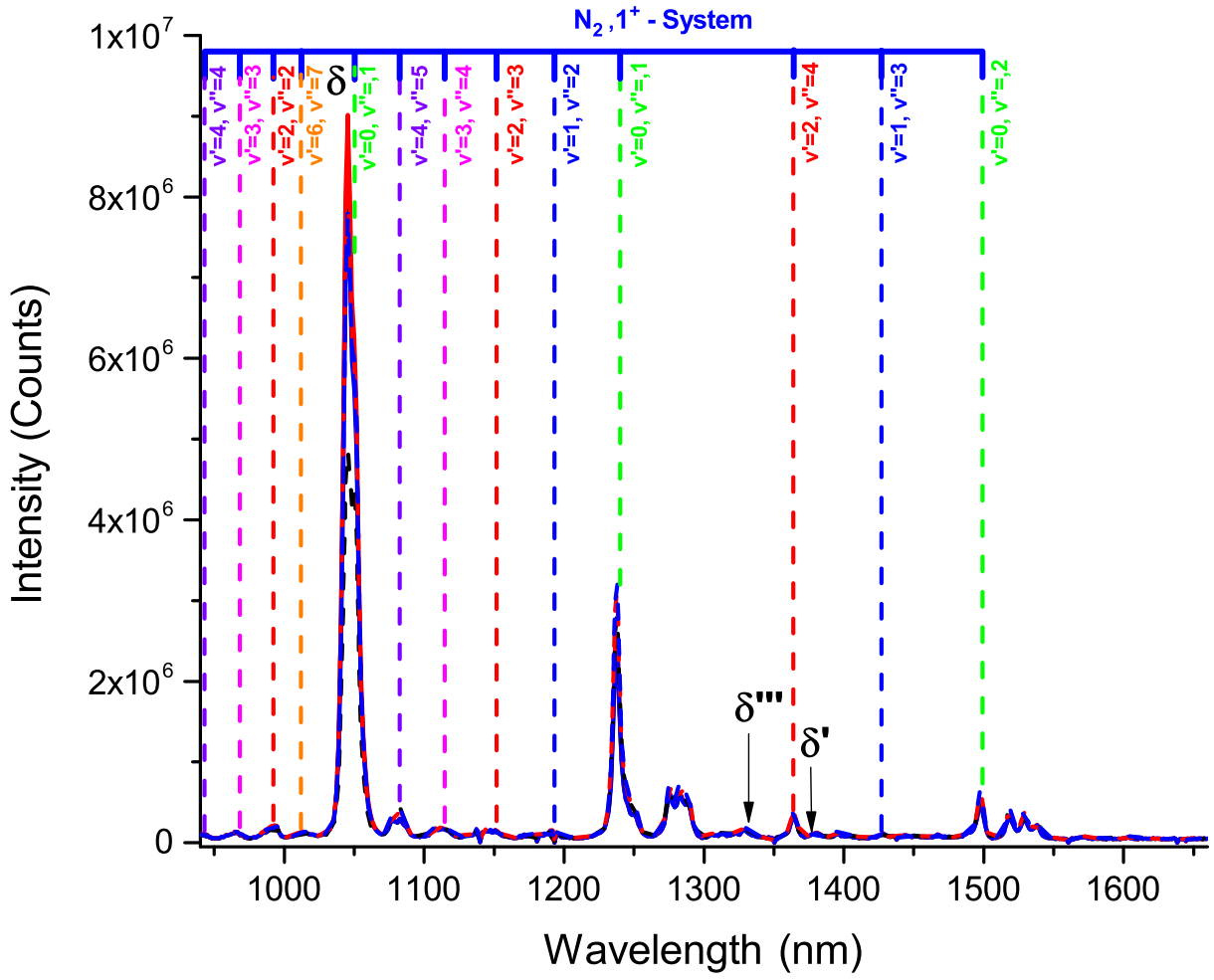

Figure 6.5: Comparison of the spectra in the range 950-1650 nm observed with the Avantes spectrometer during the injection of nitrogen-helium gas mixture N_2:He = 1:100 (solid line) and 1:200 (dashed line) into a rotating beaker with HeII for different rotational speeds: a) 3 rad/s (black), b) 4 rad/s (red), c) 7.5 rad/s (blue)

cooling down atoms and molecules entering from the gas discharge zone by passage through the cold helium vapors on the way to the surface of HeII in the collection beaker. From x-ray investigations of nanoclusters collected inside HeII an estimate of the average size of nanoclusters of the order of 5 nm has been made [27, 31]. This allows us to determine the flux of nanoclusters to be $2x10^{13}$ s^{-1} in the process of condensation of our nitrogen-helium gas mixture N_2:He=1:100 which has a flux 10^{19} s^{-1}. Each nanocluster contains on average 50 nitrogen atoms, that reside mostly on the surfaces of these nanoclusters [36]. Usually during the process of their injection into HeII,

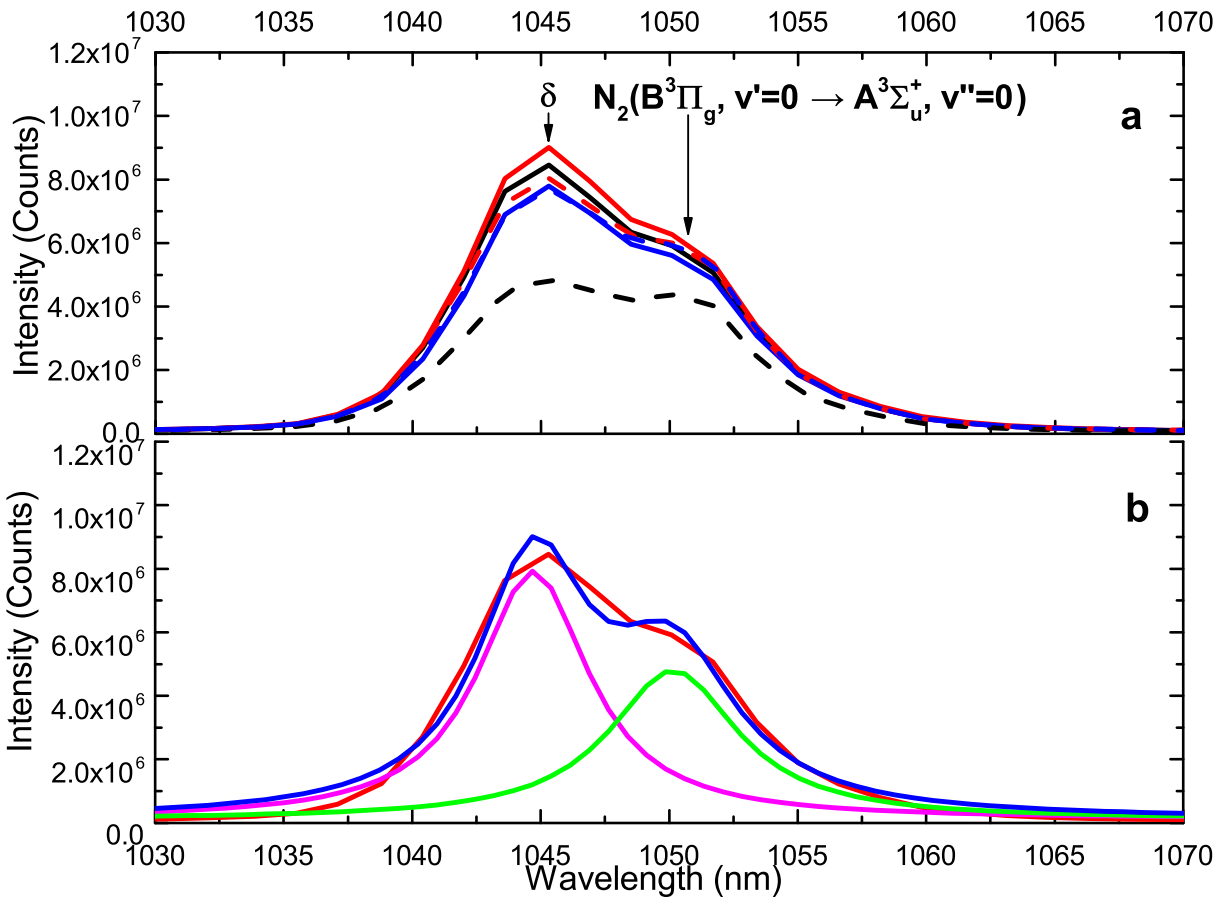

Figure 6.6: a) Comparison of the spectra of overlapping N atom δ-group and $N_2(B^3\Pi_g, v'=0 \rightarrow A^3\Sigma_u^+, v''=0)$ emissions observed during the injection of nitrogen-helium gas mixtures N_2:He = 1:100 (solid lines) and 1:200 (dashed lines) into rotating HeII for different rotational speeds: 3 rad/s (black), 4 rad/s (red), 7.5 rad/s (blue). b) Deconvolution of the overlapping spectra of δ-group and $N_2(B^3\Pi_g, v'=0 \rightarrow A^3\Sigma_u^+, v''=0)$ emissions. Experimental spectrum of these two bands recorded during injection of N_2:He = 1:100 gas mixture into beaker rotating at 4 rad/s (red), Lorentzian fitting line for δ-group emission (magenta), Lorentzian fitting line for $N_2(B^3\Pi_g, v'=0 \rightarrow A^3\Sigma_u^+, v''=0)$ emission (green), the sum of the fitting lines (blue)

the nanoclusters collide inside superfluid helium and nitrogen atoms from the adjacent nanocluster can meet each other and recombine. This leads to continuous luminescence from nanoclusters inside HeII. As a result of N atom recombination, the N_2 molecules in high vibrational states are formed. The recombination energy ($\sim$9.8 eV) is released rather slowly on the time scale of a few seconds [113, 114]. This time scale allows the removal of heat released from the nanoclusters during the process of vibrational relaxation of excited N_2 molecules by the high heat conductance

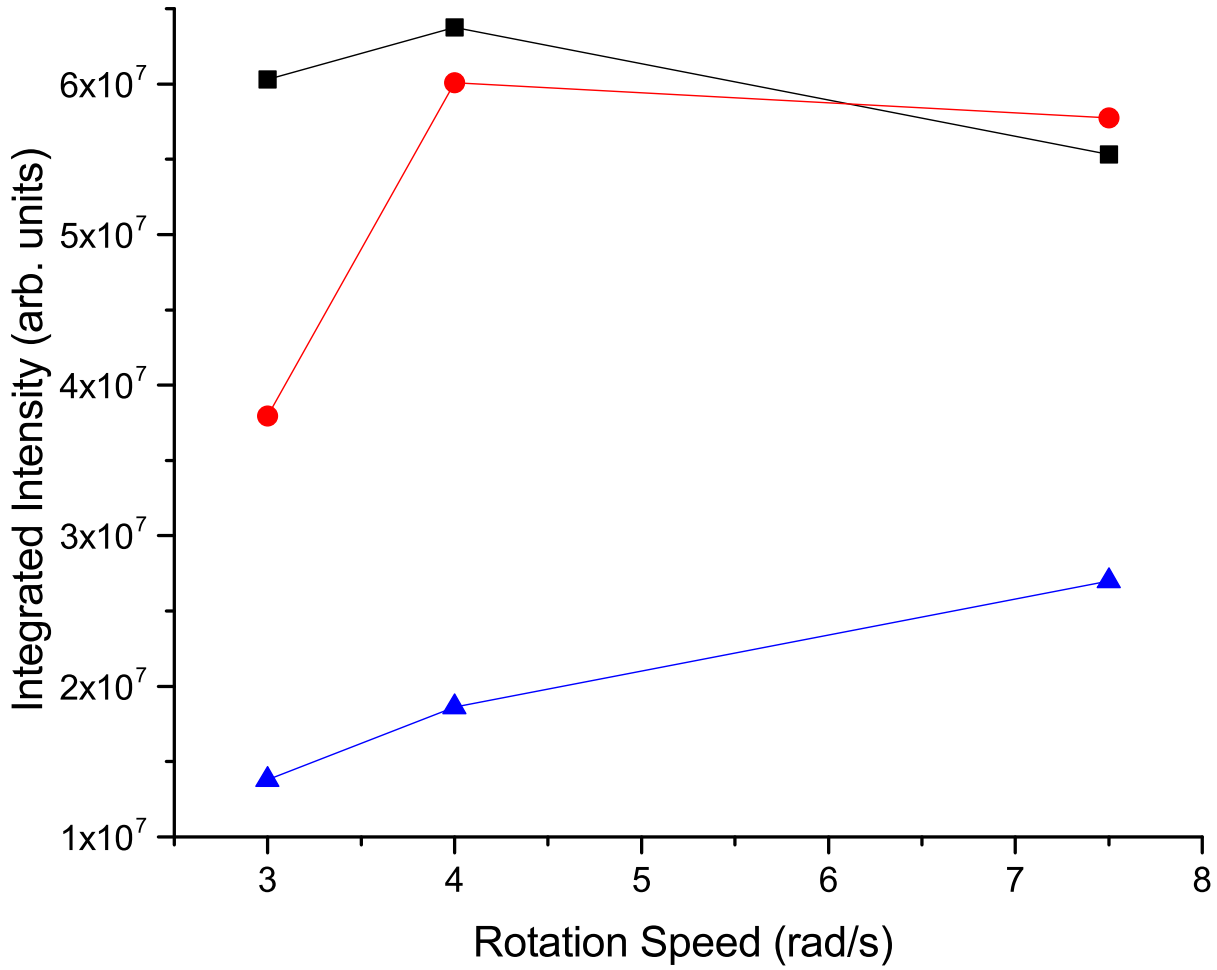

Figure 6.7: Dependence of integrated intensity of N atom δ-group observed during the injection of nitrogen-helium gas mixtures N_2 = 1:100 (black squares), 1:200 (red circles), 1:400 (blue triangles) into HeII on the rotation speed of the beaker. Integrated intensities of δ-group lines were obtained from the deconvolution of the spectra shown in Fig. 6.6a.

of superfluid helium [115]. Another part of the N_2 molecule excitation transfers efficiently to the stabilized atoms and is subsequently released by light emission. These two processes prevent the thermal explosions of nanoclusters [116]. As a consequence the ensembles of molecular nitrogen nanoclusters with high concentrations of nitrogen atoms are stable upon immersion into superfluid helium.

The mechanism of thermoluminescence in solid nitrogen containing stabilized nitrogen atoms is well understood [16, 104, 3]. Two ground state nitrogen atoms recombine to form metastable

nitrogen molecules.

$$N(^4S) + N(^4S) \rightarrow N_2(A^3\Sigma_u^+) \tag{6.1}$$

Energy from these molecules can be transferred to ground state nitrogen atoms stabilized in the nanoclusters.

$$N_2(A^3\Sigma_u^+) + N(^4S) \rightarrow N(^2D) + N_2(X^1\Sigma_g^+) \tag{6.2}$$

These excited N(^{2}D) nitrogen atoms emit the α-group.

$$N(^2D) \rightarrow N(^4S) + \alpha - group \tag{6.3}$$

Similarly for the δ-group, metastable nitrogen molecules can excite stabilized nitrogen atoms, to the higher N(^{2}P) metastable state:

$$N_2(A^3\Sigma_u^+) + N(^4S) \rightarrow N(^2P) + N_2(X^1\Sigma_g^+) \tag{6.4}$$

which emit the δ-group:

$$N(^2P) \rightarrow N(^2D) + \delta - group. \tag{6.5}$$

In this work, we studied the influence of the rotation speed of the beaker with HeII on the intensity of luminescence of nitrogen atoms in the process of injecting nanoclusters into rotating HeII. It was found experimentally (see Fig. 6.2 and 6.3) that rotation of the beaker with HeII substantially increases the intensity of luminescence of nitrogen atoms in molecular nitrogen nanoclusters immersed in HeII. Increasing the rotation speed of the beaker with HeII from 3 rad/s to 7 rad/s led to 1.5-6 fold increase of α-group intensity for the gas mixtures studied. When we increased the flux of nanoclusters by changing gas mixture from N_2:He=1:400 to gas mixture N_2:He=1:100 the intensity of luminescence from nanoclusters in rotating HeII also increased for each of the three rotation speeds investigated as seen in Fig. 6.7. In our earlier work we found that applying temperature gradients to the collection of nanoclusters immersed in HeII led to the initiation of chemical

reactions of nitrogen atoms stored on the surfaces of the nanoclusters [58]. The luminescence of ensembles of nanoclusters immersed in HeII was found to be correlated with the vortex density in bulk HeII. This correlation was explained by using a model which suggested that some loose nanoclusters were captured in the vortex cores in HeII. Inside the vortex cores, nanoclusters collide more efficiently and the recombination of nitrogen atoms residing on surfaces of nanoclusters was initiated. As a result of nitrogen atom recombination and other processes described above, nitrogen atom luminescence was observed. The intensity of this luminescence thus tended to increase with the density of vortices in the HeII. A complete discussion of the relationship between vortex density and temperature was given in Ref. [58].

We follow the same model to explain the results obtained in this work, only the method of forming vortices is more straightforward. By rotating our beaker containing HeII we created an array of quantum vortices, which aligned parallel to the axis of the beaker corresponding to the direction of the injected flux of nanoclusters entering bulk HeII. When nanoclusters enter into bulk HeII, they introduce a heat flux, which is compensated by the superfluid component of HeII. The superfluid component moves to the location of the entering nanoclusters, while simultaneously the normal component of helium moves in the opposite direction. Nanoclusters can move together with the normal component of helium. Thus nanoclusters can be captured in vortex cores. Increasing vortex density by increasing the rotation speed of the beaker should increase the efficiency for capturing nanoclusters into the array of vortex cores. Inside the vortex cores the collision rate of nanoclusters becomes larger [57]. Collisions of pairs of nanoclusters can lead to recombination of nitrogen atoms residing on their surfaces. As a result, rotation of the beaker can initiate chemical reactions between nitrogen atoms in the vortex cores, leading to formation of highly excited nitrogen molecules. The energy from excited nitrogen molecules was efficiently transferred to stabilized nitrogen atoms, which was responsible for the increased luminescence.

The flux of gas in the jet as regulated by the Brooks flow controller is $5.0{\cdot}10^{19}$ particles/sec.

$$n = \frac{5.0 \cdot 10^{19}}{6.02 \cdot 10^{23}} = 8.3 \cdot 10^{-5} mol \tag{6.6}$$

In the cold helium vapor, the atoms and molecules in the jet cool down to the temperature of 10 K. Knowing the temperature in the liquid helium in the beaker, 1.54 K, we can determine ΔT = 10 - 1.54 $\sim$ 8.46 K. The molar heat capacity of helium gas is C_v=20.78 J/(mol·K). The flux of gas gives this amount of heat each second.

$$Q = nC_v\Delta T = 14.6 \cdot 10^{-3} J \tag{6.7}$$

The heat transferred from the jet is $\approx$ 14.6 mW.

We suggest that the surface of entering nanoclusters into HeII is semi-spherical with diameter of 1 cm and surface area S,

$$S = \frac{4}{2}\pi r^2 = \frac{\pi}{2} cm^2 \tag{6.8}$$

The heat flux is:

$$q = \frac{14.6 mW}{1.57 cm^2} \simeq 9.29 \frac{mW}{cm^2} \tag{6.9}$$

The vortex density, L, is estimated using the following formula taken from Ref. [58]:

$$L^{1/2} = \gamma^{(T)} \cdot \frac{q}{\rho_s \cdot s \cdot T} \tag{6.10}$$

Where q is the heat flux in mW/cm^{-2}, ρ_s the density of the superfluid component of ^{4}He and is given from the formula from Ref. [117]:

$$\rho_s = \rho \left(1 - \left(\frac{T}{T_\lambda} \right)^{5.6} \right) \ g/cm^3 \tag{6.11}$$

The entropy, s, of the liquid helium is given by:

$$s = 1.5838 \left(\frac{T}{T_\lambda} \right)^{5.6} \ \frac{J}{g \cdot K} \tag{6.12}$$

where T is the temperature of the HeII (T = 1.54 K), and γ is the empirical coefficient 150 s ·

cm^{-2} which was experimentally determined in Ref. [118]. Plugging values into equation 6.10, we obtain:

$$\begin{aligned} L^{1/2} &= \frac{150\ s/cm^2 \cdot 9.29 \cdot 10^{-3} \frac{J}{s \cdot cm^2}}{.124\ g/cm^3 \cdot .232 \frac{J}{g \cdot K} \cdot 1.54K} \\ &= 31.5\ cm^{-1} \end{aligned} \tag{6.13}$$

Squaring, we find the estimate the vortex density created by the heat flux of the jet at the surface of the crater to be:

$$L = 993\ cm^{-2} \tag{6.14}$$

It should be noted that this estimate rapidly falls off as $\frac{1}{r^4}$ (r is the radius of hemisphere that heat travels through).

Feynman rules estimate the density of vortices created by rotation of HeII to be:

$$L = 2000\ \Omega\ cm^{-2} \tag{6.15}$$

where Ω is the rotation speed of the beaker in rad/s. In our experiments, Ω was changed from 3 to 7.5 rad/s, so L was in the range from $6{\cdot}10^3$ cm^{-2} to $1.5{\cdot}10^4$ cm^{-2}. These estimations provide evidence that rotation of the beaker in our experiments led to the formation of much larger densities of vortices than that created from the heat flux from the gas jet which was estimated in Eqn. 6.14.

Figure 6.8 shows a high resolution spectrum of α-group emission from nanoclusters recorded during rotation of the beaker of HeII with Ω = 4 rad/s integrated over a 5 minute time period. The leftmost peak of the spectrum at λ = 521 nm is emission from atoms residing on the surfaces of the nanoclusters, while the peak at λ = 522 nm is emission from atoms in interstitial sites inside the nanoclusters, and the broad feature is the phonon-induced emission of nitrogen atoms in substitutional sites[104]. The dominant experimentally observed emission of atoms residing on the surfaces of nanoclusters supports our model that the recombination of nitrogen atoms occurs mostly on the surfaces of nanoclusters trapped in vortex cores.

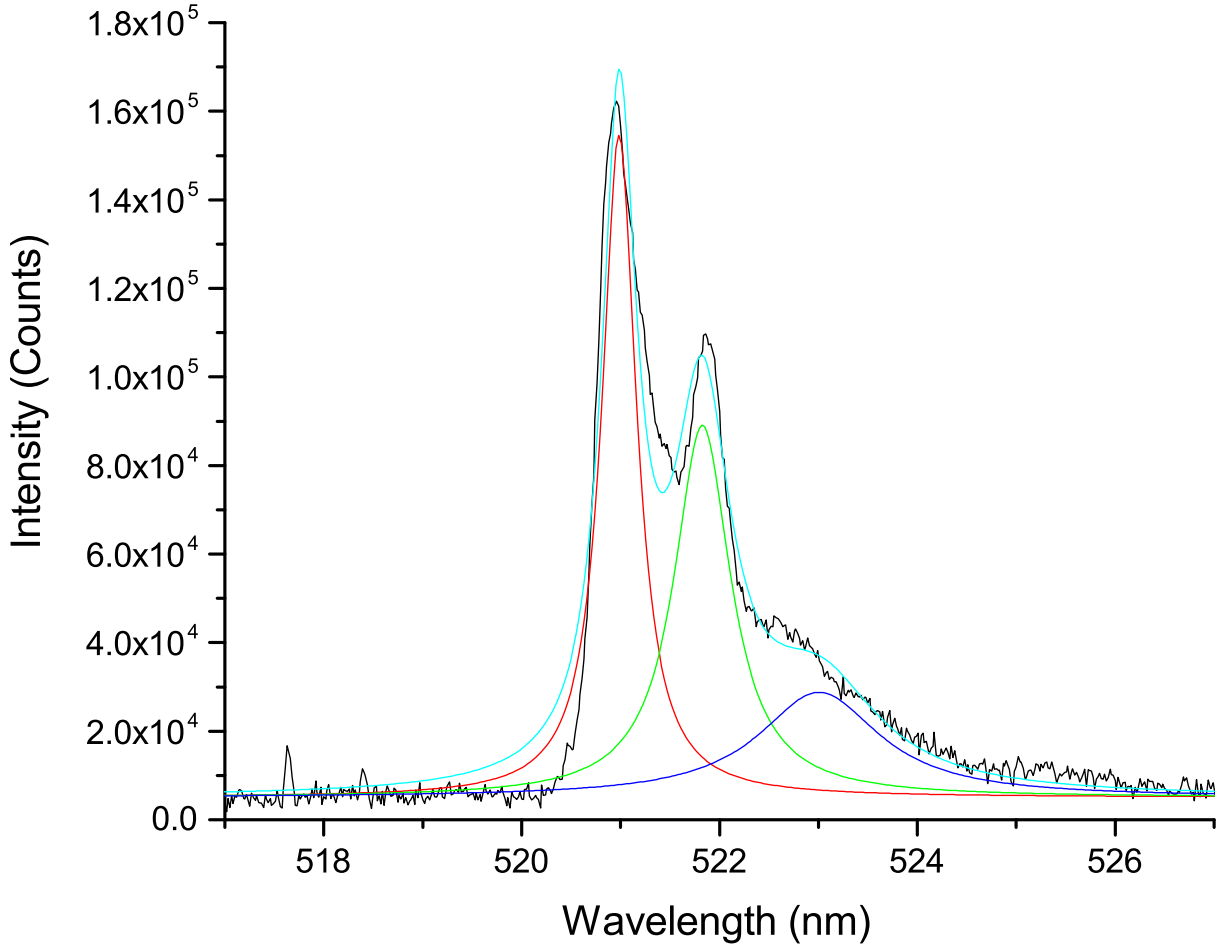

Figure 6.8: High resolution spectrum of α-group emission of nanoclusters immersed in HeII during the rotation of the beaker at Ω = 4 rad/s recorded with 3^{rd} grating of the Andor spectrometer. Emission of atoms from surfaces of nanoclusters (red), interstitial sites (green), and substitutional sites (blue), sum of Lorentzian deconvolutions (cyan).

The density of the quantized vortices in HeII, L, is given by the Feynman rules with L = 2000 Ω cm^{-2}, where Ω is the angular velocity of the beaker in rad/s. The observed increase in the intensity of N atom luminescence when rotation speed of HeII was increased from 3 to 7.5 rad/s can be explained by the proportional increase of the vortex density from 6000 cm^{-2} to 15000 cm^{-2}.

The increase in the intensity of luminescence for each rotation speed of the beaker with HeII when the content of N_2 molecules in the condensed gas mixtures was increased can be explained by an increase of the flux of nanoclusters participating in chemical reactions in the vortex cores. The model works well for explaining the behavior of α-group emission of N atoms in nanoclusters injected into a rotating beaker with HeII.

The behavior of the δ-group emission of N atoms is similar to that at low rotation speeds of HeII, but at higher rotation speed (7.5 rad/s) the intensity of δ-group emission was saturated (see Fig. 7). To understand the latter result, additional investigations are needed. It may be that differences in the behavior of α-group and δ-group emissions are somehow connected to differences in the lifetimes of the ^2D and ^2P states of nitrogen atoms in the N_2 solid matrix which are equal to 30 s and 1 ms, respectively, or related to differences in the formation of these metastable states of N atoms.

6.5 Conclusions

1. We observed direct correlation between the increase of rotation speed of the beaker with HeII and the increase of luminescence intensity of N atom α-group in molecular nitrogen nanoclusters during their injection into a rotating beaker with HeII. The increase of the luminescence intensity with increasing HeII rotation speed was explained by the initiation of chemical reactions of N atoms on the surfaces of nanoclusters trapped inside vortex cores. Increasing the rotation speed of HeII led to an increase of the vortex density and, correspondingly, an enhancement of the processes of chemical reactions involving trapped nanoclusters in the vortex cores.

2. The method of initiation of luminescence of nitrogen nanoclusters immersed in HeII can be

used to visualize vortex cores and to study quantum turbulence in HeII.

3. This method opens the possibility of initiating chemical reactions for a variety of free radicals residing on the surfaces of nanoclusters immersed in bulk HeII. It may also provide new possibilities for synthesis of exotic new species.

7. SUMMARY AND CONCLUSIONS

Luminescence during the destruction of nanoclusters containing high concentrations of nitrogen atoms was investigated in the work included in this thesis. Optical spectroscopy was used to determine the species present and the transitions that they undergo. ESR spectroscopy was used to determine the concentrations of stabilized nitrogen atoms present in our samples. Using our method of injecting gas mixtures through a radio-frequency discharge into HeII, we were able to create highly energetic samples with high concentrations of stabilized ground-state nitrogen atoms. This method provides a unique opportunity to study low temperature chemical reactions and produce unusual molecules in excited states.

7.1 Combined Optical and ESR Spectroscopy

Bands of atomic and molecular nitrogen and oxygen were present for all observed spectra. It was found that the concentration of stabilized nitrogen atoms directly correlates with the content of molecular nitrogen in the gas mixtures used to create the samples. The addition of different rare gases in the gas mixtures used to create the samples dramatically changed the optical spectra obtained during the sample destruction. Spectra observed during the destruction of samples prepared from nitrogen-krypton-helium gas mixtures contained M-bands ($a^4\Pi$, $v' = 0 \rightarrow X^2\Pi$, $v'' =$ 4-11) from the NO molecules, whereas in the spectra of nitrogen-neon-helium and nitrogen-argon-helium samples the β-bands ($B^2\Pi$, $v' = 0 \rightarrow X^2\Pi$, $v'' =$ 10-15) of NO molecules dominate.

7.2 Optical Spectroscopy

The unique conditions of our experiments allow us to form highly energetic systems, allowing us to create new exotic species. This gives a unique opportunity to observe chemical reactions at low temperatures involving unusual compounds. In our work we observed radicals such as N_4 polymeric nitrogen as well as ND radicals which were previously unobserved under these conditions. During the destruction of samples prepared from nitrogen-helium gas mixtures the weak, broad band at λ = 360 nm was identified as N_4 polymeric nitrogen. It was found that

the addition of hydrogen or deuterium greatly enhances this band. The shape of this band was unaffected by an isotopic shift when hydrogen was replaced with deuterium. Bands at λ = 336, and 473 nm were identified as the $A^3\Pi_i^+ \rightarrow X^3\Sigma^-$ and $b^1\Sigma^+ \rightarrow X^3\Sigma^-$ transitions of the ND radical. These identifications were supported by the ND($b^1\Sigma^+ \rightarrow a^1\Delta$) transition observed in spectra in the NIR region at λ = 1170 nm.

7.3 Rotationally Induced Luminescence

Correlation between the rotation speed of a beaker filled with HeII and the luminescence of nitrogen atom α-group emission of nitrogen nanoclusters during their injection into a rotating beaker filled with HeII was observed. This effect is explained by the initiation of chemical reactions of N atoms stabilized on the surfaces of nanoclusters trapped in vortex cores. As the density of the vortex cores, L, increases with the rotation speed of the beaker, the processes of chemical reactions are enhanced.

This method of initiating luminescence of nitrogen nanoclusters immersed in HeII could be used to visualize vortex cores and study quantum turbulence in HeII. Furthermore, this method opens possibilities for initiating chemical reactions of free radicals residing on the surfaces of nanoclusters immersed in HeII, possibly synthesizing new exotic species.

REFERENCES

[1] S. Mao, A. Meraki, P. T. McColgan, V. Shemelin, V. V. Khmelenko, and D. M. Lee, "Experimental setup for investigation of nanoclusters at cryogenic temperatures by electron spin resonance and optical spectroscopies," *Review of Scientific Instruments*, vol. 85, no. 7, p. 073906, 2014.

[2] A. Meraki, P. T. McColgan, R. E. Boltnev, D. M. Lee, and V. V. Khmelenko, "Electron spin resonance studies of nitrogen atoms stabilized in impurity-helium condensates," *Journal of Low Temperature Physics*, vol. 192, pp. 224–240, Aug 2018.

[3] A. Meraki, S. Mao, P. T. McColgan, R. E. Boltnev, D. M. Lee, and V. V. Khmelenko, "Thermoluminescence dynamics during destructions of porous structures formed by nitrogen nanoclusters in bulk superfluid helium," *Journal of Low Temperature Physics*, vol. 185, pp. 269–286, Nov 2016.

[4] W. Hack, R. Haubold, C. Heinrich-Sterzel, H. Keller-Rudek, U. Ohms, D. Schiöberg, and C. Strametz, *Gmelin Handbook of Inorganic and Organometallic Chemistry*, vol. N / 0-b / b / 1. Springer-Verlag Berlin Heidelberg, 8 ed., 1993. Compounds with Noble Gases and Hydrogen.

[5] R. E. Boltnev, I. B. Bykhalo, I. N. Krushinskaya, A. A. Pelmenev, S. Mao, A. Meraki, P. T. McColgan, D. M. Lee, and V. V. Khmelenko, "Spectroscopic observation of nitrogen anions N^- in solid matrices," *Phys. Chem. Chem. Phys.*, vol. 18, pp. 16013–16020, 2016.

[6] V. F. Elesin, N. N. Degtyarenko, K. S. Pazhitnykh, and N. V. Matveev, "Modeling of synthesis and dissociation of the N_4 nitrogen cluster of D_{2H} symmetry," *Russ. Phys. J.*, vol. 52, pp. 1224–1234, Nov 2009.

[7] G. G. K. Leyla Özdemir, Nurgül Atik, "The fine structure levels for ground states of negative ions of nitrogen and phosphorus," *Sakarya University Journal of Science*, vol. 17, no. 1, pp. 139–146, 2013.

[8] R. D. Cowan, C. F. Fischer, J. E. Hansen, and V. Kempter, "Excited states of the negative nitrogen ion: energies and lifetimes," *Journal of Physics B: Atomic, Molecular and Optical Physics*, vol. 30, no. 6, p. 1457, 1997.

[9] V. E. Bondybey and L. E. Brus, "Interdependence of guest radiationless transitions and localized phonon structure: NH and ND($A^3\Pi$) in rare gas lattices," *J. Chem. Phys.*, vol. 63, no. 2, pp. 794–804, 1975.

[10] A. Ramsthaler-Sommer, A. C. Becker, N. Van Riesenbeck, K.-P. Lodemann, and U. Schurath, "Branching ratios and radiative rates of matrix-isolated NH in argon: The $b^1\Sigma^+ \rightarrow a^1\Delta$, $X^3\Sigma^-$ and $a^1\Delta \rightarrow X^3\Sigma^-$ transitions," *Chem. Phys.*, vol. 140, no. 2, pp. 331–338, 1990.

[11] L. Vegard, "The auroral spectrum and the upper atmosphere," *Nature*, vol. 113, pp. 716–717, 1924.

[12] L. Vegard, "Luminescence of solid nitrogen and the auroral spectrum," *Nature*, vol. 114, pp. 357–359, 1924.

[13] A. M. Bass and H. P. Broida, "Spectra emitted from solid nitrogen condensed at 4.2°K from a gas discharge," *Phys. Rev.*, vol. 101, pp. 1740–1747, Mar 1956.

[14] M. Peyron and H. P. Broida, "Spectra emitted from solid nitrogen condensed at very low temperatures from a gas discharge," *J. Chem. Phys.*, vol. 30, no. 1, pp. 139–150, 1959.

[15] H. P. Broida and M. Peyron, "Emission spectra of N2, O2, and NO molecules trapped in solid matrices," *The Journal of Chemical Physics*, vol. 32, no. 4, pp. 1068–1071, 1960.

[16] A. Bass and H. Broida, *Formation and Trapping of Free Radicals*. Academic, New York, 1960.

[17] S. Elena, K. Ivan, U. Sergey, B. Andrey, G. Galina, P. Alexey, and B. Vladimir, "Charged defects and defect-induced processes in nitrogen films," *Physica Status Solidi C*, vol. 12, no. 1-2, pp. 49–54, 2014.

[18] E. V. Savchenko, I. V. Khyzhniy, S. A. Uyutnov, A. P. Barabashov, G. B. Gumenchuk, M. K. Beyer, A. N. Ponomaryov, and V. E. Bondybey, "Radiation effects in solid nitrogen and nitrogen-containing matrices: Fingerprints of N_4^+ species," *J. Phys. Chem. A*, vol. 119, no. 11, pp. 2475–2482, 2015.

[19] R. E. Boltnev, I. N. Krushinskaya, A. A. Pelmenev, D. Y. Stolyarov, and V. V. Khmelenko, "The thermoluminescence spectra obtained on the destruction of impurity-helium solid phase samples," *Chem. Phys. Lett.*, vol. 305, no. 3, pp. 217–224, 1999.

[20] I. N. Krushinskaya, R. E. Boltnev, V. V. Khmelenko, and D. M. Lee, "Spectroscopic studies of impurity-helium condensates containing stabilized N and O atoms," *J. of Phys.: Conf. Series*, vol. 400, pp. 01230–4, 2012.

[21] V. V. Khmelenko, D. M. Lee, I. N. Krushinskaya, R. E. Boltnev, I. B. Bykhalo, and A. A. Pelmenev, "Dynamics of thermoluminescence spectra of impurity-helium condensates containing stabilized nitrogen and oxygen atoms," *Low Temp. Phys.*, vol. 38, no. 8, pp. 688–699, 2012.

[22] V. V. Khmelenko, A. A. Pelmenev, I. N. Krushinskaya, I. B. Bykhalo, R. E. Boltnev, and D. M. Lee, "Energy release channels during destruction of impurity-helium condensates," *J. Low Temp. Phys.*, vol. 171, pp. 302–308, May 2013.

[23] R. E. Boltnev, I. B. Bykhalo, I. N. Krushinskaya, A. A. Pelmenev, V. V. Khmelenko, S. Mao, A. Meraki, S. C. Wilde, P. T. McColgan, and D. M. Lee, "Optical and electron spin resonance studies of xenon-nitrogen-helium condensates containing nitrogen and oxygen atoms," *J. Phys. Chem. A*, vol. 119, no. 11, pp. 2438–2448, 2015. PMID: 25353614.

[24] E. B. Gordon, L. P. Mezhov-Deglin, and O. F. Pugachev, "Stabilization of nitrogen atoms in superfluid helium," *J. Exp. Theor. Phys. Lett.*, vol. 19, p. 63, 1974.

[25] E. B. Gordon, L. P. Mezhov-Deglin, O. F. Pugachev, and V. V. Khmelenko, "Condensation of an atomic beam on a cold ($\leq$2 K surface)," *Cryogenics*, vol. 16(9), pp. 555–557, 1976.

[26] V. V. Khmelenko, S. Mao, A. Meraki, S. C. Wilde, P. McColgan, A. A. Pelmenev, R. E. Boltnev, and D. M. Lee, "Luminescence of oxygen atoms stimulated by metastable helium at cryogenic temperatures," *Phys. Rev. Lett.*, vol. 111, p. 183002, Oct 2013.

[27] V. Kiryukhin, B. Keimer, R. E. Boltnev, V. V. Khmelenko, and E. B. Gordon, "Inert-gas solids with nanoscale porosity," *Phys. Rev. Lett.*, vol. 79, pp. 1774–1777, Sep 1997.

[28] S. I. Kiselev, V. V. Khmelenko, D. M. Lee, V. Kiryukhin, R. E. Boltnev, E. B. Gordon, and B. Keimer, "Structural studies of impurity-helium solids," *Phys. Rev. B*, vol. 65, p. 024517, Dec 2001.

[29] E. P. Bernard, R. E. Boltnev, V. V. Khmelenko, V. Kiryukhin, S. I. Kiselev, and D. M. Lee, "ESR and X-ray investigations of deuterium atoms and molecules in impurity-helium solids," *J. Low Temp. Phys.*, vol. 134, pp. 169–174, Jan 2004.

[30] E. P. Bernard, R. E. Boltnev, V. V. Khmelenko, V. Kiryukhin, S. I. Kiselev, and D. M. Lee, "Deuterium atoms and molecules in nanoclusters of molecular deuterium," *Phys. Rev. B*, vol. 69, p. 104201, Mar 2004.

[31] V. Kiryukhin, E. P. Bernard, V. V. Khmelenko, R. E. Boltnev, N. V. Krainyukova, and D. M. Lee, "Noble-gas nanoclusters with fivefold symmetry stabilized in superfluid helium," *Phys. Rev. Lett.*, vol. 98, p. 195506, May 2007.

[32] N. V. Krainyukova, R. E. Boltnev, E. P. Bernard, V. V. Khmelenko, D. M. Lee, and V. Kiryukhin, "Observation of the fcc-to-hcp transition in ensembles of argon nanoclusters," *Phys. Rev. Lett.*, vol. 109, p. 245505, Dec 2012.

[33] S. I. Kiselev, V. V. Khmelenko, and D. M. Lee, "Investigation of ultrasound attenuation in impurity-helium solids containing liquid helium," *J. Low Temp. Phys.*, vol. 121, pp. 671–676, Dec 2000.

[34] S. I. Kiselev, V. V. Khmelenko, and D. M. Lee, "Sound propagation in liquid He in impurity-helium solids," *Low Temp. Phys.*, vol. 26, no. 9, pp. 641–648, 2000.

[35] E. Gordon, V. Khmelenko, A. Pelmenev, E. Popov, and O. Pugachev, "Impurity-helium van der Waals crystals," *Chemical Physics Letters*, vol. 155, no. 3, pp. 301 – 304, 1989.

[36] S. Mao, R. E. Boltnev, V. V. Khmelenko, and D. M. Lee, "ESR studies of nitrogen atoms stabilized in aggregates of krypton-nitrogen nanoclusters immersed in superfluid helium," *Low Temp. Phys.*, vol. 38, no. 11, pp. 1037–1042, 2012.

[37] E. P. Bernard, V. V. Khmelenko, and D. M. Lee, "Pulse electron spin resonance studies of H and D atoms in impurity-helium solids," *J. Low Temp. Phys.*, vol. 150, pp. 516–524, Feb 2008.

[38] R. E. Boltnev, E. P. Bernard, J. Järvinen, V. V. Khmelenko, and D. M. Lee, "Stabilization of hydrogen atoms in aggregates of krypton nanoclusters immersed in superfluid helium," *Phys. Rev. B*, vol. 79, p. 180506, May 2009.

[39] R. E. Boltnev, I. N. Krushinskaya, A. A. Pelmenev, E. A. Popov, D. Y. Stolyarov, and V. V. Khmelenko, "Study of the stabilization and recombination of nitrogen atoms in impurity-helium condensates," *Low Temp. Phys.*, vol. 31, no. 70, pp. 547–555, 2005.

[40] E. P. Bernard, R. E. Boltnev, V. V. Khmelenko, and D. M. Lee, "Stabilization of high concentrations of nitrogen atoms in impurity-helium solids," *J. Low Temp. Phys.*, vol. 134, pp. 199–204, Jan 2004.

[41] V. V. Khmelenko, H. Kunttu, and D. M. Lee, "Recent progress in studies of nanostructured impurity-helium solids," *J. Low Temp. Phys.*, vol. 148, no. 1, pp. 1–31, 2007.

[42] P. T. McColgan, A. Meraki, R. E. Boltnev, D. M. Lee, and V. V. Khmelenko, "Optical and electron spin resonance studies of destruction of porous structures formed by nitrogen–rare gas nanoclusters in bulk superfluid helium," *Journal of Low Temperature Physics*, vol. 187, pp. 124–139, Apr 2017.

[43] S. Mao, A. Meraki, R. E. Boltnev, V. V. Khmelenko, and D. M. Lee, "Percolation in aggregates of nanoclusters immersed in superfluid helium," *Phys. Rev. B*, vol. 89, p. 144301, Apr 2014.

[44] G. P. Bewley, D. P. Lathrop, and K. R. Sreenivasan, "Visualization of quantized vortices," *Nature*, vol. 441, no. 1, p. 588, 2006.

[45] W. F. Vinen, "An introduction to quantum turbulence," *Journal of Low Temperature Physics*, vol. 145, pp. 7–24, Nov 2006.

[46] C. F. Barenghi, L. Skrbek, and K. R. Sreenivasan, "Introduction to quantum turbulence," *Proceedings of the National Academy of Sciences*, vol. 111, no. Supplement 1, pp. 4647–4652, 2014.

[47] Y. A. Sergeev and C. F. Barenghi, "Particles-vortex interactions and flow visualization in 4he," *Journal of Low Temperature Physics*, vol. 157, p. 429, Oct 2009.

[48] G. P. Bewley, M. S. Paoletti, K. R. Sreenivasan, and D. P. Lathrop, "Characterization of reconnecting vortices in superfluid helium," *Proceedings of the National Academy of Sciences*, vol. 105, no. 37, pp. 13707–13710, 2008.

[49] E. Fonda, D. P. Meichle, N. T. Ouellette, S. Hormoz, and D. P. Lathrop, "Direct observation of kelvin waves excited by quantized vortex reconnection," *Proceedings of the National Academy of Sciences*, vol. 111, no. Supplement 1, pp. 4707–4710, 2014.

[50] M. S. Paoletti, M. E. Fisher, K. R. Sreenivasan, and D. P. Lathrop, "Velocity statistics distinguish quantum turbulence from classical turbulence," *Phys. Rev. Lett.*, vol. 101, p. 154501, Oct 2008.

[51] M. La Mantia, D. Duda, M. Rotter, and L. Skrbek, "Lagrangian accelerations of particles in superfluid turbulence," *Journal of Fluid Mechanics*, vol. 717, p. R9, 2013.

[52] W. Guo, J. D. Wright, S. B. Cahn, J. A. Nikkel, and D. N. McKinsey, "Metastable helium molecules as tracers in superfluid ^{4}He," *Phys. Rev. Lett.*, vol. 102, p. 235301, Jun 2009.

[53] D. E. Zmeev, F. Pakpour, P. M. Walmsley, A. I. Golov, W. Guo, D. N. McKinsey, G. G. Ihas, P. V. E. McClintock, S. N. Fisher, and W. F. Vinen, "Excimers He_2^* as tracers of quantum turbulence in ^{4}He in the $T = 0$ limit," *Phys. Rev. Lett.*, vol. 110, p. 175303, Apr 2013.

[54] W. Guo, S. B. Cahn, J. A. Nikkel, W. F. Vinen, and D. N. McKinsey, "Visualization study of counterflow in superfluid ^{4}He using metastable helium molecules," *Phys. Rev. Lett.*, vol. 105, p. 045301, Jul 2010.

[55] W. Guo, M. La Mantia, D. P. Lathrop, and S. W. Van Sciver, "Visualization of two-fluid flows of superfluid helium-4," *Proceedings of the National Academy of Sciences*, vol. 111, pp. 4653–4658, 2014.

[56] E. B. Gordon, A. V. Karabulin, V. I. Matyushenko, V. D. Sizov, and I. I. Khodos, "Structure of metallic nanowires and nanoclusters formed in superfluid helium," *Journal of Experimental and Theoretical Physics*, vol. 112, pp. 1061–1070, Jun 2011.

[57] E. Gordon, A. Karabulin, V. Matyushenko, V. Sizov, and I. Khodos, "The role of vortices in the process of impurity nanoparticles coalescence in liquid helium," *Chemical Physics Letters*, vol. 519-520, pp. 64 – 68, 2012.

[58] A. Meraki, P. T. McColgan, P. M. Rentzepis, R. Z. Li, D. M. Lee, and V. V. Khmelenko, "Quantum vortices and thermally induced luminescence of nitrogen nanoclusters immersed in liquid helium," *Phys. Rev. B*, vol. 95, p. 104502, Mar 2017.

[59] H. E. Hall and W. F. Vinen, "The rotation of liquid helium II. I. experiments on the propagation of second sound in uniformly rotating helium II," *Proceedings of the Royal Society of London A: Mathematical, Physical and Engineering Sciences*, vol. 238, no. 1213, pp. 204–214, 1956.

[60] E. B. Gordon, M. I. Kulish, A. V. Karabulin, V. I. Matyushenko, E. V. Dyatlova, A. S. Gordienko, and M. E. Stepanov, "Realization of mechanical rotation in superfluid helium," *Low Temperature Physics*, vol. 43, no. 9, pp. 1055–1061, 2017.

[61] M. Chergui, R. Schriever, and N. Schwentner, "Electronic and vibrational relaxation in rydberg and valence states of NO in Ne matrices," *The Journal of Chemical Physics*, vol. 89, no. 12, pp. 7083–7093, 1988.

[62] I. Y. Fugol and Y. B. Poltoratski, "Luminescence and biexcitons in nitrogen crystals," *Solid State Communications*, vol. 30, no. 8, pp. 497 – 500, 1979.

[63] R. E. Boltnev, V. V. Khmelenko, and D. M. Lee, "Stabilization of H and D atoms in krypton-helium nanocondensates," *Low Temperature Physics*, vol. 36, no. 5, pp. 382–391, 2010.

[64] R. P. Frosch and G. W. Robinson, "Emission spectrum of NO in solid rare gases: The lifetime of the a 4Π state and the spectrum of the a $4\Pi \rightarrow$X 2Π and B $2\Pi \rightarrow$X 2Π transitions," *The Journal of Chemical Physics*, vol. 41, no. 2, pp. 367–374, 1964.

[65] J. Fournier, J. Deson, and C. Vermeil, "Photolysis of NO trapped in a rigid matrix at 6 K," *The Journal of Chemical Physics*, vol. 68, no. 11, pp. 5062–5065, 1978.

[66] J. Eloranta, K. Vaskonen, H. Häkkänen, T. Kiljunen, and H. Kunttu, "193 nm photodynamics of NO in rare gas matrices: Fluorescence, thermoluminescence, and photodissociation," *The Journal of Chemical Physics*, vol. 109, no. 18, pp. 7784–7792, 1998.

[67] M. Chergui, N. Schwentner, and A. Tramer, "Spectroscopy of the NO molecule in N_2 and mixed N_2/Kr matrices," *Chem. Phys. Lett.*, vol. 201, no. 1, pp. 187–193, 1993.

[68] W. Walker, R. Taylor, and K. Monahan, "Photoluminescence spectra of NeO in a solid matrix," *Chemical Physics Letters*, vol. 84, no. 2, pp. 288 – 289, 1981.

[69] R. V. Taylor and W. C. Walker, "Photoluminescence of ArO and KrO in doped rare-gas matrices," *The Journal of Chemical Physics*, vol. 70, no. 1, pp. 284–287, 1979.

[70] R. V. Taylor, W. Scott, P. R. Findley, Z. Wu, W. C. Walker, and K. M. Monahan, "Matrix interactions with rare-gas oxide excimers," *The Journal of Chemical Physics*, vol. 74, no. 7, pp. 3718–3722, 1981.

[71] R. N. Clark, R. Carlson, W. Grundy, and K. Noll, "Observed ices in the solar system," in *The Science of Solar System Ices* (M. S. Gudipati and J. Castillo-Rogez, eds.), vol. 356 of *Astrophysics and Space Science Library*, pp. 3–46, New York: Springer, 1 ed., 2013.

[72] E. B. Gordon, A. A. Pelmenev, O. F. Pugachev, and V. V. Khmelenko, "Hydrogen and deuterium atoms, stabilized by condensation of an atomic beam in superfluid helium," *J. Exp. Theor. Phys. Lett.*, vol. 37, no. 5, pp. 237–239, 1983.

[73] S. I. Kiselev, V. V. Khmelenko, and D. M. Lee, "Hydrogen atoms in impurity-helium solids," *Phys. Rev. Lett.*, vol. 89, p. 175301, Oct 2002.

[74] V. V. Khmelenko, E. P. Bernard, S. . Vasiliev, and D. M. Lee, "Tunnelling chemical reactions of hydrogen isotopes in quantum solids," *Russ. Chem. Rev.*, vol. 76, no. 12, pp. 1107–1121, 2007.

[75] P. C. Samartzis and A. M. Wodtke, "All-nitrogen chemistry: How far are we from N_{60}?," *Int. Rev. Phys. Chem.*, vol. 25, no. 4, pp. 527–552, 2006.

[76] A. Douglas and W. J. Jones, "The 2700Å bands of the N_3 molecules," *Can. J. Phys.*, vol. 43, no. 12, pp. 2216–2221, 1965.

[77] R. Tian and J. Michl, "Fast-particle bombardment of solid nitrogen," *Faraday Discuss. Chem. Soc.*, vol. 86, pp. 113–124, 1988.

[78] J. C. Amicangelo, J. R. Collier, C. T. Dine, N. L. Saxton, and R. M. Schleicher, "Matrix isolation infrared observation of N_3 using a nitrogen microwave discharge plasma source," *Mol. Phys.*, vol. 105, no. 8, pp. 989–1002, 2007.

[79] Y.-J. Wu, H.-F. Chen, S.-J. Chuang, and T.-P. Huang, "Far ultraviolet absorption spectra of N_3 and N_2^+ generated by electrons impacting gaseous N_2," *The Astrophysical Journal*, vol. 779, no. 1, pp. 40–46, 2013.

[80] E. Savchenko, I. Khyzhniy, S. Uyutnov, M. Bludov, G. Gumenchuk, and V. Bondybey, "Emission spectroscopy of solid nitrogen," *Radiat. Meas.*, vol. 90, no. Supplement C, pp. 1–5, 2016. Proceedings of the 9th International Conference on Luminescent Detectors and Transformers of Ionizing Radiation (LUMDETR 2015).

[81] K. O. Christe, W. W. Wilson, J. A. Sheehy, and J. A. Boatz, "N_5^+: A novel homoleptic polynitrogen ion as a high energy density material," *Angew. Chem., Int. Ed.*, vol. 38, no. 13-14, pp. 2004–2009, 1999.

[82] A. Vij, W. W. Wilson, V. Vij, F. S. Tham, J. A. Sheehy, and K. O. Christe, "Polynitrogen chemistry. synthesis, characterization, and crystal structure of surprisingly stable fluoroantimonate salts of N_5^+," *J. Am. Chem. Soc.*, vol. 123, no. 26, pp. 6308–6313, 2001. PMID: 11427055.

[83] M. T. Nguyen, "Polynitrogen compounds: 1. structure and stability of N_4 and N_5 systems," *Coord. Chem. Rev.*, vol. 244, no. 1, pp. 93–113, 2003. 13th Main Group Chemistry.

[84] V. E. Zarko, "Searching for ways to create energetic materials based on polynitrogen compounds (review)," *Combustion, Explosion, and Shock Waves*, vol. 46, pp. 121–131, Mar 2010.

[85] F. Cacace, G. de Petris, and A. Troiani, "Experimental detection of tetranitrogen," *Science*, vol. 295, no. 5554, pp. 480–481, 2002.

[86] E. E. Rennie and P. M. Mayer, "Confirmation of the "long-lived" tetra-nitrogen (N_4) molecule using neutralization-reionization mass spectrometry and ab initio calculations," *J. Chem. Phys.*, vol. 120, no. 22, pp. 10561–10578, 2004.

[87] J. P. Zheng, J. Waluk, J. Spanget-Larsen, D. M. Blake, and J. Radziszewski, "Tetrazete (N_4). can it be prepared and observed?," *Chem. Phys. Lett.*, vol. 328, no. 1, pp. 227–233, 2000.

[88] E. V. Savchenko, I. V. Khyzhniy, S. A. Uyutnov, M. A. Bludov, A. P. Barabashov, G. B. Gumenchuk, and V. E. Bondybey, "Radiation effects in solid nitrogen," *J. Low Temp. Phys.*, vol. 187, pp. 62–70, Apr 2017.

[89] W. R. M. Graham and H. Lew, "Spectra of the $d^1\Sigma^+ - c^1\Pi$ and $d^1\Sigma^+ - b^1\Sigma^+$ systems and dissociation energy of NH and ND," *Can. J. Phys.*, vol. 56, no. 1, pp. 85–99, 1978.

[90] G. W. Robinson and M. McCarty, Jr., "Electronic spectra of free radicals at 4°K-HNO, NH, and OH," *J. Chem. Phys.*, vol. 28, no. 2, p. 350, 1958.

[91] M. McCarty, Jr. and G. W. Robinson, "Imine and imine-d radicals trapped in argon, krypton and xenon matrices at 4.2°K.," *J. Am. Chem. Soc.*, vol. 81, no. 17, pp. 4472–4476, 1959.

[92] P. A. Lund, Z. Hasan, P. N. Schatz, J. H. Miller, and L. Andrews, "Matrix isolation magnetic circular dichroism (MCD) spectrum of NH radical produced by a glow discharge technique," *Chem. Phys. Lett.*, vol. 91, no. 6, pp. 437–439, 1982.

[93] O. Schnepp and K. Dressler, "Photolysis of ammonia in a solid matrix at low temperatures," *J. Chem. Phys.*, vol. 32, no. 6, pp. 1682–1686, 1960.

[94] C. E. P. M. Van De Bult, L. J. Allamandola, F. Baas, L. V. Ijzenboorn, and J. M. Greenberg, "Chemiluminescence of N_2, NH, and O_2 in argon matrices," *J. Mol. Struct.*, vol. 61, no. Supplement C, pp. 235–238, 1980.

[95] J. Goodman and L. E. Brus, "Long range vibrational energy transfer from ND and NH($A^3\Pi$) to CO and N_2 in solid Ar," *J. Chem. Phys.*, vol. 65, no. 3, pp. 1156–1164, 1976.

[96] V. E. Bondybey and J. H. English, "Effect of matrix on vibrational relaxation: NH and ND $X^3\Sigma^-$ in rare gas solids," *J. Chem. Phys.*, vol. 73, no. 1, pp. 87–92, 1980.

[97] D. A. Ramsay and P. J. Sarre, "The $c^1\Pi - a^1\Delta$ system of the NH molecule," *J. Mol. Spectrosc.*, vol. 93, no. 2, pp. 445–446, 1982.

[98] W. Y. Cheung, B. Gelernt, and T. Carrington, "New bands in the ND $c^1\Pi - a^1\Delta$ system: Spectroscopic constants of the $a^1\Delta$ state," *Chem. Phys. Lett.*, vol. 66, no. 2, pp. 287–290, 1979.

[99] R. W. Lunt, R. W. B. Pearse, and E. C. W. Smith, "The λ 4502 band of NH," *Proc. R. Soc. London, Ser. A*, vol. 151, no. 874, pp. 602–609, 1935.

[100] F. L. Whittaker, "The $c^1\Pi - b^1\Sigma^+$ band system of NH and ND," *J. Phys. B: At. Mol. Phys.*, vol. 1, no. 5, pp. 977–982, 1968.

[101] F. L. Whittaker, "Observation of the $d^1\Sigma - b^1\Sigma^+$ system of NH and ND in the vacuum ultraviolet," *Can. J. Phys.*, vol. 47, no. 12, pp. 1291–1293, 1969.

[102] H. Esser, J. Langen, and U. Schurath, "Spectrum and lifetime of NH($a^1\Delta \rightarrow X^3\Sigma^-$) in inert gas matrices," *Berichte der Bunsengesellschaft für physikalische Chemie*, vol. 87, no. 8, pp. 636–643, 1983.

[103] V. Hizhnyakov, K. Seranski, and U. Schurath, "Homogeneous lineshapes and shifts of the $b^1\Sigma^+ \leftarrow X^3\Sigma^-$ transition in matrix-isolated NH: Comparison with quadratic coupling theory," *Chem. Phys.*, vol. 162, no. 2, pp. 249–256, 1992.

[104] O. Oehler, D. A. Smith, and K. Dressler, "Luminescence spectra of solid nitrogen excited by electron impact," *J. Chem. Phys.*, vol. 66, no. 5, pp. 2097–2107, 1977.

[105] F. Coletti and A. M. Bonnot, "Emission spectrum of electron excited solid nitrogen," *Chem. Phys. Lett.*, vol. 45, no. 3, pp. 580–582, 1977.

[106] I. Y. Fugol, Y. B. Poltoratski, and Y. I. Rybalko, "Self-localization of high-frequency triplet excitations in solid nitrogen," *Low Temp. Phys.*, vol. 4, pp. 1048–1052, 1978.

[107] E. Savchenko, I. Khyzhniy, S. Uyutnov, A. Barabashov, G. Gumenchuk, A. Ponomaryov, and V. Bondybey, "Charged defects and defect-induced processes in nitrogen films," *Phys. Status Solidi C*, vol. 12, no. 1-2, pp. 49–54, 2015.

[108] R. J. Loveland, P. G. L. Comber, and W. E. Spear, "Charge transport in the diatomic molecular solids and liquids: N_2, O_2, and CO," *Phys. Rev. B*, vol. 6, pp. 3121–3127, Oct 1972.

[109] K. Hiraoka and G. Nakajima, "A determination of the stabilities of $N_2^+(N_2)_n$ and $O_2^+(N_2)_n$ with $n = 1-11$ from measurements of the gas-phase ion equilibria," *J. Chem. Phys.*, vol. 88, no. 12, pp. 7709–7714, 1988.

[110] D. E. David, T. F. Magnera, R. Tian, D. Stulik, and J. Michl, "Cluster ions from keV-energy ion and atom bombardment of frozen gases," *Nucl. Instrum. Methods Phys. Res., Sect. B*, vol. 14, no. 4, pp. 378–391, 1986.

[111] B. Stenum, J. Schou, H. Sørensen, and P. Gürtler, "Luminescence from pure and doped solid deuterium irradiated by kev electrons," *J. Chem. Phys.*, vol. 98, no. 1, pp. 126–134, 1993.

[112] P. T. McColgan, A. Meraki, R. E. Boltnev, D. M. Lee, and V. V. Khmelenko, "Luminescence of molecular nitrogen nanoclusters containing stabilized atoms," *J. Phys. Chem. A*, vol. 121, pp. 9045–9057, 2017. PMID: 29112821.

[113] A. A. Ovchinnikov, "Localized long-lived vibrational states in molecular crystals," *Sov. Phys. J. Exp. Teor. Phys.*, vol. 30, no. 1, pp. 147–150, 1970.

[114] K. Dressler, O. Oehler, and D. A. Smith, "Measurement of slow vibrational relaxation and fast vibrational energy transfer in solid N_2," *Phys. Rev. Lett.*, vol. 34, pp. 1364–1367, Jun 1975.

[115] V. Arp, "Heat transport through helium II," *Cryogenics*, vol. 10, no. 2, pp. 96 – 105, 1970.

[116] E. B. Gordon, L. P. Mezhov-Deglin, O. F. Pugachev, and V. V. Khmelenko, "Thermal stability of condensed systems that contain trapped atoms," *Sov. Phys. J. Exp. Teor. Phys.*, vol. 46, no. 3, pp. 502–507, 1977.

[117] S. W. V. Sciver, *Helium Cryogenics*. 1st ed. Plenum, New York and London, 1986.

[118] S. Babuin, M. Stammeier, E. Varga, M. Rotter, and L. Skrbek, "Quantum turbulence of bellows-driven ^{4}He superflow: Steady state," *Phys. Rev. B*, vol. 86, p. 134515, Oct 2012.